APPLICATIONS OF FRP IN REINFORCING AND STRENGTHENING CONCRETE MASONRY BEAMS

Munir Alp Enginsal

A Thesis

in

The Department

of

Building, Civil, and Environmental Engineering

Presented in Partial Fulfillment of the Requirements

for the Degree of Master of Applied Science (Civil Engineering) at

Concordia University

Montréal, Québec, Canada

September 2009

Your file Votre référence
ISBN: 978-0-494-63072-3
Our file Notre référence
ISBN: 978-0-494-63072-3

ABSTRACT

APPLICATIONS OF FRP IN REINFORCING AND STRENGTHENING CONCRETE MASONRY BEAMS

MUNIR ALP ENGINSAL

An experimental and analytical study is conducted in order to investigate the flexural behaviour of masonry beams when reinforced or strengthened with Fibre-Reinforced Polymers (FRP) composite materials. Nine reinforced masonry beams with 4.0 m and 2.4 m clear spans were constructed to be tested under four point bending setup. The beams were subjected to increasing monotonic load up to failure, and then unloaded. Two beams have two courses of hollow concrete masonry units, and the remaining seven beams have three courses. Three masonry beams were reinforced using conventional steel rebars two of which were considered as the control specimens, while the remaining beam strengthened using two layers of Carbon Fibre-Reinforced Polymers (CFRP) sheets that were externally bonded to both sides of the beam. The remaining six beams were internally reinforced using Glass Fibre Reinforced Polymers (GFRP) rods with different reinforcement ratios. Beams were detailed to have sufficient shear reinforcement such that they do not fail in shear. Comparisons were conducted between the GFRP-reinforced and steel-reinforced control beams as well as CFRP-strengthened and steel-reinforced control beam of the flexural capacity, deformation and strains of the tested specimens. Using the acquired data from the experimental and analytical studies, effectiveness of GFRP rods as internal reinforcement for concrete masonry beams as well as the effectiveness CFRP sheets for strengthening steel-reinforced concrete masonry beams are demonstrated.

To my beloved family

ACKNOWLEDGEMENT

First of all, I would like to acknowledge the financial supports of Natural Sciences and Engineering Research council of Canada (NSERC), le Fonds Québécois de la Recherche sur la Nature et les Technologies (FQRNT), and Centre d' Études Interuniversitaire sur les Structures sous Charges Extrêmes (CEISCE).

The experimental phase of this project became possible with the endless support and sincere collaboration of l'Association des Entrepreneurs en Maçonnerie du Québec (AEMQ), Normand Turenne (Président) and Denis Brisebois (Directeur Général). Furthermore, Canada Masonry Design Centre (CMDC) is greatly acknowledged for their contribution in enlightening us with ideas at the very beginning of this project.

I would also like use this opportunity to show my deepest gratitude to my supervisor Dr. Khaled Galal for tenaciously believing in me throughout this project. Without his financial and academic support, it would be impossible to realize this extensive investigation.

I would also like to acknowledge the assistance and technical support of laboratory technicians Mr. Mark Elie and Mr. Tiberiu Aldea. Their innovative ideas helped me significantly during the experimental phase of this thesis.

I wish to express my acknowledgements to my dear colleague Navid Sasanian for sincerely supporting me throughout this project. Without his valuable contributions and clever ideas, finalizing this task would take much longer.

I am also grateful that I have had chance to work with Ricardo Gioia, who helped me extensively during several experimental phases of this project. I will forget neither the laughs we had in the structural laboratory nor the lessons he taught me on construction.

I also would like to extend my sincere gratitude to all my other colleagues namely; Sherif, Hossein, Nima, Mossab, Hossam, Hany, Ihab and Behnam for supporting me and helping me in the structural laboratory to complete my experimental work.

Finally, I would like to thank Bercis Misirli for always and unconditionally being there for me whenever I sought for an asylum.

TABLE OF CONTENTS

LIST OF FIGURES

LIST OF TABLES

LIST OF SYMBOLS

A_{frp}	Total area of the GFRP reinforcement in beam cross-section, mm^2
A_s	Total area of steel reinforcement in beam cross-section, mm^2
A_{sb}	Balanced area of steel reinforcement, mm^2
a	Shear span of the reinforced masonry beam, mm
b	Width of the cross-section, mm
c	Depth of the compression zone in the cross-section of the beams, mm
d	Effective depth of internal longitudinal reinforcement, mm
d_b	Diameter of the reinforcing bars, mm
E_{cfrp}	Young's modulus of CFRP laminate, GPa
E_m	Young's modulus of masonry assemblage, GPa
E_{frp}	Young's modulus of GFRP bars, GPa
$E_{elastic}$	Elastic energy absorbed by the masonry beam
$E_{inelastic}$	Inelastic energy absorbed by the masonry beam
E_{steel}	Young's modulus of steel reinforcement, GPa
E_{total}	Total energy absorbed by the masonry beam
f_{frp}	Stress in the GFRP rods, MPa
f'_c	Compressive strength of concrete, MPa
f'_m	Compressive strength of the masonry assemblage, MPa
f_{frpu}	Ultimate tensile strength of the GFRP rods, MPa
f_y	Yield stress of the steel reinforcement, MPa
h	Height of the reinforced masonry beam, mm
I_{cr}	Moment of inertia of fully cracked section, mm^4

I_{eff}	Effective moment of inertia of the cracked section, mm^4
I_g	Moment of inertia of the gross section, mm^4
l	Reinforced masonry beam span, mm
M_a	Applied moment on the reinforced concrete masonry beams, kN.m
M_{cr}	Cracking moment of the reinforced concrete masonry beams, kN.m
M_n	Nominal flexural resistance of the masonry beams, kN.m
M_r	Moment resistance of the reinforced masonry beam cross-section, kN.m
M_s	Serviceability moment of the reinforced concrete masonry beams, kN.m
P	Load applied by the hydraulic actuator, N
Ps	Weight of the specimen, N
R, f_r	Modulus of rupture of the masonry assemblage, MPa
S	Section modulus of the actual net area, mm^3
α_1	Stress block factor
β	Constant dependent on the mode of failure
β_1	Stress block factor
ε_c	Compressive strain of concrete
ε_{cfrp}	Tensile strain of the CFRP laminate
ε_{frpu}	Ultimate tensile strain of the GFRP
ε_m	Compressive strain of masonry
ε_{mu}	Ultimate compressive strain of masonry
μ	Deformability index
σ_m	Compressive stress in masonry
ρ_{frp}	GFRP reinforcement ratio

ρ_{frpb}	Balanced GFRP reinforcement ratio of the masonry beam cross-section
ψ_s	Curvature of the reinforced concrete masonry beams at service stage
ψ_u	Curvature of the reinforced concrete masonry beams at ultimate stage
χ	Modification factor to account for the direction of the compressive stress and continuity of grout in the masonry assemblage

LIST OF ABBREVIATIONS

ACI	American Concrete Institute
ASTM	American Society of Testing and Materials
CFRP	Carbon Fibre-Reinforced Polymer
CSA	Canadian Standards Association
DF	Deformability Factor
FRP	Fibre-Reinforced Polymer
GFRP	Glass Fibre-Reinforced Polymer
ISIS	Intelligent Sensing for Innovative Structures
LSD	Limit States Design
NSM	Near-Surface Mounted
RBM	Reinforced Brick Masonry
RC	Reinforced Concrete
RCM	Reinforced Concrete Masonry

CHAPTER 1

INTRODUCTION

1.1 Background and Problem Definition

Masonry is one of the ancient construction methods and has been used by number of civilizations for centuries. Although many different materials have been employed as masonry units such as alluvial deposits, stones, ice blocks, glass ...etc, concrete masonry units were first designed and molded in mid-1800s with the increase in the cement quality. Since the very first concrete masonry units were solid and heavy, they could not attract the attention of the construction industry. Later on, techniques were developed to make hollow concrete blocks and the first hollow concrete masonry was introduced in 1866 (Figure 1.1). The concrete masonry units that are used in this research are almost identical to their predecessors in terms of shape.

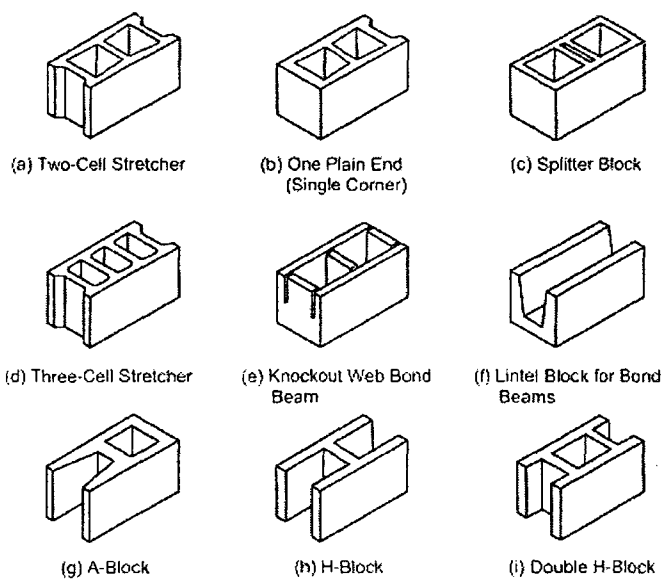

Figure 1.1 Various types of concrete masonry units (Drysdale and Hamid, 2005)

Romans started constructing low-rise unreinforced masonry buildings as early as the first century A.C. Some of those structures were five or more stories high and had one meter thick unreinforced load bearing masonry walls all around their parameters. Unreinforced masonry beams were utilized in order to allow for door and window openings on the façade and within the interior masonry walls of the structures (Figure 1.2).

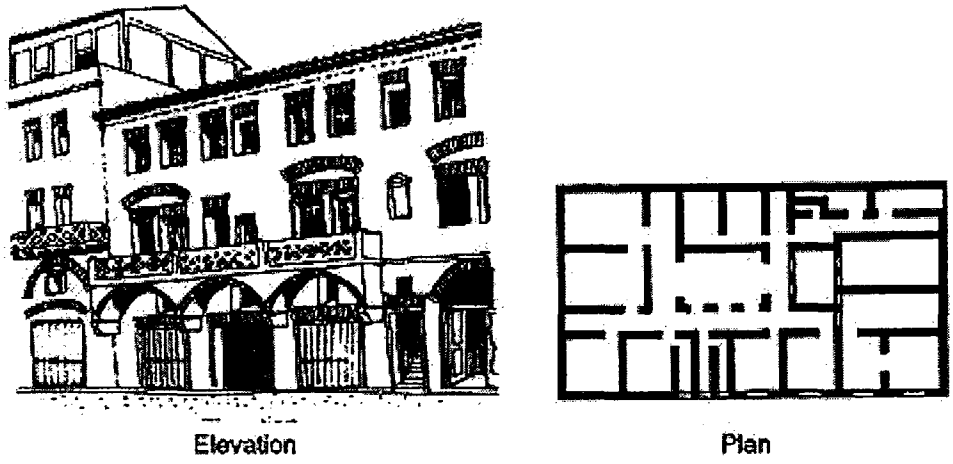

Figure 1.2 Early multistory load-bearing masonry structure (Drysdale and Hamid, 2005)

Beams in masonry construction are mostly utilized as bond beams or lintel beams. They are located at the roof level or at floor levels and may have multiple functions such as tying the structure around its perimeter, transferring the diaphragm action of the roof to the shear walls and spanning over the openings in the walls supporting the gravity loads coming from above (Figure 1.3 and Figure 1.4).

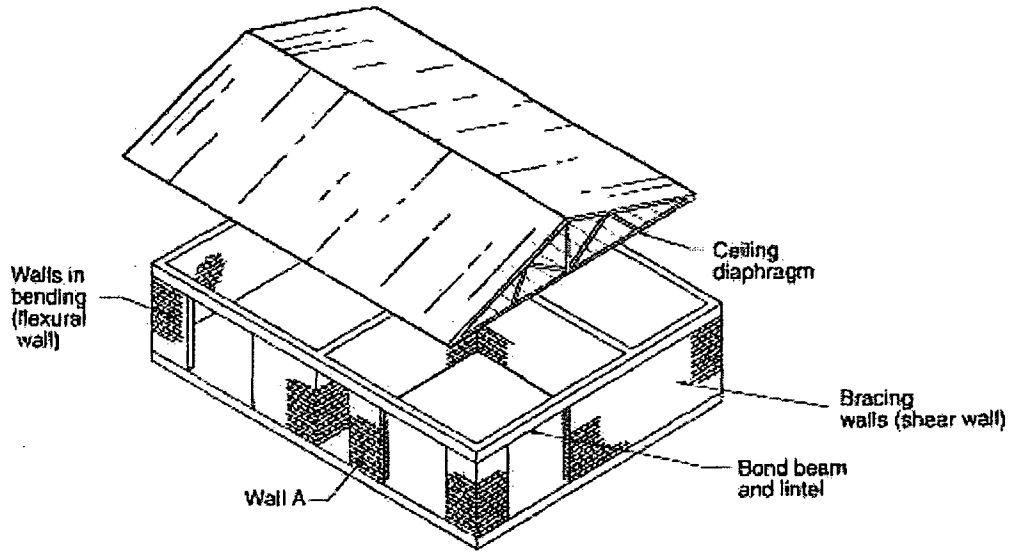

Figure 1.3 Lateral load resisting structural system of a single-storey masonry structure. (Drysdale and Hamid, 2005)

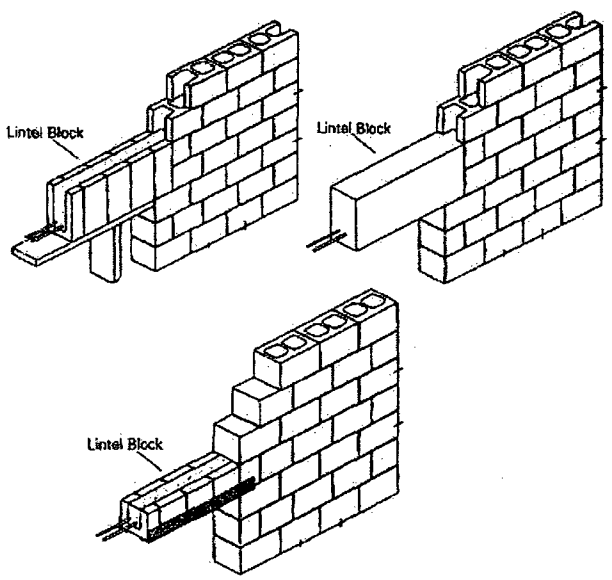

Figure 1.4 Reinforced concrete lintel masonry units supporting opening located in an unreinforced masonry wall (Taly, 2001)

Although some of the structural principles hardly ever changed in masonry design, with the introduction of stronger concrete blocks and steel reinforcement, contemporary structural masonry elements that are presently being used differ greatly

from their ancient ancestors. Foremost, today's limit states design (LSD) design guideline for reinforced masonry structures CSA S304.1 (2004) does not permit the use of unreinforced masonry beams since tensile strength of masonry alone cannot be relied upon. Instead, even for barely loaded short spans, longitudinal wire reinforcement located at bed joints have to be used (Figure 1.5).

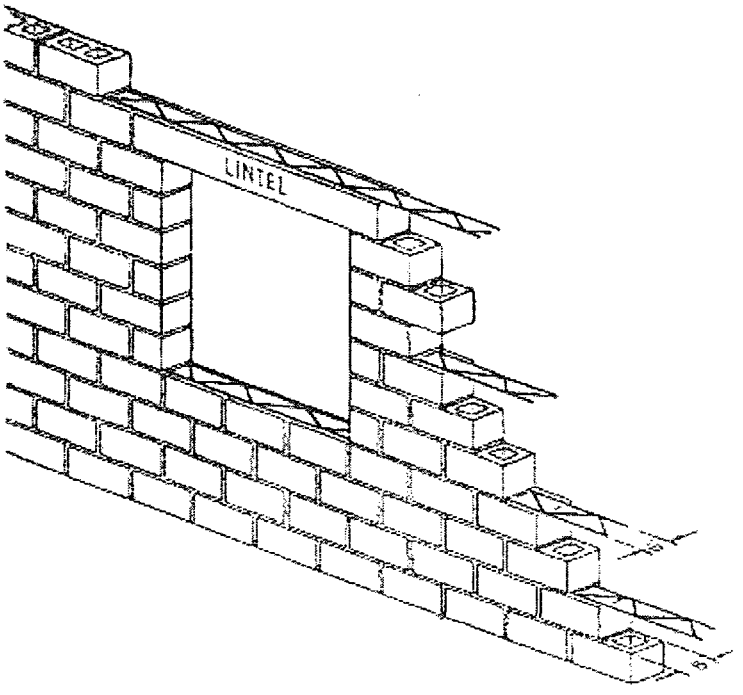

Figure 1.5 Lintel over an opening in a wall, supported by truss-type longitudinal wire reinforcement (Taly, 2001)

Although shear resistance capacity of masonry beams can be sufficient for small openings such as doors and windows on masonry walls, for larger spans, adequate shear reinforcement is enforced. Implementation of steel reinforcement in the field of masonry not only improved the performance of the low-rise structures by increasing their ability to resist axial and lateral loads, but also made it possible to construct high-rise structures such as Place Louis Riel apartment building located in Winnipeg, Canada (Figure 1.6).

Structure was constructed using high strength, grout filled masonry units that had internal steel reinforcement. In addition to that, there were several other high-rises built in the early 1970s in the province of Ontario. Recently several other reinforced masonry structures were constructed in USA, one of which is the 17 storey apartment building located in Cleveland, Ohio, completed in 1995.

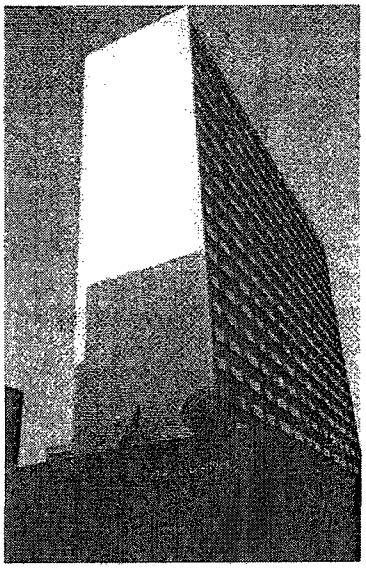

Figure 1.6 Place Louis Riel apartment building located in Winnipeg, Canada (Drysdale and Hamid, 2005)

Earlier researchers, namely Khalaf (1981), Suter and Fenton (1986), have commenced establishing design criteria for reinforced masonry in the beginning of 1980s. Their areas of interest were mostly ultimate compressive and tensile strains, equivalent rectangular stress block, ductility and deflection properties of reinforced masonry beams. Conducted tests revealed that loaded reinforced masonry flexural members behave to the reinforced concrete members. However design difficulties may be encountered with conventional steel bars due to the limited width of the masonry units. Considering the under-reinforced design principle of the steel reinforced masonry, the design of larger

beam cross-sections is inevitable for most of the cases, giving rise to higher material and labor costs.

The introduction of Fibre-Reinforced Polymer (FRP) composites into reinforced masonry design will allow engineers to overcome steel related problems that the conventional reinforced masonry has been facing for decades. Although FRP possesses several limitations such as higher initial costs and low fire resistance in comparison to conventional steel reinforcement, fire resistance should not be an issue for masonry construction as minimum cover requirements are naturally satisfied due to the shell thickness of concrete masonry units. Moreover, higher initial cost of FRP is not being seen as a major limitation anymore as this material is becoming increasingly abundant and competitive in the construction industry. More importantly, due to the high maintenance costs of steel reinforcement, the life cycle cost of FRP is less than the cost of conventional steel bars for some structures. FRP also comes with several significant advantages over steel such as high durability, non-corrosiveness, high strength-to-weight ratio and resistance against fatigue. Unlike conventional steel reinforcement, FRP uses over-reinforced design approach meaning that there will not be any upper limit for reinforcement ratio as long as the deflections are within the allowable limits set by the design guidelines of ISIS Canada (2001) and ACI 440-2R (2002). Moreover, FRP-reinforced masonry beams may be used in the same fashion as the pre-stressed reinforced concrete beams for the constructions taking place at remote areas where the delivery of factory made pre-stressed structural members is cumbersome. In this sense, it is suitable to say that one can maximize the versatility of both FRP and reinforced masonry elements once they are implemented to be utilized concurrently.

FRP-reinforced concrete has been extensively examined by the researchers such as Benmokrane and Theriault (1998), Ombres and Aiello (2000) in the past decade and has been identified as an alternate construction material for reinforcing and strengthening concrete primarily due to its promising strength and durability characteristics. There are several researches investigating the applications of CFRP in strengthening and rehabilitating previously built reinforced masonry elements such as masonry beams and masonry shear walls. However, applications of FRP as an internal reinforcement for reinforced masonry beams have not been investigated, yet. Although design guidelines such as Canada (2001) and ACI 440-2R (2002) for the applications of FRP in reinforced concrete are already available for the designers, a design guideline addressing the applications of FRP in the design of reinforced masonry elements has not yet been published.

It is a known fact that the existing ancient structures constructed using unreinforced masonry do not meet the requirements of today's buildings codes and are prone to failure when subjected to excessive lateral loads such as seismic loads and wind loads. For instance, a recent earthquake with a magnitude of 6.3 shook Abruzzo region of Italy, severely damaged several historical villages, killing at least 100 civilians and injuring 1500 other (CNN, 2009). Moreover, most of those ancient masonry structures have severely deteriorated structural members that need urgent retrofitting. As a remedy, Carbon Fibre-Reinforced Polymers (CFRP) is being used in the construction industry in order to rehabilitate, retrofit and strengthen existing masonry structural members. CFRP exhibits similar properties with other fiber reinforced polymers such as high strength-to-weight ratio, non-corrosiveness and high durability and it has already been used for

rehabilitation purposes of reinforced concrete bridges. As its usage is becoming more popular in reinforced concrete structures, researchers have already started to test CFRP strengthened masonry structural members such as shear walls and columns and they have been able to acquire promising results. To the author's knowledge, CFRP sheets have not yet been tested on steel-reinforced masonry beams excluding a research conducted by Hao, Z. (2007) in retrofitting steel reinforced masonry deep beams using CFRP sheets.

1.2 Objectives and Scope

This research is primarily targeting to examine the flexural response of fully-grouted and internally GFRP-reinforced full-scale concrete masonry beams. For that purpose, six GFRP-reinforced concrete masonry beams were prepared having different reinforcement ratios. In addition to that, three other fully-grouted steel reinforced full-scale beams were built and tested as control specimens, one of which was strengthened using CFRP sheets in order to assess the contribution of CFRP to the flexural resistance and stiffness of a reinforced concrete masonry beams.

The scope of this research consists of the following items in order to fulfill the objectives;

- To investigate and demonstrate the flexural performance of internally GFRP reinforced fully-grouted concrete masonry beams.
- To evaluate the contribution of CFRP strengthening to the flexural resistance and stiffness properties of conventional steel reinforced fully-grouted concrete masonry beams.

- To propose a design diagram based on the performance of the tested GFRP reinforced masonry beams that will contribute to develop design guidelines for FRP reinforced masonry.
- To investigate the deformability of the GFRP reinforced masonry beams in order to determine if they are able meet the deformability requirements of the building codes in effect.
- To propose a new concrete masonry unit design that is not only intended to contribute to the flexural performance of the masonry assemblages but also enhances the workability of the masonry units.

The author of this thesis would like to point out that, this research investigates the flexural performances of the FRP reinforced masonry beams, meaning that the beams were detailed to have adequate shear resistance such that they were forced to fail in flexure. In addition to that, it is assumed that GFRP rods maintained perfect bonding with the surrounding grout filling during the test.

1.3 Organization of the Thesis

Chapter one is an introductory chapter summarizing the history of masonry being one of the oldest methods of construction. This chapter also provided the reader with brief information regarding the importance and objectives of this research and was written to deliver the necessary knowledge regarding the materials that have been used in order to better comprehend the rest of the thesis.

Chapter two is a review of related researches that have been previously conducted and elaborates them in five main headlines; steel-reinforced masonry, general usage of

FRP in structural elements, FRP-reinforced masonry, general usage of CFRP in strengthening and rehabilitation of structural elements and finally CFRP strengthened and rehabilitated reinforced masonry elements.

Chapter three presents the experimental program of this study. It contains detailed information regarding the used materials, test setup, instrumentation and constructed specimens.

Chapter four reports, interprets and discusses the acquired test data of each specimen with corresponding charts, tables and photographs.

Chapter five focuses on the analytical modeling and design of the tested specimens. This chapter mainly compares the expected flexural strength, stiffness and deformability values of the specimens with the test results. Proposed design diagrams are included in this section as well.

Chapter six discusses the proposed new concrete masonry unit designed to be used in reinforced masonry beams and walls.

Chapter seven consists of the summary and conclusion sections of this experimental project followed by a list of recommendations for future studies.

CHAPTER 2

LITERATURE REVIEW

2.1 Steel-Reinforced Masonry Beams

Tests on conventional steel-reinforced masonry assemblages have been conducted for decades as seismic design codes enforced the use of reinforcement for the masonry assemblages. Since most of the experimental work that has been done is related to the behaviour of reinforced masonry walls, there exists little amount of published experimental work on the behaviour of the reinforced masonry beams.

Khalaf (1981) conducted an experimental investigation on eight steel reinforced four-course concrete block masonry beams with different percentages of reinforcement and different configurations of grouting including twenty one compressive prisms in which the authors tried to implement the ultimate strength design for reinforced concrete to reinforced masonry. Khalaf (1981) also tried to acquire a suitable guideline to determine a representative value of compressive strength (f'_m) for concrete masonry units with a correct method of prisms testing. In order to do so, tests were conducted on unfilled, partially filled and completely grouted two-block prisms under axial and eccentric loads. In addition, they tried to determine the correct values of modulus of elasticity (E_m), modulus of rupture and cracking patterns for reinforced concrete masonry beams under load. The effect of discontinuities in the concrete fill, poor bond between the concrete masonry block, grout and mortar on the flexural performance of the beam was also studied. Based on the test results, the author reached the following conclusions; limit states design approach of reinforced concrete can be safely used for reinforced concrete

beams by assuming the maximum usable strain as 0.003 and by designating f'_m instead of f'_c, the value of f'_m can be estimated correctly by testing concrete masonry blocks in the direction in which they will be stressed and the reinforced masonry beams exhibit lower ductility then similarly reinforced concrete beams due to the stress concentrations at the void areas that has not been perfectly filled by the poured infill. It was also reported that the use of horizontal mortar joints reinforcement at the compression zone of masonry should not be recommended as the buckling of this material under loading conditions tends to destroy the horizontal mortar joint, provoking splitting.

Suter and Fenton (1986) have tested 97 masonry beams of which 78 were reinforced specimens. Tested specimens were mostly fully-grouted concrete masonry blocks while several others were partially grouted and fully grouted brick prisms with reinforcement ratios ranging from 0.4 to 2.5 percent. They not only tested reinforced concrete masonry (RCM) specimens but also conducted tests on reinforced brick masonry (RBM) specimens and they tried to contribute to the limit states design of reinforced masonry by suggesting design formulas for ultimate flexural capacity of the section, depth of equivalent stress block, minimum reinforcement and balanced section. The failure of their specimens was generally initiated by crushing or spalling of the shell of concrete masonry unit that was located at the compressive zone. They concluded by saying that the flexural behavior of the beams were very similar to those of reinforced concrete. They found the average ultimate compressive strain of the grouted masonry unit as 0.003.

Voon and Ingham (2005) conducted structural testing of eight single storey concrete masonry walls with various window and door openings in order to address the bracing capacity of the walls containing openings. All of the constructed specimens were partially grout filled as only the cells enclosing reinforcement were grouted. In addition to that, walls had variations in lintel reinforcement detailing. A suitable strut-and-tie model and a plastic hinge model were utilized to evaluate the performance of the reinforced concrete masonry walls under lateral loading. Consequently the authors concluded that the results clearly demonstrate effects of the size of the openings and the detailing of the lintel beam reinforcement on the lateral strength of the walls. Also, extending the lintel reinforcement below the top edge of the window was proved to increase the lateral strength of the wall (Figure 2.1).

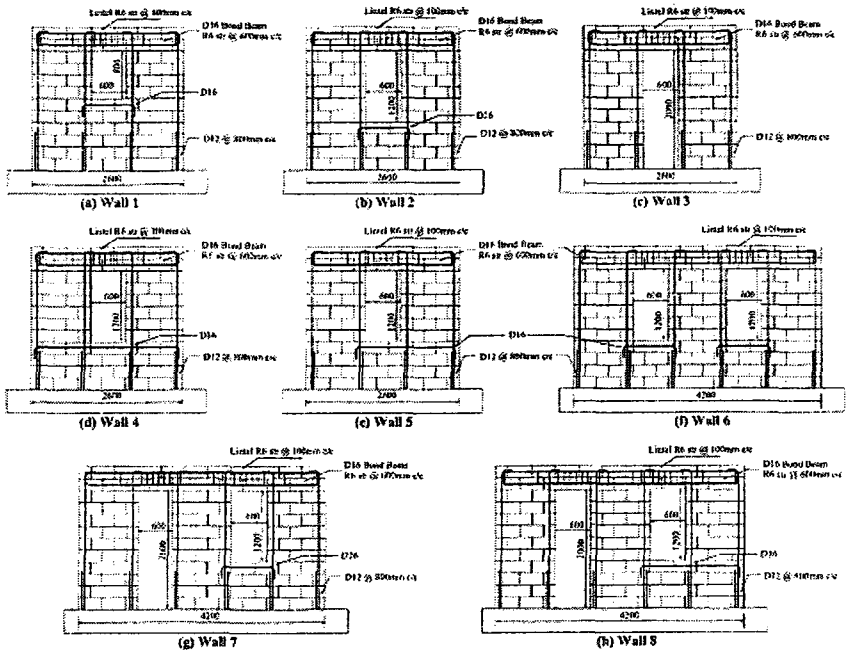

Figure 2.1 Reinforcing details and dimensions of tested walls with reinforced concrete masonry lintels (Voon and Ingham, 2005)

Bennett *et al.* (2007) compared six different methods that are presently being used to predict the deflections of unreinforced and reinforced concrete masonry beams with the deflection data obtained from test conducted on fourteen full-scale specimens. The tested beams had 3.6 meters clear span and were two, three and four courses high. Comparison of the deflections demonstrated the fact that the deflection prediction methods either underestimated or overestimated the actual deflections. Since among all the other methods, ACI 318 method seemed to predict the most accurate effective moment of inertia (I_{eff}) of the beam cross-section and consequently able to predict deflection values close to actual deflections, they also recommended this method for prediction of deflections for unreinforced and reinforced concrete masonry beams. It is also suggested that the beams with span/depth ratio less than or equal to 8 should not be controlled by deflections. Beams exceeding this limit do not have to be increased in size, but rather usage of shores is recommended to provide sufficient stiffness during construction.

2.2 GFRP-Reinforced Concrete

Benmokrane, and Theriault (1998) carried out monotonic and cyclic tests on twelve GFRP reinforced concrete beams having 1800mm clear spans and identical cross-sections of 130 x 180mm. The main parameters investigated in this study were the reinforcement ratio of GFRP and strength of concrete. The researchers tried to find the effects of changed parameters on crack width, deflection, flexural capacity and deformability of the reinforced beams. Although several conclusions were withdrawn using the experimental data, relative outcomes for this experimental program are; the residual crack width decreases as the reinforcement ratio of the beam increases, even

though the ultimate moment capacity of the beams increase as the reinforcement ratio increases, this increase is controlled and limited by the strains in concrete, using the deflection calculations for steel reinforced concrete can be misleading for GFRP reinforced concrete and should be estimated using the proposed model and following the calculation of J-factor recommended by Jaeger, tested beams were considered to be safe in terms of deformability (Figure 2.2).

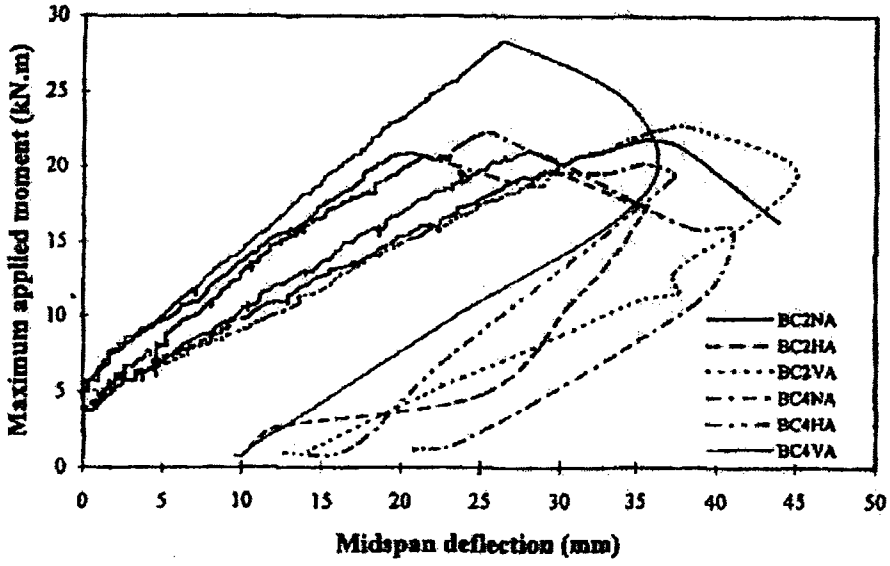

Figure 2.2 Plot demonstrating the effect of GFRP reinforcement ratio on the maximum mid-span deflection of reinforced concrete (RC) beams.
(Theriault and Benmokrane, 1998)

Ombres and Aiello (2000) further investigated the deformability properties of GFRP reinforced concrete beams since their performance is controlled by their serviceability and deformability conditions. Theoretical predictions were compared with an experimental analysis that had been accomplished using nine GFRP reinforced concrete beams spanning 2610mm and they were subjected to four-point bending. Theoretical calculations included estimations of an accurate I_{eff} for deflection calculations, usage of block models and bond-slip law to evaluate the deformability of the

beams. Although the above-mentioned theoretical methods agreed with the results of the experimental tests, block models method appeared to be overwhelming and cumbersome from the computational point of view. On the other hand, they observed that the utilized bond-slip law accurately predicts the interaction of GFRP with the surrounding concrete.

Saikia *et al.* (2007) have examined ten reinforced concrete beams in order to improve the existing crack width and slippage estimation models since the serviceability criteria of the limit states design of GFRP reinforced beams is controlled by the maximum crack width. Seven of the tested beams were GFRP reinforced while the remaining were steel reinforced and used as control specimens. The proposed methods for crack width and slippage showed close agreement with the experimental data. Deflections were predicted using one of the available methods in literature was proved to work well with the actual results.

Ashour (2006) reported the test results of twelve GFRP reinforced concrete beams loaded using four-point bending setup. Ratio of GFRP reinforcement and the beam depth were the two main parameters investigated in this research. He aimed to develop a simplified method to calculate the flexural capacity of the beams and to examine the shear capacity using available methods in the literature for reinforced concrete. During the tests, both shear and flexural failures were observed since over-reinforced beams failed in flexure and under-reinforced ones failed in shear. None of the beams had shear reinforcement. Consequently, although the developed flexural capacity predictions provided good correlation with the experimental data, comparisons of the shear capacity were inconsistent and proved the fact that further research has to be conducted in that area.

Abdalla (2002) conducted tests on concrete beams reinforced with three different types of FRP bars that include GFRP (Isorod) produced by Pultrall, Canada; GFRP (c-bar) produced by Marshall Industries Composites, USA and CFRP (Leadline) produced by Mitsubishi Kasei, Japan. In total, fifteen simply supported slabs and beams were prepared to be tested under four-point loading system. Five specimens out of fifteen were GFRP reinforced concrete beams. Objective of the research was to investigate primarily the deflections, cracking and ultimate capacity properties of the FRP reinforced concrete elements. The researcher observed that the ACI-440 guidelines for FRP reinforced concrete members estimated the deflections to be lower than the test results. On the other hand, deflections predicted by ISIS Canada (2001) were in good agreement with the experimental results (Figure 2.3).

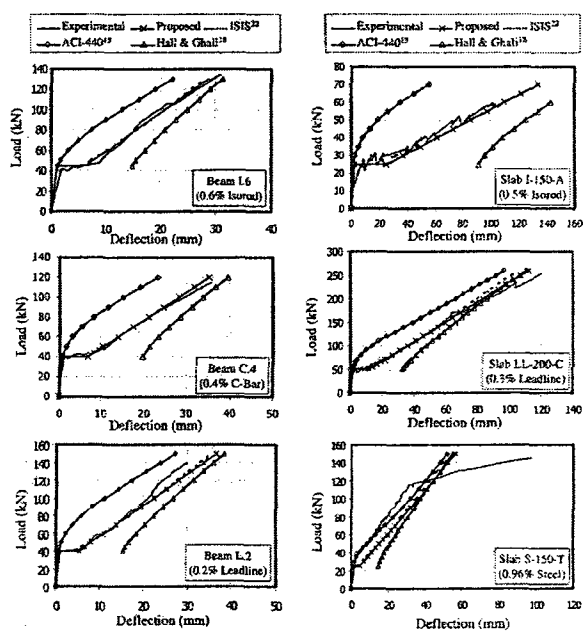

Figure 2.3 Experimental and analytical load-deflection comparisons of GFRP and steel reinforced concrete beams (Abdalla, 2002)

2.3 GFRP-Reinforced Masonry

As mentioned earlier, even though researchers have started conducting tests on conventional steel reinforced masonry assemblages decades ago, to the author's knowledge, literature regarding internally FRP-reinforced masonry assemblages is limited mainly for two reasons. First of all, the use of FRP reinforcement in concrete structures is a relatively new technique and dependability of its applications are still being investigated by researchers. As it satisfies present codes and regulations of reinforced concrete, its usage will be promoted for other types of structural design methods such as reinforced masonry design and steel design. On the other hand, since majority of the masonry structures are relatively old, in order to adapt today's requirements, they have to be repaired, retrofitted and strengthened. Consequently, although literature regarding retrofitting and strengthening masonry assemblages using composite materials can easily be found, research on masonry reinforced with internal FRP reinforcement lately has started attracting the attention of researchers, pointing a field that is in need of investigation.

Recently, Sasanian (2009) investigated the out-of-plane flexural performance of GFRP reinforced concrete masonry walls. Eight full-scale walls were constructed using internally GFRP reinforced, either partially or fully-grouted concrete masonry blocks. Walls were tested using monotonic four-point bending system imitating lateral loads that can arise from wind, soil pressure and earthquake forces. The researcher primarily tried to investigate and evaluate the flexural capacity and lateral deflection of the walls. Based on the comparisons of experimental tests and analytical predictions, it was concluded that; higher flexural capacities compared to steel reinforced masonry walls can be

achieved with acceptable deformability, walls showed sufficient flexural forewarning deformability prior failure and grouting of the cells with no reinforcement found to be ineffective (Figure 2.4).

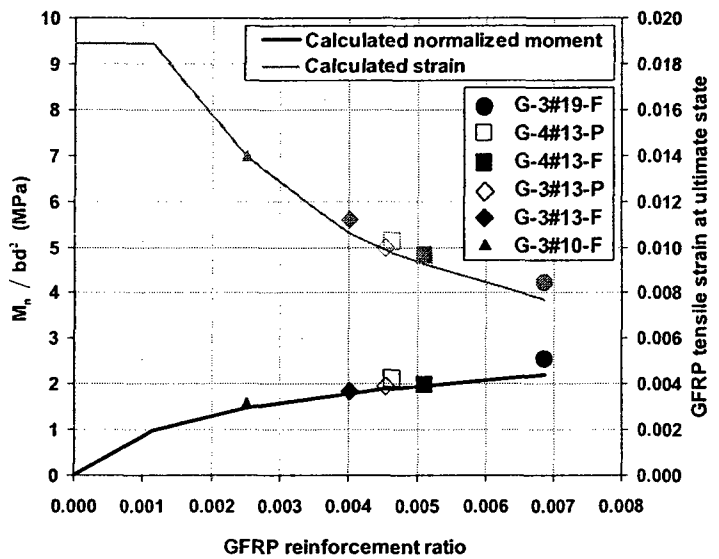

Figure 2.4 Proposed capacity chart for designing masonry walls reinforced with GFRP rods (Sasanian, 2009)

Galati *et al.* (2005) worked on strengthening of unreinforced masonry walls (URM) using near surface mounted (NSM) FRP rods. They constructed and tested fifteen URM walls with different percentages and types of FRP reinforcement. The influence of the dimension of the groove, rod shape and type of bonding material on the flexural capacity was also studied. The specimens exhibited different types of failures such as; debonding of FRP reinforcement, flexural failure either due to crushing of concrete or rupture in FRP and shear failure in case of over-reinforced specimens. Consequently, up to 14 times increase was observed in the flexural capacity of the wall compared to URM control specimen.

2.4 Reinforced Concrete Strengthened Using CFRP

Alagusundaramoorthy *et al.* (2003) studied the contribution and effectiveness of externally bonded CFRP sheets in increasing the flexural performance of reinforced concrete beams. In order to accomplish the objectives, four-point bending tests were conducted on two control beams and twelve other CFRP strengthened reinforced concrete beams with different layouts of strengthening. All the beams were designed to have sufficient shear reinforcement to prevent failure in shear. The conducted analytical and experimental investigation proved that; the flexural strength of the CFRP strengthened beams increased up to 49% while the beams having anchored CFRP sheets had up to 58% increase in their flexural capacities. Consequently, it was reported that the Whitney's stress block approach was suitable to predict the failure load for CFRP strengthened reinforced concrete beams.

Lee and Moy (2007) conducted a research in order to achieve an effective maximum CFRP laminate strain to better estimate the contribution of strengthening to the overall flexural performance of the reinforced concrete beam. Premature failure due to debonding of the CFRP sheets is a common mode of failure in strengthening; not allowing CFRP laminates to reach their ultimate tensile strengths and strains. The experimental program of this research included nine reinforced concrete beams having spans from two meters to seven meters. All the beams were heavily reinforced in shear to ensure flexural failure. Conducted test showed that the proposed method can predict the premature failing load with 6.8% error on average.

Esfahani, M.R. (2006) investigated the effect of steel reinforcement ratio on the flexural strength of reinforced concrete beams. Experimental program comprised twelve specimens having there different reinforcement ratios and clear spans of two meters. Comparisons between the experimental program and analytical calculations yielded that the flexural capacities of the strengthened beams increased compared to the control specimens as explained in previous studies. It was also concluded that the present design guidelines of ACI and ISIS Canada (2001) overestimates the effect of CFRP flexural strengthening of the beams with small reinforcement ratios.

Garcen and Hollaway (1998) studied the influence of the plate end anchorages on the CFRP laminates. Premature failure due to debonding of the CFRP sheets is a common mode of failure in strengthening therefore several researches were conducted on anchoring the laminate to the beam using different anchoring techniques and types in order to delay or in some cases to prevent premature failure. They reported that beams having shear span-to-depth ratio lower than 3, the anchorage improved the composite action between the laminate and the concrete thus increasing the flexural capacity and stiffness of the beam.

Bahn, B.Y., and Harichandran, R.S., (2008) aimed at improving the bonding behavior of CFRP laminates that are being used to strengthen and retrofit reinforced concrete beams using an effective epoxy mortar since it was observed that 60% of the anchor stiffened CFRP laminates on strengthened beams debonded prematurely prior to failure. In this study, various configurations of epoxy mortar applied at the both ends of the beams and compared with beams having anchor bolts and beams without any anchors. In total, 11 specimens were designed, built and tested. In conclusion, epoxy mortar

performed well in delaying and preventing premature failure of CFRP laminates. It was observed that the mortar patch length has noticeable influence on the bond strength of the epoxy mortar. In addition to that, a wavy surface between the epoxy mortar and CFRP laminate improves the bond in between.

2.5 Reinforced Concrete Masonry Strengthened with CFRP

Hao, Z., (2007) examined the applications of CFRP laminates in strengthening reinforced masonry deep beams. For this purpose, CFRP plates were bonded to the surface of the beams on both sides. The flexural response of the beams was investigated having the percentage of steel reinforcement and percentage of CFRP reinforcement as variables. In total, eight full-scale fully grouted masonry deep beams were constructed and tested. Authors observed that; the flexural capacities and the ductility of specimens increased noticeably after strengthening; use of CFRP plates delayed the emergence of the first visible cracks and delamination of the CFRP laminates dominated the failure modes of the beams that are strengthened from the soffit (Figure 2.5).

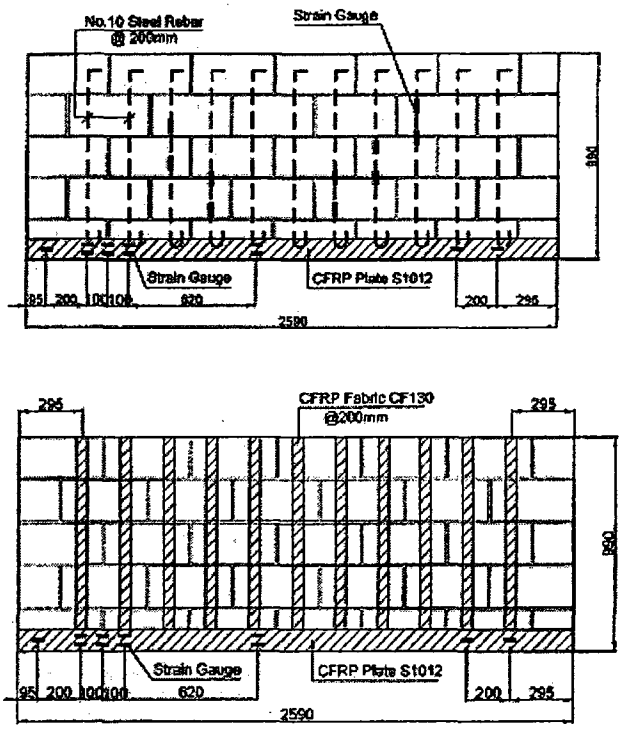

Figure 2.5 Layout of longitudinal and transverse CFRP strengthening applied on reinforced concrete masonry deep beams (Hao, Z., 2007)

Ghobarah and Galal (2004) investigated out-of-plane resistance of CFRP laminate strip strengthened URM walls under extreme lateral loads. For that purpose, five full-scale unreinforced concrete masonry walls were constructed. Walls had various openings such as; single window, double window, single wide window and a single door. Based on the results of the experimental program, researchers withdrew the following conclusions; the strengthened walls out-of-plane resistances increased up to five times compared to the control specimen, walls behaved in a ductile manner dissipating considerable amount of energy and proper anchoring at the end locations of the CFRP laminates improved bonding between the CFRP strips and masonry blocks (Figure 2.6).

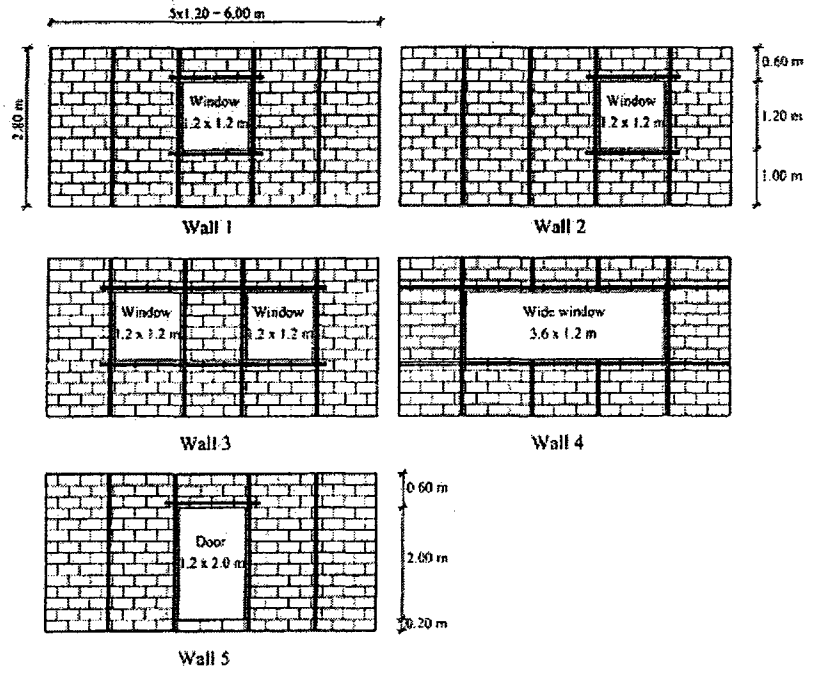

Figure 2.6 Elevation of strengthened unreinforced masonry walls with openings (Ghobarah and Galal, 2004)

Moon *et al.* (2007) conducted tests on a full-scale unreinforced masonry structure to investigate the effectiveness of several strengthening techniques since URM is highly vulnerable against extreme lateral loads. FRP sheets, near surface mounted rods and vertical post-tensioning were the techniques used for strengthening. Structure was subjected to slowly apply lateral load cycles. They reported that all of the strengthening techniques proved to be effective in improving the seismic resistance of the tested specimen. For the case of FRP, progressive debonding of the sheets acted as a warning sign for brittle failure of the URM and contributed to highly nonlinear and ductile system response.

Kiss *et al.* (2002) studied the effect of strengthening of FRP on the flexural performance of URM beams. Two types of FRP were used with two different types of resins as strengthening material; chopped glass fibre with epoxy resin, chopped glass

fibre with polyester resin, glass fabric cloth with epoxy resin and glass fabric cloth with polyester resin. FRP sheets were applied to completely cover both sides of the beams. The influence of type of FRP, thickness of FRP, and type of resin on the flexural performance of the strengthened beam was the points of interest of this project. Consequently, the following observations were made during the tests; the FRP strengthening increased both the cracking moment and the ultimate moment capacity of the sections and the strengthened beams had higher ductility values compared to the control beam.

2.6 Discussions

An extensive literature review has been conducted, analyzing the previously completed researches that were investigating; conventional steel-reinforced masonry, FRP-reinforced concrete, FRP-reinforced masonry, CFRP-strengthened concrete and CFRP-strengthened masonry. This literature survey was concluded by pointing out the fact that, there is plenty of literature available related to the use of FRP as an internal reinforcement method and external strengthening method for reinforced concrete structural members and both methods were found to be effective and practical. In addition to that, these previous researches had significant contributions to the development of design guidelines for FRP-reinforced concrete, such as ISIS Canada (2001).

On the other hand, previous researches conducted on applications of FRP in reinforced concrete masonry have been focused on developing CFRP-strengthening techniques for conventional steel-reinforced structural masonry members. However, to the author's knowledge, research related to the applications of FRP as an internal reinforcing material for structural masonry elements scarcely exists. In particular, research regarding internally GFRP-reinforced masonry beams has never been presented.

Hence, this research program is targeting to assess the reliability and effectiveness of GFRP rods as internal reinforcement for concrete masonry beams as well as the effectiveness of CFRP sheets for strengthening steel-reinforced concrete masonry beams. The proposed design diagram based on the performance of the tested GFRP-reinforced masonry beams will contribute to develop design guidelines for FRP reinforced masonry.

CHAPTER 3

EXPERIMENTAL PROGRAM

3.1 Materials' Characteristics

Masonry specimens tested in this project were constructed using locally available structural materials such as concrete masonry blocks, dry sand, Portland cement, masonry cement, coarse aggregate, self-leveling mortar, steel reinforcement GFRP rods and CFRP sheets. All the beams and auxiliary specimens were constructed by experienced masons certified in province of Québec, under the surveillance of the author and their quality of workmanship was judged to be above average. Below listed are the detailed specifications of constituent materials that were used in the construction the specimens for this project.

3.1.1 Concrete Masonry Units

Hollow rectangular masonry blocks with dimensions 190x190x390mm, square blocks with dimensions 190x190x190mm and lintel blocks with dimensions 190x190x390mm were utilized for the construction of the specimens. Lintel blocks were used as the bottom course in order to be able to position the internal reinforcement easily into the masonry beams. Compressive resistance of concrete masonry blocks were reported as 15MPa by the manufacturer's technical datasheet. All the concrete masonry units were provided by a local supplier Simard-Beaudry (2001). Figure 3.1 shows the concrete masonry units used for the construction of the test specimens.

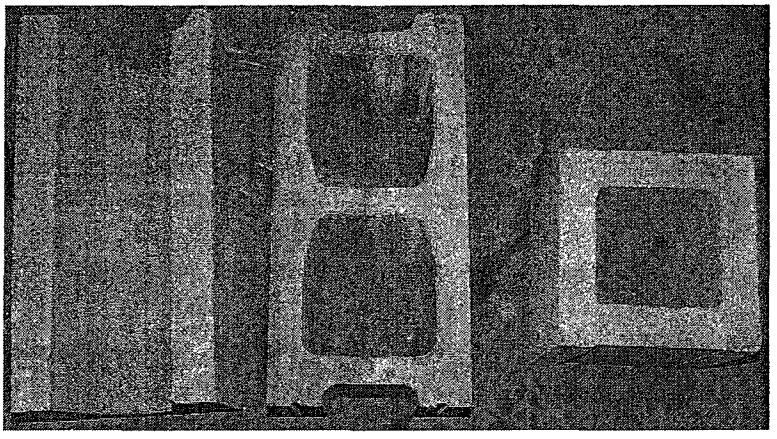

Figure 3.1 Hollow concrete masonry units used for experimental work

3.1.2 Mortar

During the construction, Type "S" mortar was used in accordance with the masonry standards ASTM C270 (2002) and CSA A179 (2002). The volumetric proportions of the mix were as follows; 0.7 unit of water, 0.5 unit of Portland cement, 1.0 unit of masonry cement and 2.9 units of dry sand. Ten mortar cubes with dimensions 50 x 50mm were prepared in order to be tested 7 days and 28 days after construction. Following average compressive resistances of the mortar cubes were found to be 7.9 MPa and 14.5 MPa. Detailed results of the mortar cube tests are shown in Table 3.1. Average compressive strength of the tested mortar cubes was within the allowable limits set by the above mentioned masonry standards.

Table 3.1 Compressive strength test data of the mortar cubes

Cube Number	Age (days)	Failure Load(kN)	Compressive Strength(MPa)
1	7	19.6	7.82
2	7	19.6	7.83
3	7	19.7	7.89
4	28	35.4	14.18
5	28	36.9	14.78
6	28	35.8	14.31
7	28	37.1	14.83
8	28	35.9	14.40

3.1.3 Grout

The concrete grout used to fill the tested specimens was "coarse" grout, prepared in accordance with the masonry standards ASTM C476 (2002) and CSA A179 (2002). The volumetric proportions of the mix was as follows; one unit of Portland cement, two units of ¼ inch aggregate, 2.8 units of dry sand and 0.9 units of water. Five cylinders filled with the grout mix were prepared in order to be tested 28 days after construction. Following average compressive resistances of the grout cylinders were found to be 14.2 MPa. Detailed results of the cylinder tests are shown in Table 3.2. Average compressive strength of the tested cylinders was within the allowable limits set by the above mentioned masonry standards.

Table 3.2 Compressive strength test data of the grout cylinders

Cylinder Number	Age (days)	Failure Load(kN)	Compressive Strength(MPa)
1		115.6	14.72
2		108.9	13.87
3	28	112.5	14.33
4		109.4	13.93
5		110.5	14.07

3.1.4 Longitudinal Steel Reinforcement

Steel reinforcement used for the tested control beams and the CFRP-strengthened beam was conventional M15 rebar with 492MPa yield strength and 698MPa ultimate strength. Both ends of the steel rebars were bended 90 degrees in the factory in order to increase its anchoring capacity. Steel reinforcement for this project was provided by a local structural steel supplier Metal M-Pact Inc of Montréal.

3.1.5 GFRP Rods

GFRP rods, also known as "V-ROD^{TM}", that were utilized in this project were provided by Pultrall Inc. of Québec. They are manufactured by pultrusion procedure of continuous glass fibers and thermosetting polyester resin. Surface of the rod is wrapped by glass fiber strings and sand coated in order to improve its bond characteristics. In order to have a variety of GFRP reinforcement percentages, different diameters and

numbers of rods were utilized as an internal reinforcement for the specimens. Table 3.3 provides detailed information on the strength characteristics of the rods.

Table 3.3 Properties of the GFRP rods used in the experimental program (V-ROD^{TM}) (Pultrall, 2007)

Metric Size	Nominal Diameter	Area (mm^2)	Modulus of Elasticity(GPa)	Ultimate Tensile Strength(MPa)	Ultimate Tension Strain ($x10^{-6}$)
13	12.7	126.7	46.3	786	17000
16	15.875	197.9	48.2	751	15600
19	19.050	285	47.6	728	15300

3.1.6 CFRP Sheets

The CFRP sheets and the corresponding epoxy resin used in this research were provided by FYFE Co. and were Tyfo SCH-11UP Composite and Tyfo S Epoxy by the manufacturer. Epoxy mix consists of Component A and Component B that were mixed in laboratory conditions by the author with the help of laboratory technicians prior to application, following the producers mix ratios. Typical dry fiber properties, epoxy material properties and the composite laminate properties are tabulated on Table 3.4.

Table 3.4 Properties of the CFRP sheets used in the experiments (Tyfo® SCH-11UP using Tyfo® S Epoxy) (Fyfe Co., 2008)

Dry Fiber Properties				Composite Gross Laminate Properties			
Tensile Strength (MPa)	Tensile Modulus (GPa)	Ultimate Strain ($x10^{-6}$)	Thickness (mm)	Tensile Strength (MPa)	Tensile Modulus (GPa)	Ultimate Strain ($x10^{-6}$)	Thickness (mm)
3790	230	17000	0.127	903	86.9	10500	0.25

3.1.7 Wooden Platforms

Platforms were constructed in order to avoid mobility problems while transferring the reinforced masonry beams to the test setup. On the other hand, beams had the risk of achieving their cracking moments (M_{cr}) due to their own weight as they were being transferred to the test setup. For that reason, they were supposed to be braced and carried from underneath to the test area with the help of a crane.

Surface of the platforms were prepared using 2"x10" timbers and two other 2"x4" pieces were screwed on the sides in order to increase their stiffness. Self-leveling mortar was poured on the surface in order to cover any imperfections and to achieve a leveled surface for construction. They were anchored to the strong floor beneath to prevent cracking of self-leveling due to torsion and shrinkage of the timber. Figure 3.2 shows the details of the platforms constructed.

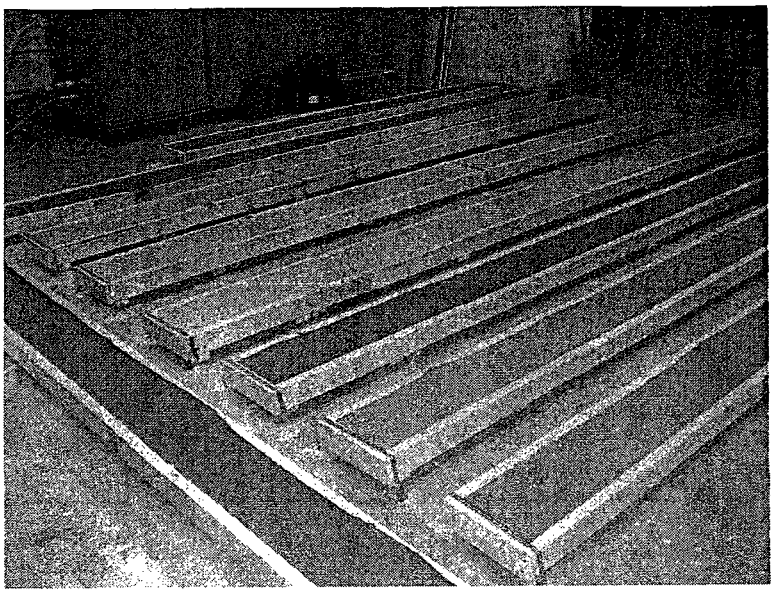

Figure 3.2 Wooden platforms that were prepared prior to construction of the specimens

3.1.8 External Shear Reinforcement (Clamps)

Application of exterior shear clamps is a common technique that is being used to strengthen beams thus it can be also used to ensure sufficient shear capacity in shear zone in order to obtain flexural failure. Previous researches conducted on shear clamps (shown in Figure 3.3) by Kim and White (1999), Altin *et al.* (2003) and Anil (2007), showed great similarity between the strengthened beams and the control specimens in terms of rigidity and crack patterns. The steel clamps used for this experiment were prepared under laboratory controlled conditions and were made of two square hollow steel sections, two 10 mm diameter threaded bars, eight high strength nuts and four washers. While three clamps were used for each shear span of the short-spanned beams, four clamps were used for each shear span of large-spanned beams. Figure 3.3 shows a sample clamp while Figure 3.4 crack pattern and load deflection relationship of reinforced concrete beams utilizing shear clamps as tested and reported by Kim and White (1999).

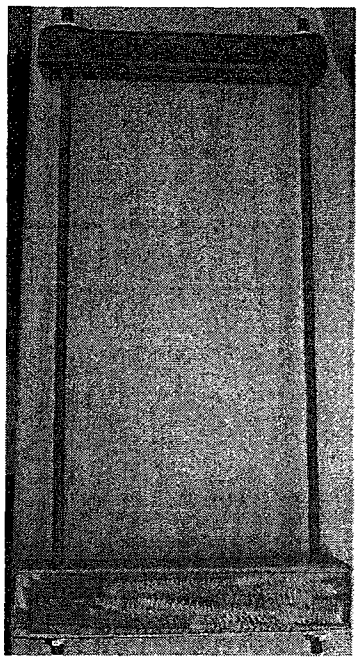

Figure 3.3 Sample external shear reinforcement

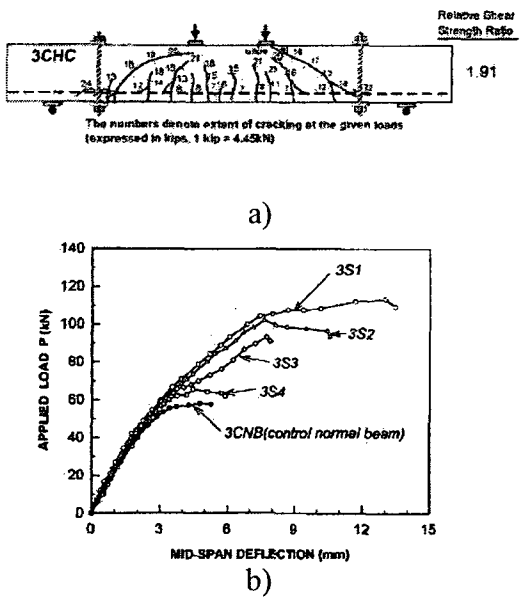

Figure 3.4 a) Reinforced concrete beam reinforced using shear clamps, b) Load-deflection comparison of clamped and unclamped beams (Kim and White, 1999)

3.2 Auxiliary Laboratory Tests

3.2.1 Compressive Strength Normal to the Bed Joint

It is impossible to determine the compressive strength of the masonry assemblages by looking at individual compressive strengths of its constituents, i.e. grout cylinders, mortar cubes and hollow concrete masonry units. In order to determine the compressive strength (f'_m) of grouted masonry assemblages normal to the bed joint, five one-block wide and five-block high unreinforced grouted masonry prisms were constructed following the guidelines of ASTM C1314 (2002). Two high precision potentiometers were placed on both faces of the prisms to measure the axial deformations which later on were used to plot axial stress-strain relationships of the prisms. The mean value of the compressive strength of the masonry prisms was found to be 13.66 MPa and the Young's modulus (E_m) was obtained from the slope of the stress-strain curves, using the section between 5% and 33% of the ultimate loads. The average E_m of the prisms was determined to be 7.5 GPa. Conical breaks and face shell splitting were among the fracture types experienced before failure. Comprehensive strengths of the prisms did not demonstrate much variation proving that the quality of the workmanship was reasonable since imperfections can severely affect the results of the compressive tests. Detailed results and stress-strain diagrams of the prism tests are shown in Table 3.5 and Figure 3.7. Test setup and failed prisms can be viewed at Figure 3.6.

Figure 3.5 Constructed five-block high and seven-block high masonry prisms

Table 3.5 Test results of the compressive prisms loaded normal to the bed joint

Specimen	Failure Load(kN)	Compressive Strength(MPa)
1	824.9	13.4
2	822.2	13.3
3	901.9	14.6
4	817.4	13.2
5	854.7	13.8

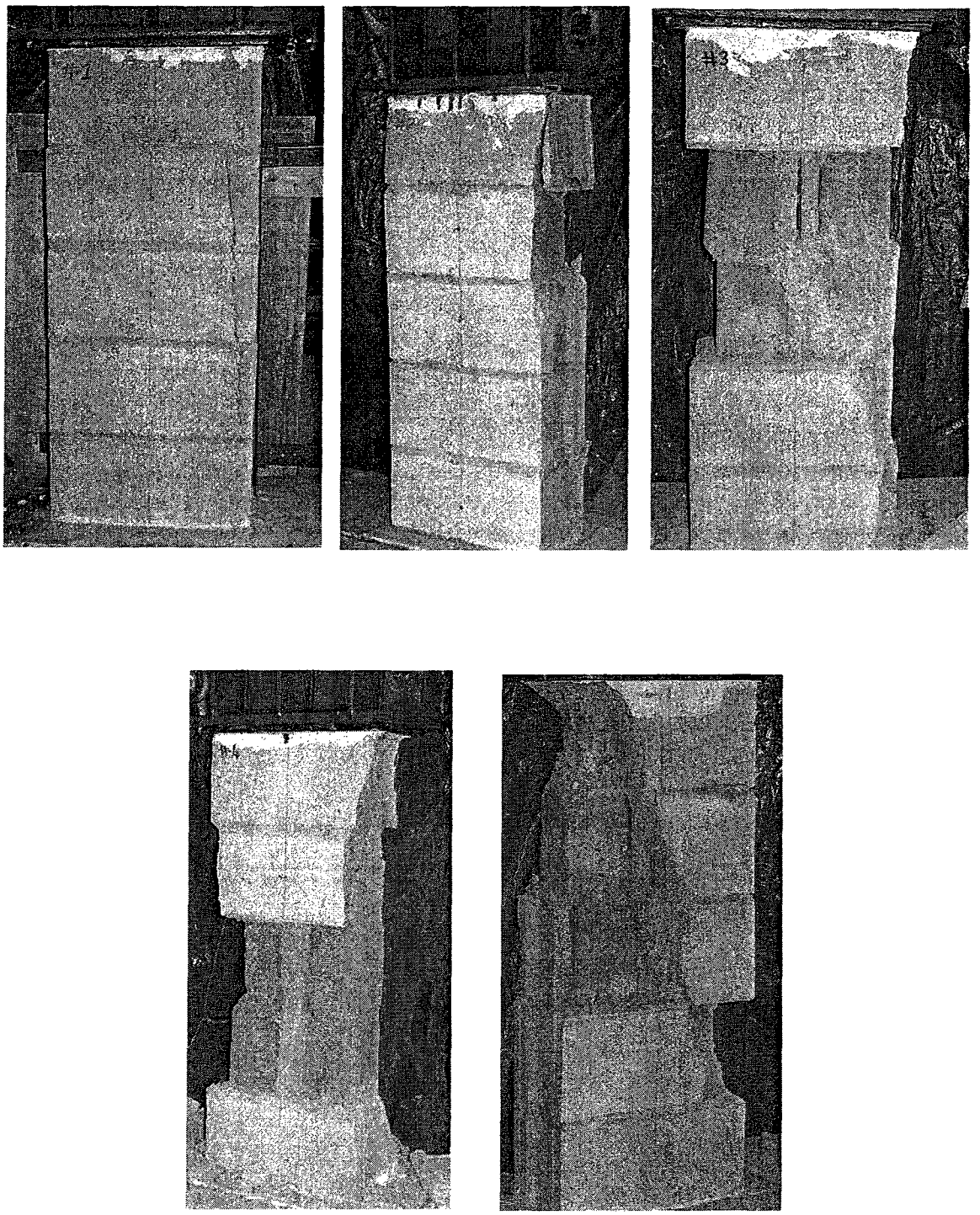

Figure 3.6 Compressive masonry prisms loaded normal to their bed joints after failure

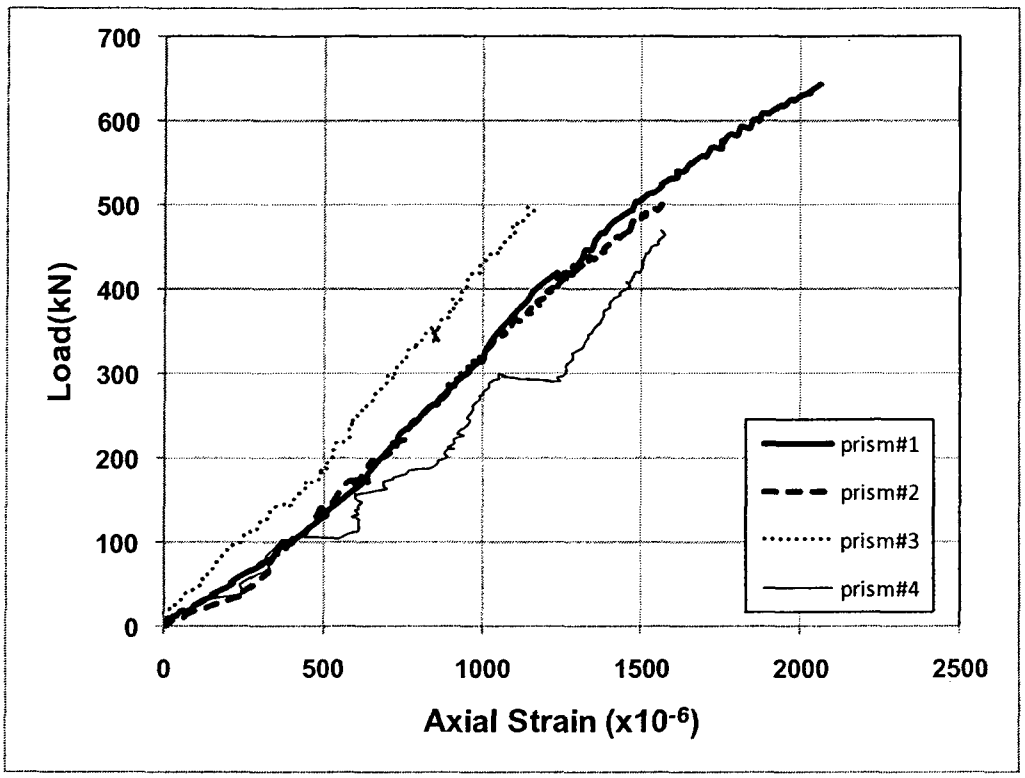

Figure 3.7 Load-strain relationship of the prisms loaded normal to the bed joint

3.2.2 Compressive Strength Parallel to the Bed Joint

While reinforced masonry members such as walls and columns, rely on the block's compressive strength normal to the bed joint, beams, on the contrary, are influenced by the block's compressive strength parallel to the bed joint due to the compression zone located at the top course of the beam. Researchers such as Khalaf (1981) previously conducted tests on prisms axially loaded parallel to the bed joints and proved that grout filled hollow concrete units fail at lower stresses exhibiting different failure modes compared to those loaded normal to the bed joint. For that purpose, CSA 304.1 (2004) provides correction factor χ for f'_m to be used for reinforced masonry beam design. The correction factor χ can range from 0.5 to 0.7 depending on the conditions as stated by CSA 304.1 (2004) Clause 10.2.6

Consequently, five one block wide and five blocks high unreinforced grouted masonry prisms were constructed (Figure 3.7). Dimensions of the prisms and test setup were determined to be identical to the preciously tested compressive prisms to enhance the comparison conditions between prisms. The mean value of the compressive strength of the masonry prisms was found to be 6.0 MPa. Detailed results of the prism tests are shown in Table 3.6. Test setup and failed prisms can be viewed at Figure 3.8

Table 3.6 Test results of the compressive prisms loaded parallel to their bed joints

Specimen	Failure Load(kN)	Compressive Strength(MPa)
1	401.5	6.5
2	358.9	5.8
3	373.8	6.1
4	349.5	5.7
Average	369.9	6.0

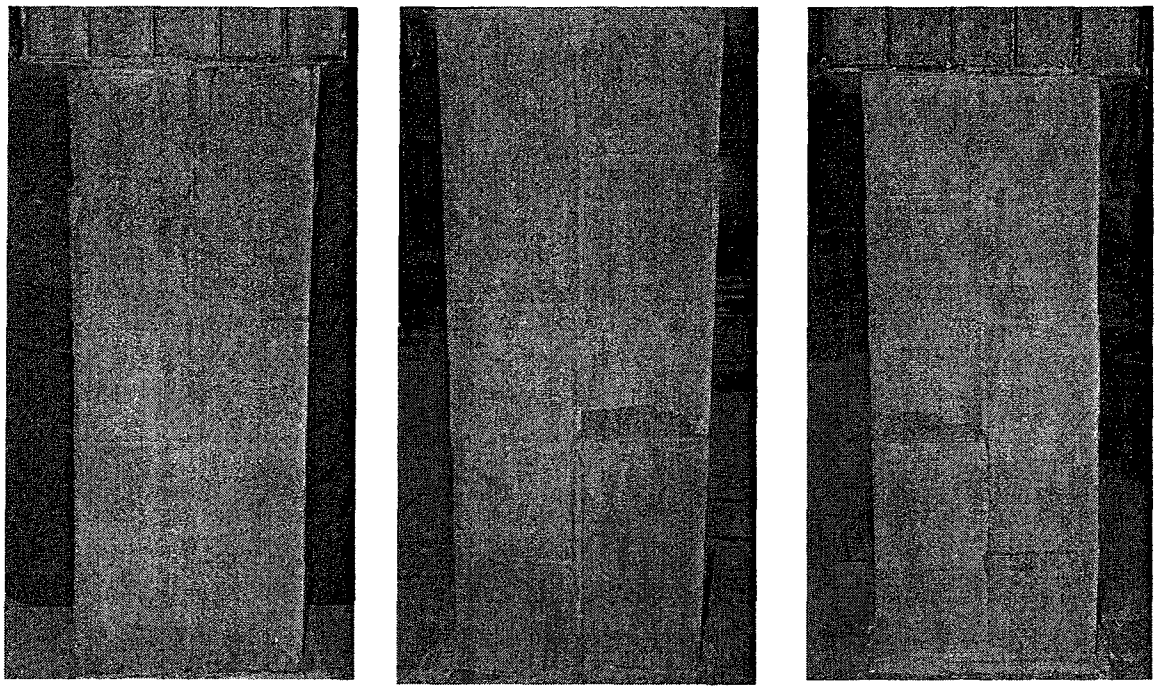

Figure 3.8 Compressive masonry prisms loaded parallel to their bed joints after failure.

3.2.3 Flexural Bond Strength

In order to determine the cracking moment (M_{cr}) of the reinforced masonry assemblages, flexural tensile strength normal to the bed joints of the grouted hollow concrete masonry blocks has to be determined. For this purpose, following the guidelines of ASTM E518 (2002), seven five-blocks high and one block wide unreinforced grouted masonry prisms were constructed and tested under four point bending test setup (Figure 3.8). Using a single potentiometer and a dial gauge, mid-span deflection of the prisms were recorded during loading. One of the specimens showing signs of poor workmanship had visible joint imperfections and failed prematurely during transportation. The average flexural bond strength, also known as modulus of rupture (R) of the remaining prisms was 0.72 MPa. Detailed results of the prism tests are shown in Table 3.7. Test setup and

failed prisms can be viewed at Figure 3.9. ASTM E518 (2002) calculates the modulus of rupture of specimens prepared using hollow masonry units as follows:

$$R = \frac{(0.167P + 0.125P_s)l}{S} \qquad 3.1$$

where:

P = maximum load applied, N

P_s = weight of specimen, N

l = span, mm

S = section modulus of actual net area, mm^3

Table 3.7 Test results of the flexural bond strength prisms

Specimen	Failure Load(kN)	Modulus of Rupture(MPa)
1	6.7	0.63
2	6.2	0.60
3	10.1	0.91
4	7.8	0.73
5	-	-

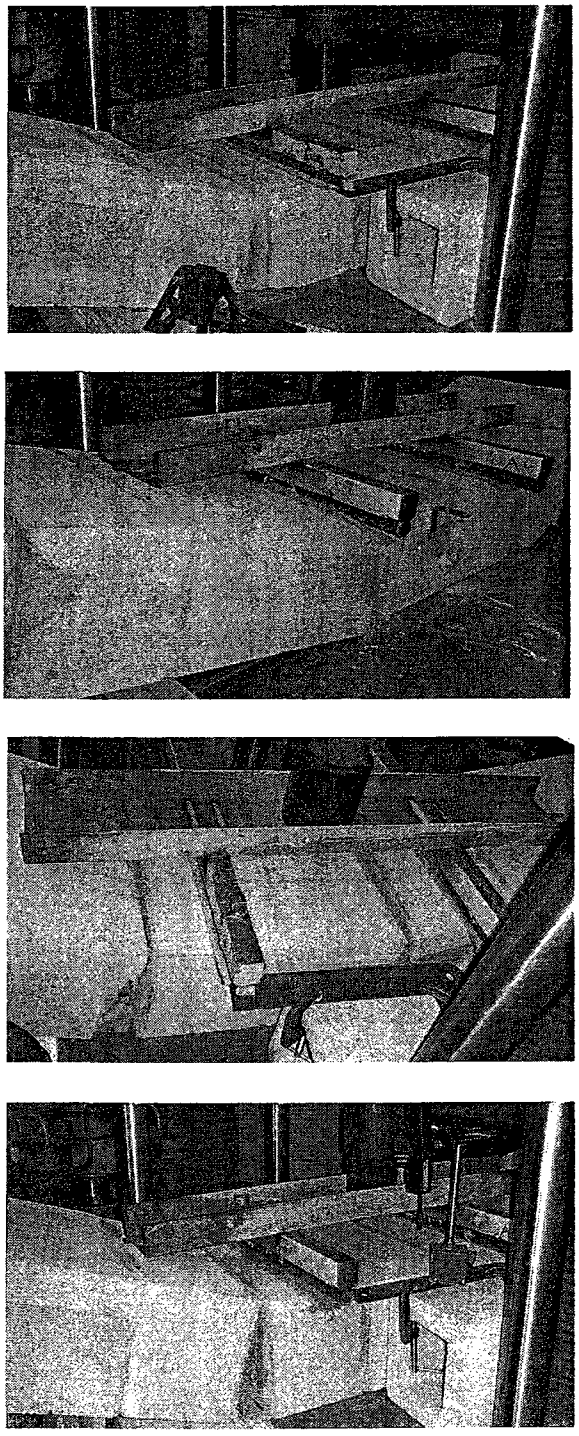

Figure 3.9 Flexural masonry prisms after failure

3.3 Discussion

Grout filled hollow concrete units are stronger when axially loaded normal to the bed joints and tend to fail at lower stresses if the axial load is parallel to the bed joints. Keeping this characteristic of the hollow masonry units in mind, grout filled masonry units with holes going through their webs are expected to be stronger compared to regular hollow units when axially loaded parallel to the bed joints due to their continuous cylindrical grout cores acting against compression. In addition to this advantage, they are going to be lighter than regular hollow concrete units making them a lot easier to handle compared to their predecessors.

In order to improve the concrete masonry blocks performance, an innovative block design is experimentally evaluated and further discussed in chapter 6 of this thesis.

3.4 Full Scale Reinforced Concrete Masonry Beams

3.4.1 Construction of the Test Specimens

Nine reinforced fully grouted concrete masonry beams with 4.0 m and 2.4 m clear spans were constructed by three experienced masons on the previously prepared wooden frames. Two beams had two courses of hollow concrete masonry units, and the remaining seven beams had three courses. Three masonry beams were reinforced using conventional steel rebars two of which were considered as the control specimens, while the remaining beam was later on strengthened using two layers of CFRP sheets that were externally bonded to both sides of the beam. The other six beams were internally reinforced using GFRP rods with different reinforcement ratios. Beams were detailed to have sufficient

shear reinforcement such that they do not fail in shear. Figure 3.10 exhibits photos that were taken during construction of the beams.

Beams were designated with letters and numbers to indicate its internal reinforcement type (FRP or Steel), height in terms of courses of units (2 or 3), type and amount of internal reinforcement(1#13, 1M15) and existence of clamps (Clamped). Thus F-3-1#13C indicates internally single #13 GFRP rod reinforced three course clamped beam. Following Table 3.7 lists all the tested full-scale beams in detail with corresponding designations. Figure 3.11 demonstrates the schematics of cross-sections.

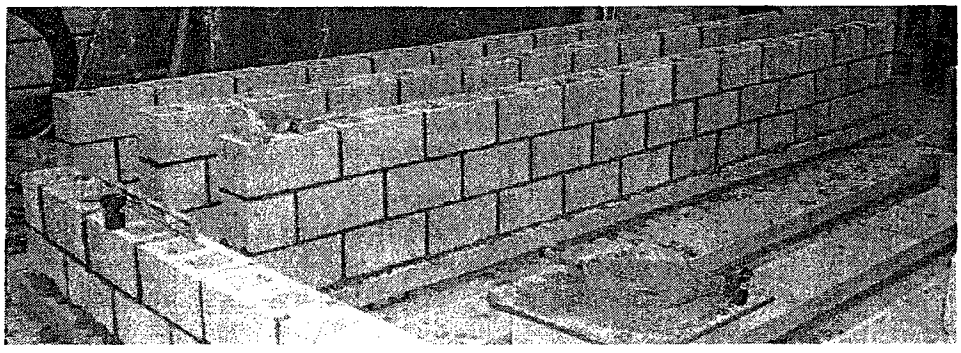

a)

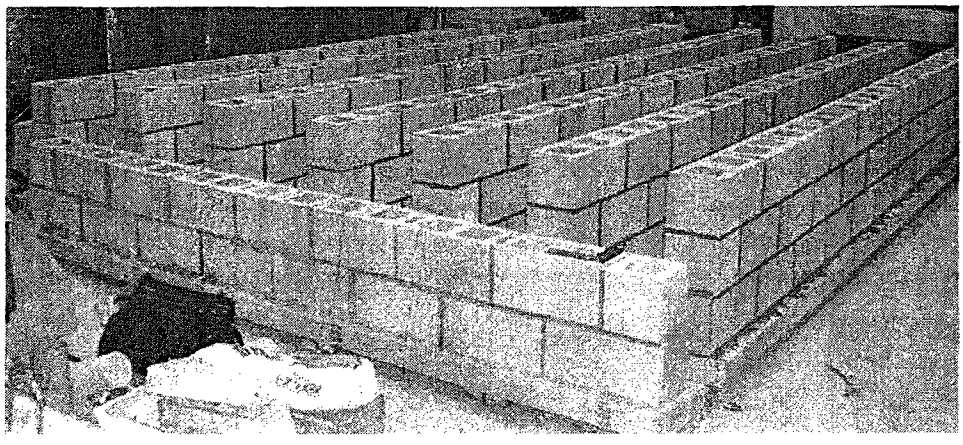

b)

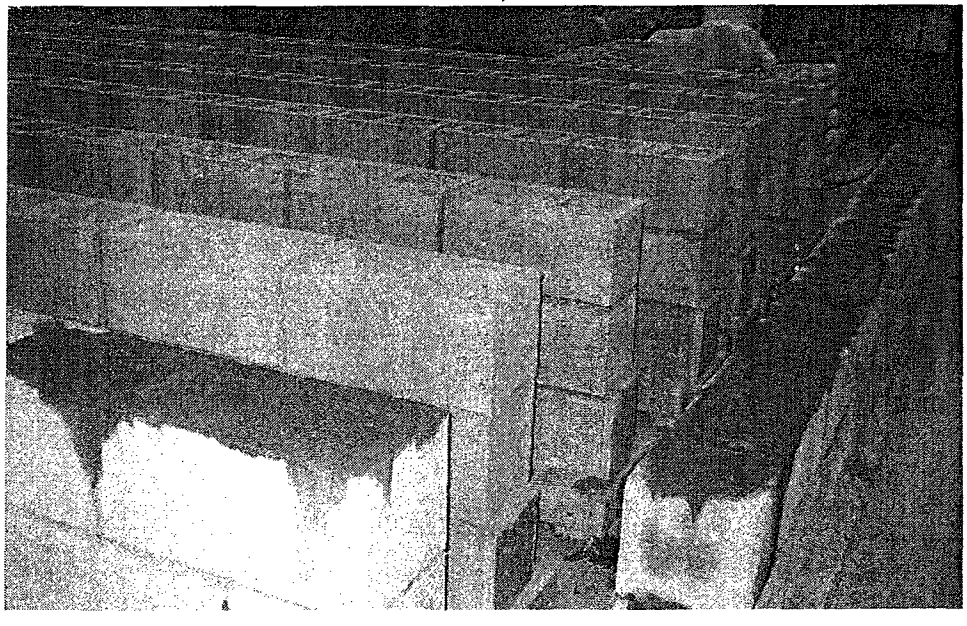

c)

Figure 3.10 a) Construction of full-scale reinforced masonry beams b) Beams after construction c) Grouting of the beams

Table 3.8 Tested full-scale reinforced concrete masonry beams

Beam	Reinforcing Material	Courses	Exterior Shear Reinf.	Span (mm)	ρ (%)	Effect Of	
						GFRP reinforcement ratio	CFRP strengthening
S-3-1-15M	Steel	3	No	4000	0.2	■	■
S-3-1-15M-C	Steel	3	Yes	4000	0.2	■	■
F-2-2#19	GFRP	2	No	2400	0.93	■	
F-2-2#16-C	GFRP	2	Yes	2400	0.65	■	
F-3-1#13-C	GFRP	3	Yes	4000	0.13	■	
F-3-1#19-C	GFRP	3	Yes	4000	0.29	■	
F-3-2#16-C	GFRP	3	Yes	4000	0.4	■	
F-3-2#19&1#16-C	GFRP	3	Yes	4000	0.78	■	
S-3-1-15M-C-CFRP	Steel+CFRP	3	Yes	4000	0.2		■

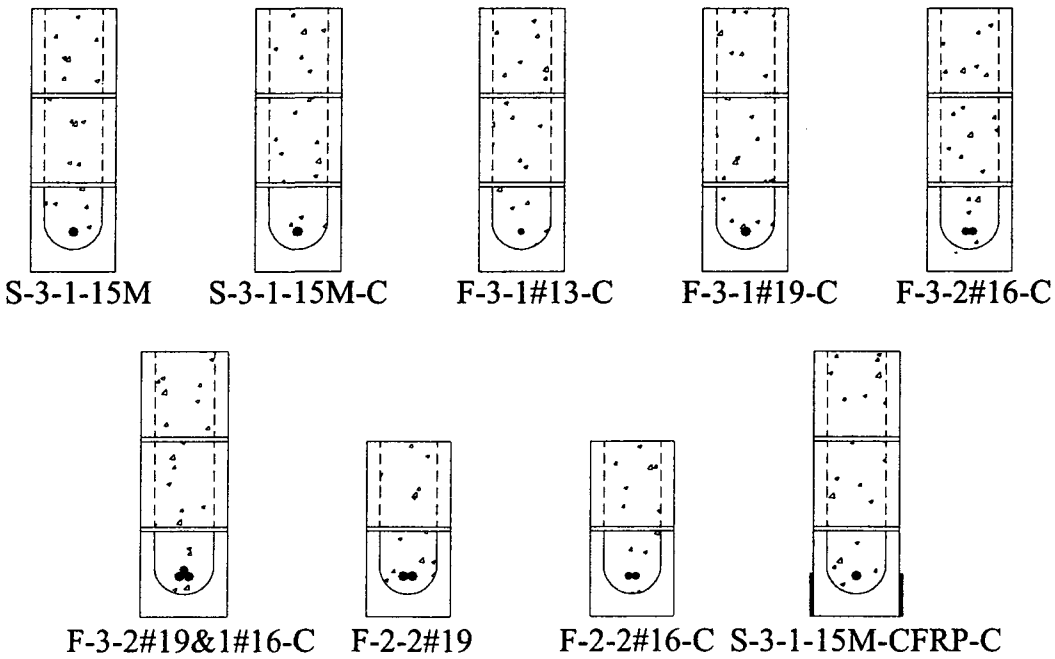

Figure 3.11 Cross-sections of the full-scale reinforced concrete masonry beams

3.4.2 Test Setup and Testing Procedure

Each and every beam was picked up from underneath via a 5 ton capacity crane to prevent any cracking and was transferred to the test frame on the previously prepared wooden frames. Prior to loading, beams were supported by two permanent supports (hinged and roller) located at the last vertical joint at both ends and one temporary support located at the mid-point. Temporary support was removed before each test as soon as the data acquisition system was turned on to monitor and record the initial strains and deflections due to self-weight before applying any load. All the beams were tested under four point bending setup. The beams were subjected to an increasing monotonic load up to failure, and then unloaded when possible to determine the permanent deflection and energy dissipation characteristics of the beams. Monotonic load was applied by a 15-ton hydraulic actuator and transferred to the beam through a stiffened steel I-beam. In order to prevent stress concentrations at the two loading points, the loading apparatus was placed on two wide steel channels.

Strain gauges were installed on the steel reinforcement, GFRP rods and CFRP sheets in order to record the strain response of the reinforcement at different load levels. Each and every interior reinforcing bar had five gauges installed prior to construction; two at the mid-points of the shear spans, two under loading points and another one at the mid-span. Surface mounted CFRP sheets had two other additional strain gauges at the mid-span in order to be able to record the distribution of the strains along their widths. Figure 3.12 showing a strain gauge as it is being installed in a GFRP rod is provided below. Figure 3.12, Figure 3.13

In total, five cable-operated potentiometers were used during the tests in order to be able to monitor the load-deflection relationship of each specimen. Potentiometers were positioned at the same location as the strain gauges; two at the mid-points of the shear spans, two under loading points and another one at the mid-span. Mid-span deflection was controlled using an additional measurement tool named dial-gauge in order to make sure that the deflections recorded by the potentiometers were the actual deflections. Figure 3.13, Figure 3.14

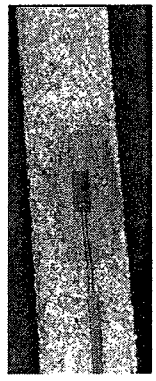

Figure 3.12 Sample installed strain gauge on one of the GFRP rods.

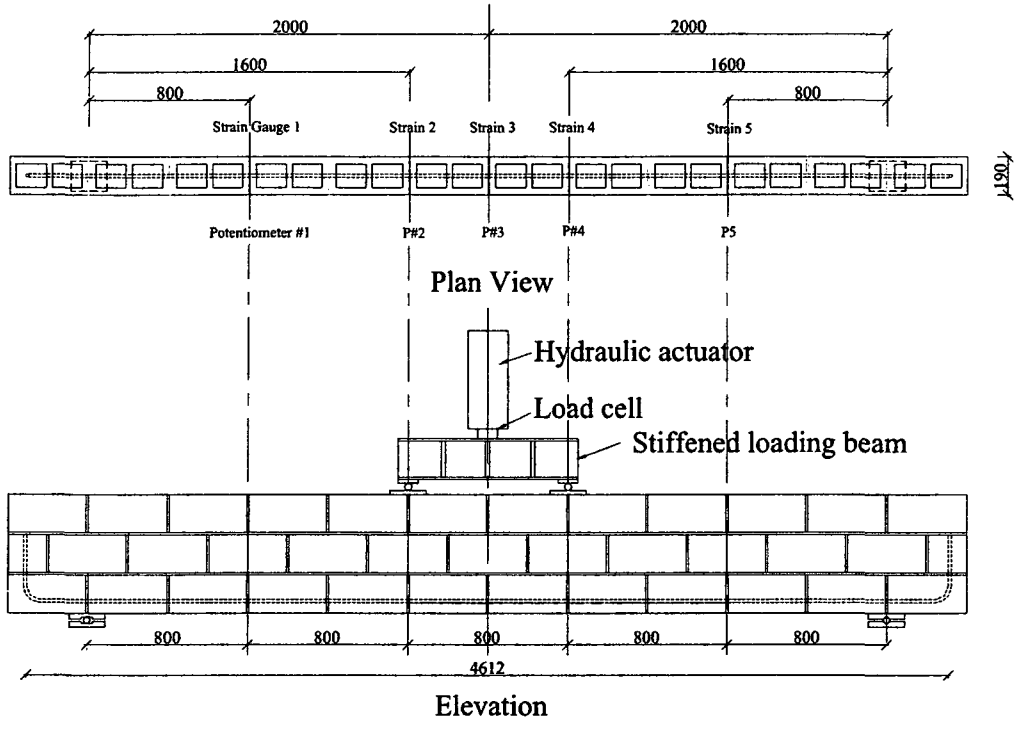

Figure 3.13 Elevation and plan view of three-course reinforced masonry specimens showing locations of strain gauges and potentiometers.

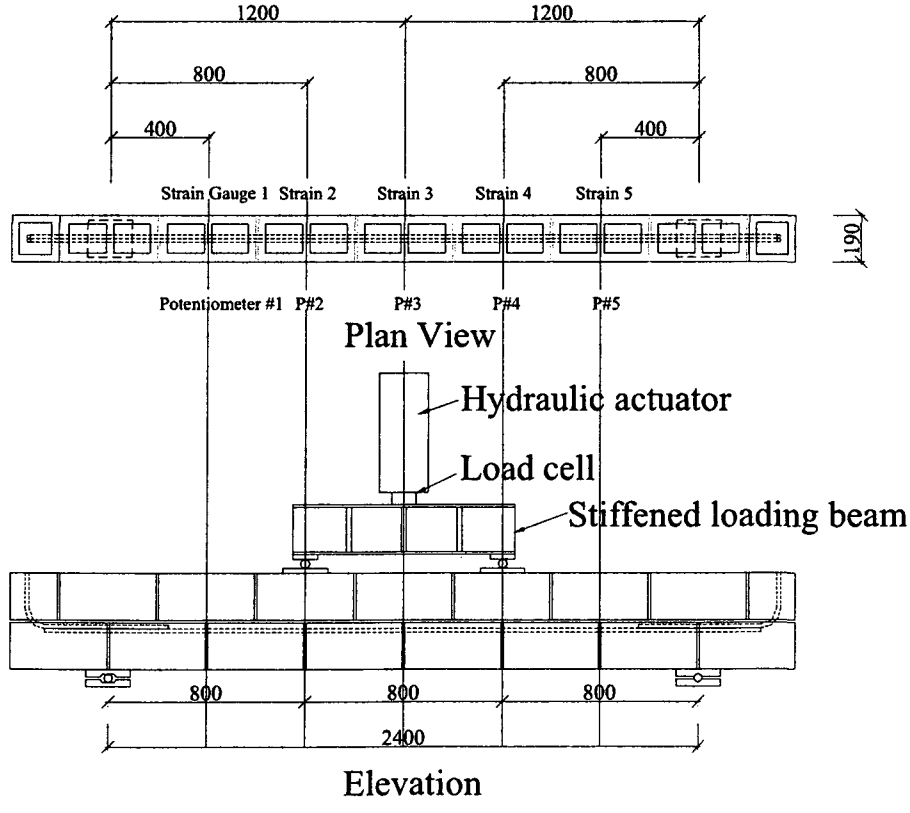

Figure 3.14 Elevation and plan view of two-course reinforced masonry specimens showing locations of strain gauges and potentiometers

CHAPTER 4

TEST RESULTS OF THE REINFORCED MASONRY BEAMS

4.1 Introduction

This chapter explains in detail the observations that were made during each and every conducted test. Main points of interests that were explained and interpreted in this section are the flexural strengths of the beam sections, tensile strains of reinforcing and strengthening materials, deflections and ductility characteristics of the beams and their modes of failure.

Self-weight of the fully-grouted reinforced masonry beam was calculated and was corresponding to a distributed load of 2.6 kN/m in case of a 3 course beam and 1.6 kN/m for a 2 course beam. These distributed loads are equivalent to 6.5 kN and 3 kN point loads respectively and they were added to the loading data of the corresponding beams. Table 4.1 shows a summary of test results of the nine tested reinforced masonry beams.

All the beams had a pure flexure zone that was designed to be 800 mm in length, which was located between the supports of the loading apparatus. Shear span-to-depth ratio of the beams were varied. Two short-spanned beams had a shear span-to-depth ratio of 2.05 while the remaining seven beams had a ratio of 2.7

All the beams were designed to have 400mm additional length beyond the support points at both ends in order to provide sufficient development length and anchorage for the internal reinforcement. The internal conventional steel reinforcement had 90 degree hooked ends in order to prevent any slippage even though the provided development length was in accordance with CSA S304.1 (2004) Clause 12.4.2.3. Although GFRP rods

of the three course beams had sufficient development length as required by ISIS Canada (2001), an increase in anchorage was required for the short-spanned two course GFRP reinforced masonry beams. It order to overcome this problem, two L shaped GFRP rods with the same diameters were spliced with the main internal GFRP reinforcement at both ends.

Shear clamps were used in the shear zones of seven beams in order to prevent premature shear failure since one of the two course beams failed in shear before reaching its flexural capacity. A steel reinforced three course masonry beam was later on tested without clamps and compared with an unclamped control beam in order to make sure that the clamps do not alter the deflection values of the beam.

The moment, strain and deflection values mentioned in the following detailed test results of the beams are referring to the values recorded at the mid-span which is the primary point of interest of this project.

4.1.1 Beam S-3-1-15M

This fully-grouted three course high reinforced concrete masonry beam was designed as an under-reinforced beam, having a conventional 492 MPa steel reinforcement ratio of 0.21%. It was tested to be used as a control specimen to observe the load-deflection response of an "unclamped" reinforced masonry beam. The first crack appeared at 15.6 kN, corresponding to a 12.48 kN.m moment. Although this first crack was not visible to the eye, it caused a 0.2 kN drop in the load. As the load increased, cracks at the mortar joints close to the mid-span started to widen and propagated vertically towards the compression zone. Steel reinforcement started to yield at 52.5 kN,

corresponding to 42 kN.m moment. The mid-span deflection at the yield was recorded as 8.46 mm. After the yield of the reinforcement, flexural shear cracks close to the pure flexure zone started to intensify as the load increased gradually but not considerably. Crushing of the vertical mortar joint and splitting of the block shells in the compression zone resulted with failure at 67 kN corresponding to 53.6 kN.m moment and 46.71 mm of deflection. After the failure, the applied load was gradually removed to be able to observe the permanent deflection of the beam. The corresponding load-deflection curve, strains readings of the interior steel reinforcement and pictures of the beam during loading and after failure are shown in Figures 4.2 and 4.3

4.1.2 Beam F-2-2#19

The test was conducted on a fully-grouted two course high over-reinforced beam. Two #19 GFRP rods were used to achieve a reinforcement ratio of 1.0%. The first crack appeared at 6.5 kN, corresponding to a 2.6 kN.m moment. Shear cracks close to the pure flexure zone widened rapidly and extended as the beam continued carrying more load. The beam prematurely failed in shear at 47.5 kN corresponding to 19 kN.m moment, experiencing 21.6 mm of deflection. The corresponding load-deflection curve, strains readings of the interior GFRP reinforcement and pictures of the beam during loading and after failure are shown in Figures 4.4 and 4.5

4.1.3 Beam S-3-1-15M-C

Test specimen was a fully-grouted three course high reinforced concrete masonry beam that was identical to the control specimen. It was an under-reinforced beam, having a conventional 492 MPa steel reinforcement ratio of 0.21%. It was tested to observe the load-deflection response of a "clamped" reinforced masonry beam. The first crack appeared at 17.4 kN, corresponding to a 13.92 kN.m moment. Although this first crack was not visible to the eye, it caused a 0.3 kN drop in the load. Slightly inclined shear-flexure cracks in the shear span started to appear as well due to the continuously increasing load. Steel reinforcement started to yield at around 52.5 kN, corresponding to 42 kN.m moment. The mid-span deflection at the yield was recorded as 7.78 mm. After the yield of the reinforcement, flexural shear cracks close to the pure flexure zone started to intensify as the load increased gradually but not considerably. The beam finally failed due to splitting of the face shells of the masonry units located in the compression zone at 70 kN corresponding to 56 kN.m moment, experiencing 52.3 mm of deflection. The corresponding load-deflection curve, strains readings of the interior steel reinforcement and pictures of the beam during loading and after failure are shown in Figures 4.6 and 4.7

4.1.4 Beam F-2-2#16-C

This test was conducted on a fully-grouted two course high reinforced concrete masonry beam. It was over-reinforced having a reinforcement ratio of 0.69% provided by two internal #16 GFRP rods. Shear clamps were used in the shear zones in order to prevent premature failure of the beam in shear. The first crack appeared at 17.4 kN, corresponding to a 13.92 kN.m moment. Although this first crack was not visible to the

eye, it caused a slight drop in the load. After the first crack, the beam continued carrying more load as significant number of cracks started to appear and mortar joints close to the soffit of the beam started splitting at the constant moment zone. The beam finally failed at 70 kN corresponding to 28 kN.m moment due to the crushing and splitting of masonry blocks located at the first row of compression zone, experiencing 35.86 mm of deflection. The corresponding load-deflection curve, strains readings of the interior GFRP reinforcement and pictures of the beam during loading and after failure are shown in Figures 4.8 and 4.9

4.1.5 Beam F-3-1#13-C

The test was conducted on a fully-grouted three course high reinforced concrete masonry beam. Although ISIS (2001) strictly recommends over-reinforced design approach for FRP reinforced beams due to the brittle failure behavior of the FRP rods, this beam was detailed to be under-reinforced with a reinforcement ratio of 0.13%, having one internal #13 GFRP rod. Shear clamps were used in the shear zones in order to prevent premature failure of the beam in shear. The first crack appeared at 15.3 kN, corresponding to a 12.24 kN.m moment. As expected, the beam suddenly failed at 58 kN corresponding to 46.4 kN.m moment due to rupture of the internal GFRP rod, at 50.5 mm of deflection. The corresponding load-deflection curve, strains readings of the interior GFRP reinforcement and pictures of the beam during loading and after failure are shown in Figures 4.10 and 4.11

4.1.6 Beam F-3-1#19-C

This fully-grouted three course high over-reinforced masonry beam had a reinforcement ratio of 0.3% provided by one internal #19 GFRP rod. Shear clamps were used in the shear zones in order to prevent premature failure of the beam in shear. The first crack appeared at 16.5 kN, corresponding to a 13.2 kN.m moment. The beam failed at 86 kN corresponding to 69 kN.m due to crushing of the blocks and the mortar joints in compression area of the pure flexure zone, at 68.21 mm of deflection. The corresponding load-deflection curve, strains readings of the interior GFRP reinforcement and pictures of the beam during loading and after failure are shown in Figures 4.12 and 4.13

4.1.7 Beam F-3-2#16-C

This specimen was a fully-grouted three course high over-reinforced masonry beam with reinforcement ratio of 0.42% provided by two internal #16 GFRP rods. Shear clamps were used in the shear zones in order to prevent premature failure of the beam in shear. The first crack appeared at 14.6 kN, corresponding to an 11.68 kN.m moment. After the first crack, the beam continued carrying more load as the visible flexural cracks started to appear and mortar joints close to the soffit of the beam started splitting at the constant moment zone. The beam failed at 79.5 kN corresponding to 63.6 kN.m due to crushing of the blocks and the mortar joints in compression area of the pure flexure zone, at 28.6 mm of deflection. The corresponding load-deflection curve, strains readings of the interior GFRP reinforcement and pictures of the beam during loading and after failure are shown in Figures 4.14 and 4.15

4.1.8 Beam F-3-2#19&1#16-C

This specimen was a fully-grouted three course high over-reinforced masonry beam with reinforcement ratio of 0.8% provided by two #19 and one #16 GFRP rods. Shear clamps were used in the shear zones in order to prevent premature failure of the beam in shear. The first crack appeared at 15.5 kN, corresponding to a 12.4 kN.m moment. The beam failed at 86.5 kN corresponding to 69 kN.m due to crushing of the blocks and the mortar joints in compression area of the pure flexure zone, at 16.29 mm of deflection. The corresponding load-deflection curve, strains readings of the interior GFRP reinforcement and pictures of the beam during loading and after failure are shown in Figures 4.16 and 4.17

4.1.9 Beam S-3-1-15M-C-CFRP

Last tested beam was a fully-grouted three course high reinforced concrete masonry beam that was identical to the clamped control specimen. It was an under-reinforced beam, having a conventional 492 MPa steel reinforcement ratio of 0.21%. This beam was strengthened in flexure using one block wide CFRP sheets. CFRO sheets were applied on both sides of the beam along its length, extending beyond the supports. The first crack appeared at 20 kN, corresponding to a 16 kN.m moment. Although the load was increased continuously and gradually, there were neither visible cracks on both sides of the beam nor any debonding in the CFRP laminate. Steel reinforcement started to yield at around 79.5 kN, corresponding to 63.6 kN.m moment. The mid-span deflection at the yield was recorded as 9.97 mm. After the yield of the reinforcement, the beam continued carrying more load. The beam failed due to splitting of the face shells of the masonry

units located in the compression zone at 110.9 kN corresponding to 88.72 kN.m moment, experiencing 25.86 mm of deflection. Even without any mechanical anchorage, CFRP laminate did not debond from the original beam. The corresponding load-deflection curve, strains readings of the interior steel reinforcement and pictures of the beam during loading and after failure are shown in Figures 4.18 and 4.19

4.2 Discussions on Performance of Tested Beams

This section briefly comments on the visual observations that were encountered during the conducted tests. Crack patterns, deformations, reinforcement strains and modes of failures were compared and interpreted. Following quantitative analysis chapter of this thesis includes a more detailed numerical analysis and numerical comparisons of the beams.

4.2.1 Cracking Patterns

As expected, majority of the beams reached their cracking moments (M_{cr}) as soon as the loading process started. Those first cracks were not visible however they resulted with a significant drop in the load.

Excluding the CFRP-strengthened beam, after the first crack, beams continued carrying more load as the visible flexural cracks started to appear and mortar joints close to the soffit of the beam in the constant moment zone started splitting. As the load increased, cracks at the mortar joints close to the mid-span began widening and propagated vertically towards the compression zone. Cracks did not necessarily follow

the mortar joints and propagated through the masonry blocks as well. Shear cracks in the shear span started to appear as well with the continuous increase in the applied load.

On the other hand, visual comparison of the tested clamped and unclamped steel reinforced masonry beams proved that they had similar flexural and shear crack patterns, meaning that the clamps in the shear zone did not limit the formation of shear cracks but prevented them from widening. Clamps were deliberately placed before or after mortar joint in order to allow the joints separate freely during loading. In the case of steel reinforced beams, flexural cracks widened significantly as soon as the steel reinforcement reached yielding load.

During the tests, separation of the joints in the constant moment zone was monitored and recorded at intervals of 10 kN. As soon as joints started separating, using a scaled transparency, images of the joints were taken. As much as 10mm of separation at the mortar joints were observed (Figure 4.1). Since the CFRP-strengthened beam's mortar joints were covered with the CFRP laminate, conditions of the joints and cracks on the masonry units along the beam could not be monitored. Strengthening steel reinforced masonry beam significantly reduced the crack propagation, there were neither any flexural not any shear cracks visible even in the vicinity of failure load.

Internally GFRP-reinforced concrete masonry beams showed great similarities with GFRP-reinforced concrete beams in terms of crack patterns. Previous tests conducted on GFRP-reinforced concrete beams showed that, similar to GFRP-reinforced concrete masonry, crack formation was initiated when cracking moment M_{cr} point was reached. The cracks in the constant moment zone cracks propagated vertically and widened as the load increased. Cracking in the shear zone started with vertical cracks as

well and the cracks started to incline as the shear stresses became dominant in the shear zone.

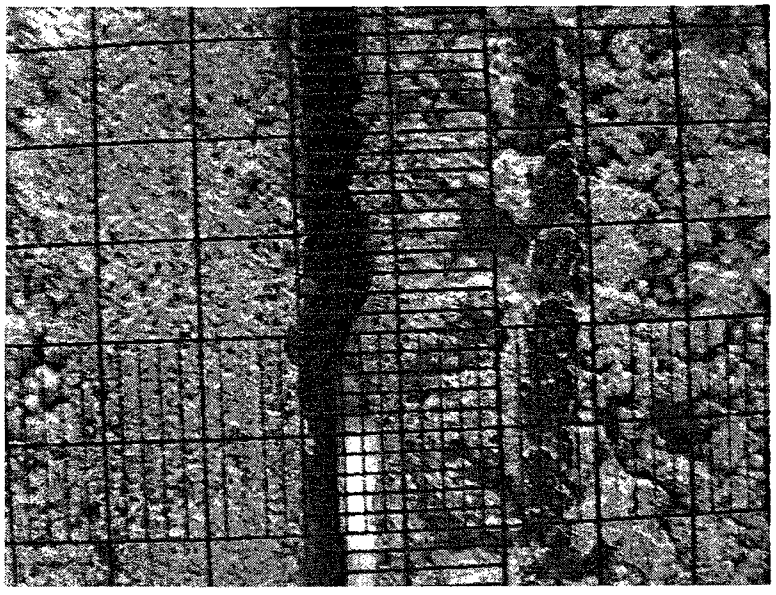

Figure 4.1 Observed head joint crack located at the constant moment zone of a specimen

4.2.2 Comparative Load-Deflection Performance

When plotting the load-deflection relationships of the beams, dead load acting on the beams due to their own weight was incorporated. The own weight was converted into an equivalent point load and added to the load measured by the load-cell every one tenth of a second.

In general, none of the beams experienced significant amount of deflection prior to the cracking moment as can be observed in the longitudinal profile drawings. Load-deflection curves for all the specimens were initially linear. In case of steel-reinforced beams S-3-1-15M and S-3-1-15M-C, load-deflection curve started to flatten as the internal steel reinforcement yielded. All the other GFRP-reinforced masonry beams had close to linear load-deflection relationship up to their ultimate loads except beam F-2-2#19 which failed prematurely in shear before reaching its flexural capacity.

Compared to the other tested beams, GFRP under-reinforced masonry beam F-3-1#13-C experienced highest mid-span deflection as expected at failure load of 58 kN. Other GFRP-reinforced masonry beams were all stiffer as the reinforcement ratios were increased. They were all over-reinforced as required by ISIS Canada (2001). F-3-2#19&1#16-C had the highest GFRP reinforcement ratio among the other GFRP-reinforced three course masonry beams and was a lot stiffer than the steel reinforced shear clamped control beam S-3-1-15M-C. This shows that GFRP over-reinforced masonry beams can provide high flexural resistances with reasonable deformability.

CFRP-strengthened beam S-3-1-15M-C-Sheet was significantly stiffer than steel reinforced control specimen S-3-1-15M-C. Although the control specimen had relatively less mid-span deflection prior to yield mainly due to the level of applied load, in the vicinity of failure load, mid-span deflection of the control specimen was significantly higher, as much as 102.25 mm. On the other hand, strengthened beam S-3-1-15M-C-Sheet resisted 60% more load compared to the control beam and failed at 88.72 kN.m, experiencing only 25.86 mm of deflection.

4.2.3 Comparative Load-Strain Performance

As expected, conventional 492 MPa steel reinforcement of the steel reinforced masonry beams S-3-1-15M, S-3-1-15M-C and S-3-1-15M-C-CFRP yielded at strains around 2400 micro strains. Their load-strain relationships were satisfactory as well since the plotted curves were linear up to yield, flattened as the steel started yielding and exhibited post-yielding plateau as the beams were reaching their ultimate loads.

GFRP rods exhibited linear stress-strain relationship until flexural failure of the beams. Only the under-reinforced GFRP beam F-3-1#13-C reached its ultimate strain in tension and ruptured. I was able to monitor the strains of the #13 GFRP rod up to 14000 micro strains before the strain-gauge went off-scale and the rod ruptured. Manufacturer reported the ultimate strain of that rod as 17000 micro strains. Since the rest of the specimens were all over-reinforced, failures of the specimens were compression controlled and the rods stayed intact (i.e. they did not fail by rupture). Examinations performed on GFRP rods of the failed specimens showed that the sand coating on the surface of the bars were fully existent, showing no signs of slippage and proving that the provided anchorage was sufficient.

Strain-gauges installed on the CFRP laminate at the mid-span recorded a variation of maximum strains from 2500 to 4500 micro strains depending on the location of the gauge on the width of the CFRP laminate, 4500 micro strains being the strain value nearest to the soffit of the beam. Ultimate strain of the composite CFRP laminate is reported as 10000 micro strains by the manufacturer meaning that CFRP laminate was able to reach 50% of its capacity without any mechanical anchorage and did not get debonded.

4.2.4 Modes of Failures

Compression failure in the constant moment zone was the desired type of failure for all the over-reinforced specimens. Compression failure started with crushing of the vertical mortar joint located between the masonry units on the top row at the mid-span. As the load increased, horizontal cracks started to form on the face of the concrete

masonry unit located at the top row of the mid-span, right beneath the loading apparatus. As the loading continued and horizontal cracks widened, and splitting of the block shells in the compression zone occurred and the flexural resistance of the specimen decreased significantly.

Conventional steel-reinforced, under-reinforced concrete masonry beams S-3-1-15M, S-3-1-15M-C and S-3-1-15M-C-CFRP were failed in compression after the yielding of steel reinforcement. All the failures were ductile since the internal steel reinforcement gradually went through plastic deformation after yielding.

GFRP reinforced unclamped specimen F-2-2#19 failed prematurely in shear. A forty five degree shear crack was formed and widened as the applied load increased between the roller support of the beam and the support of the loading apparatus.

Under-reinforced GFRP specimen F-3-1#13-C failed due to the rupture in the GFRP rod as expected without experiencing compression failure in grout-filled masonry units.

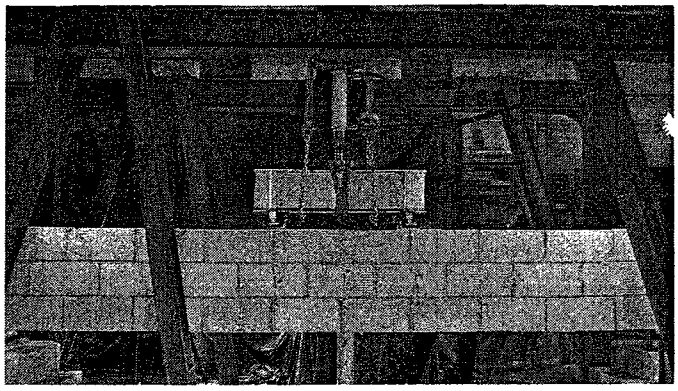

(a)

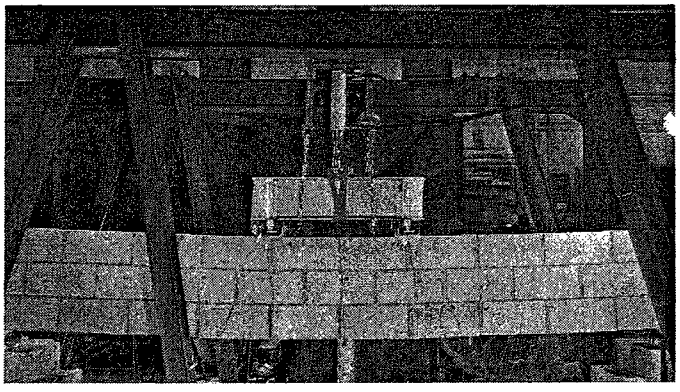

(b)

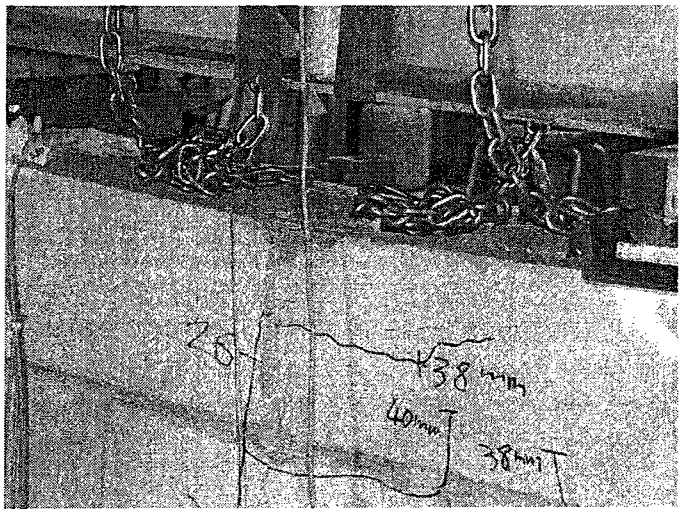

(c)

Figure 4.2 Pictures corresponding to beam S-3-1-15M; a) beam soon after cracking, b) close to failure load, c) failed section

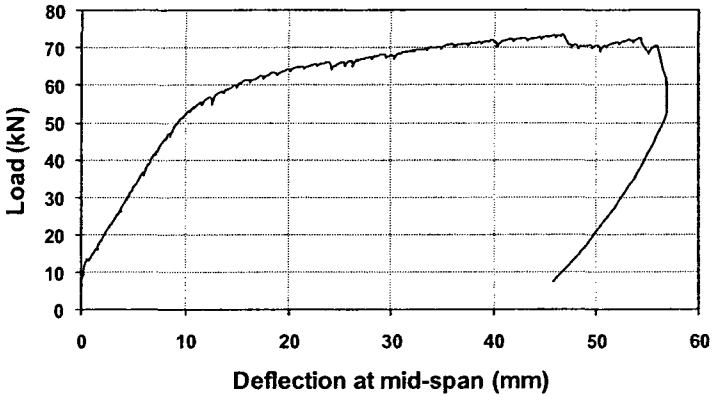

(a)

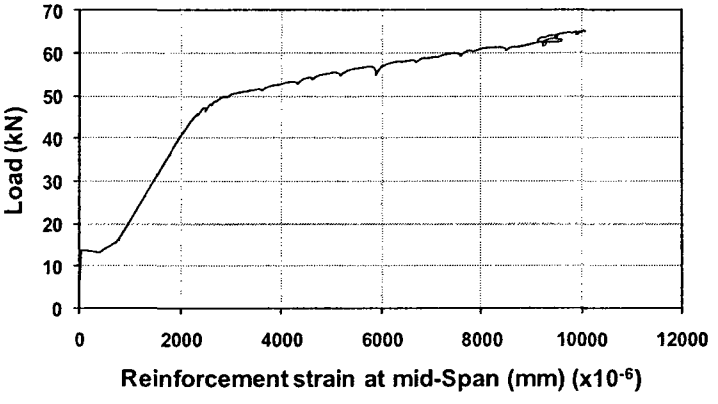

(b)

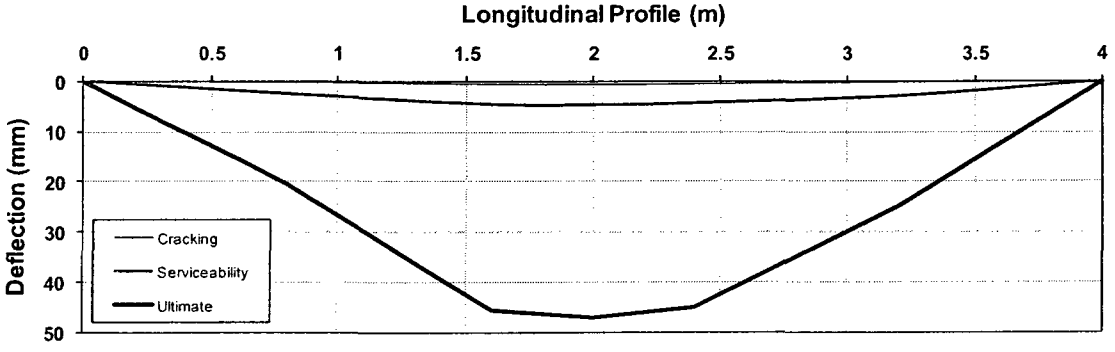

(c)

Figure 4.3 Test results of S-3-1-15M; a) load-deflection at Mid-Span, b) load-Strain at mid-span c) longitudinal profile at different stages of loading

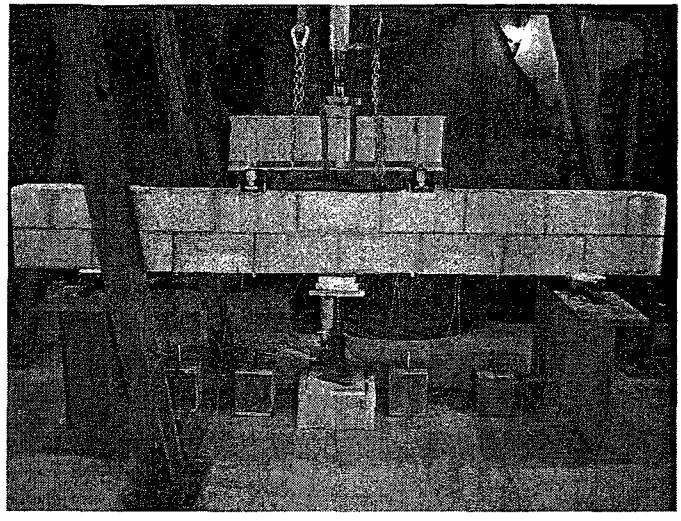

(a)

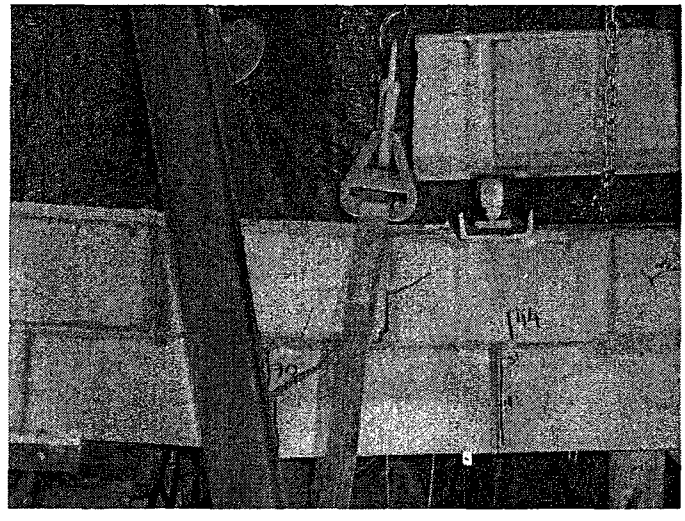

(b)

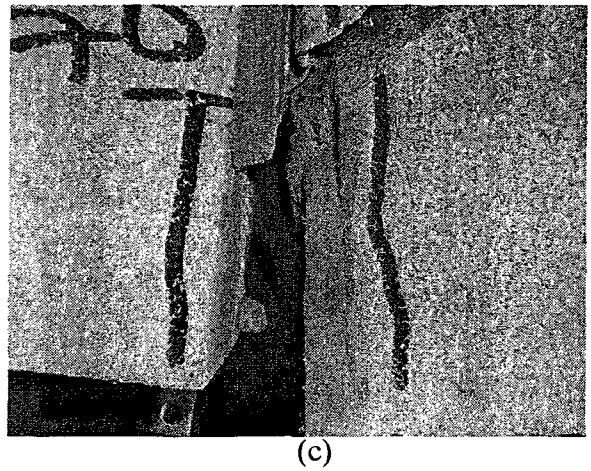

(c)

Figure 4.4 Pictures corresponding to beam F-2-2#19; a) beam before loading, b) beam at failure c) failed section

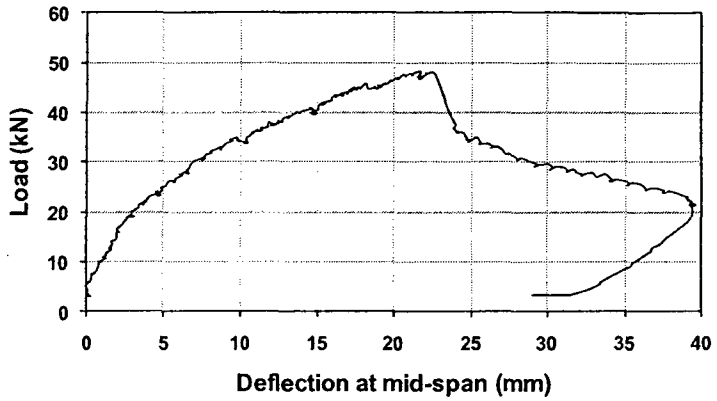

(a)

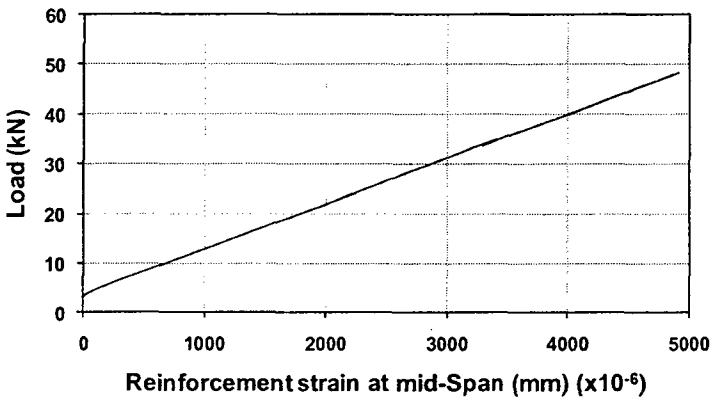

(b)

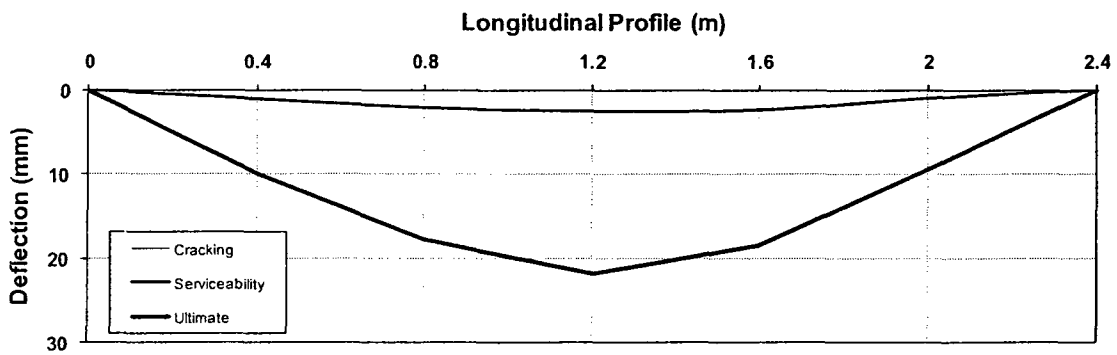

(c)

Figure 4.5 Test results of F-2-2#19; a) load-deflection at Mid-Span, b) load-Strain at mid-span c) longitudinal profile at different stages of loading

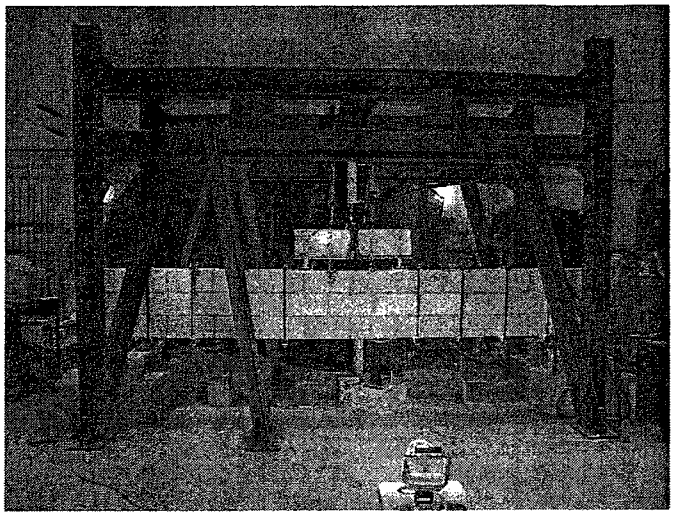

(a)

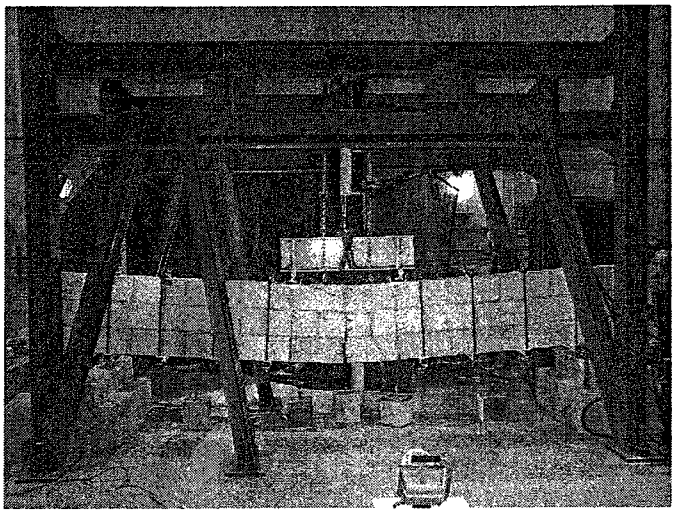

(b)

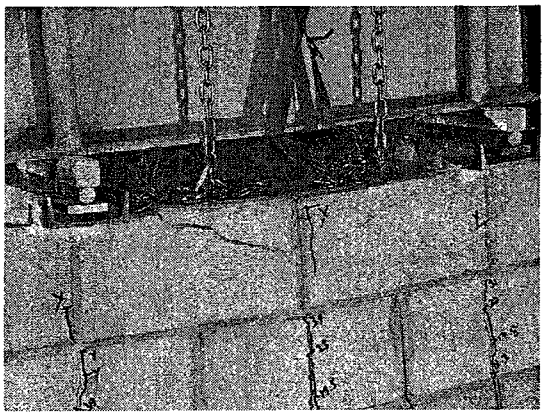

(c)

Figure 4.6 Pictures corresponding to beam S-3-1-15M-C; a) beam before commencement of loading, b) close to failure load, c) failed section

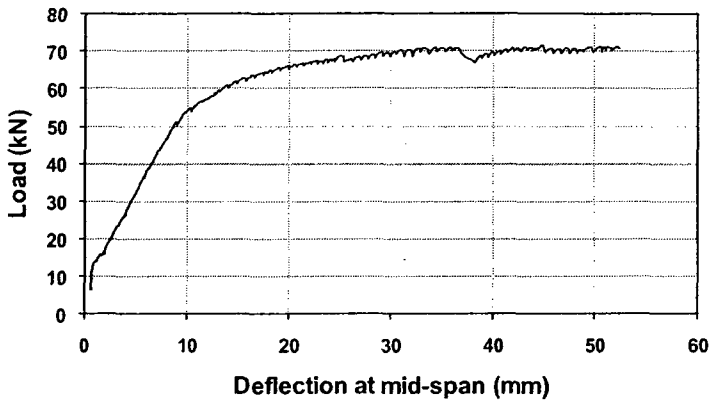

(a)

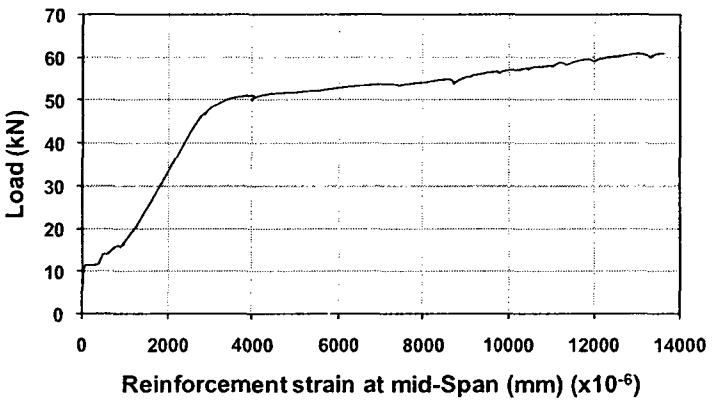

(b)

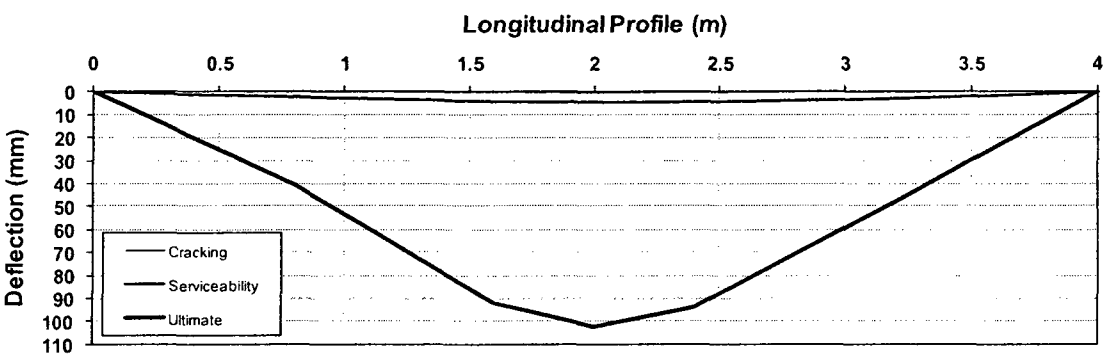

(c)

Figure 4.7 Test results of S-3-1-15M-C; a) load-deflection at Mid-Span, b) load-Strain at mid-span c) longitudinal profile at different stages of loading

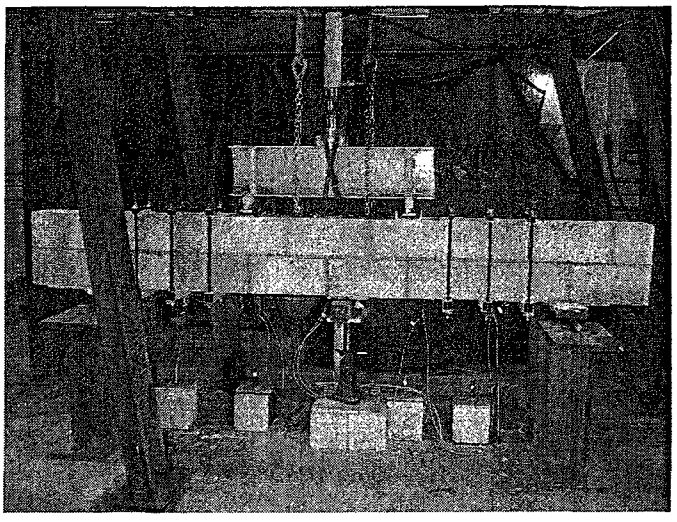

(a)

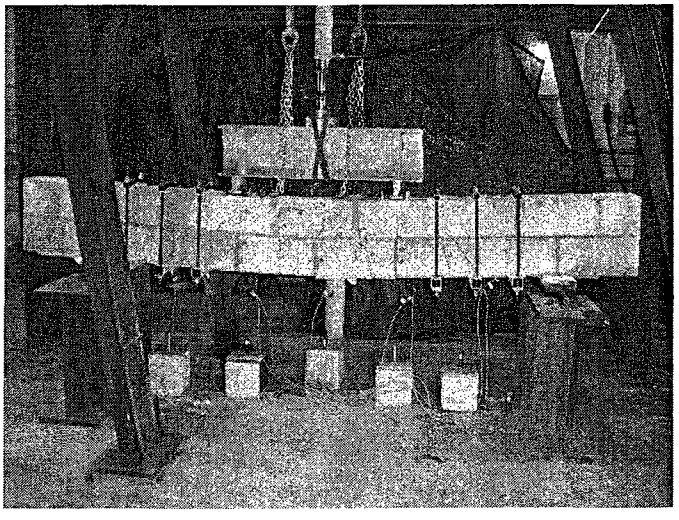

(b)

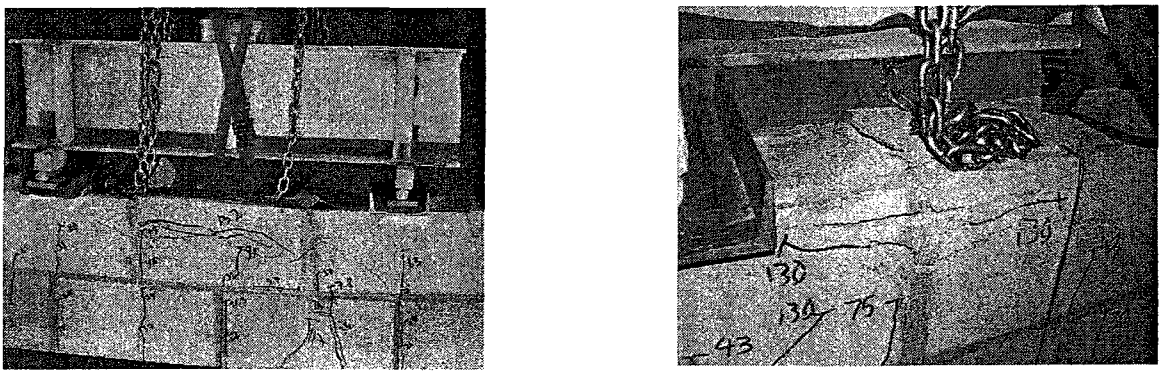

(c)

Figure 4.8 Pictures corresponding to beam F-2-2#16-C; a) beam before commencement of loading, b) close to failure load, c) failed section

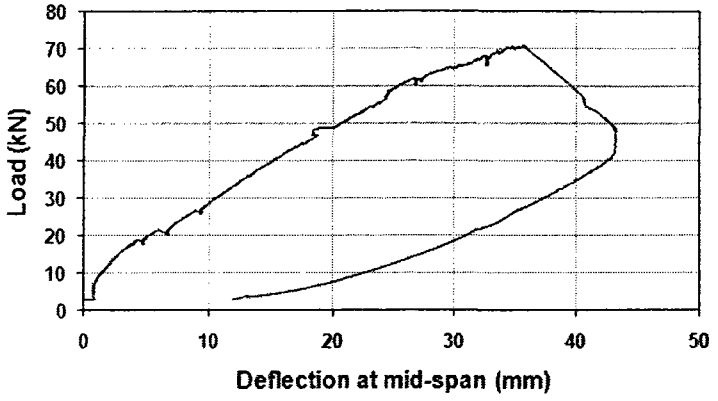

(a)

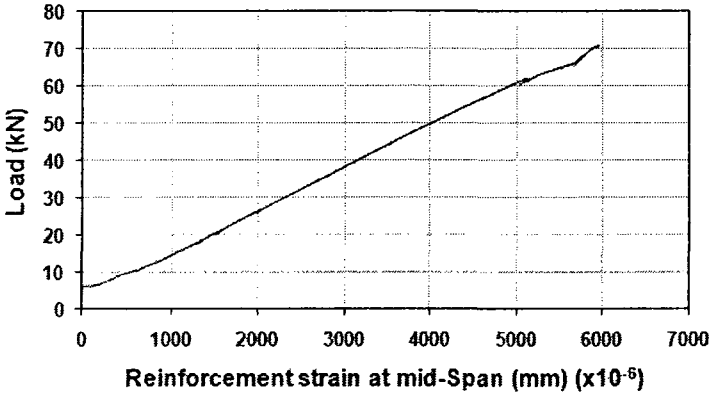

(b)

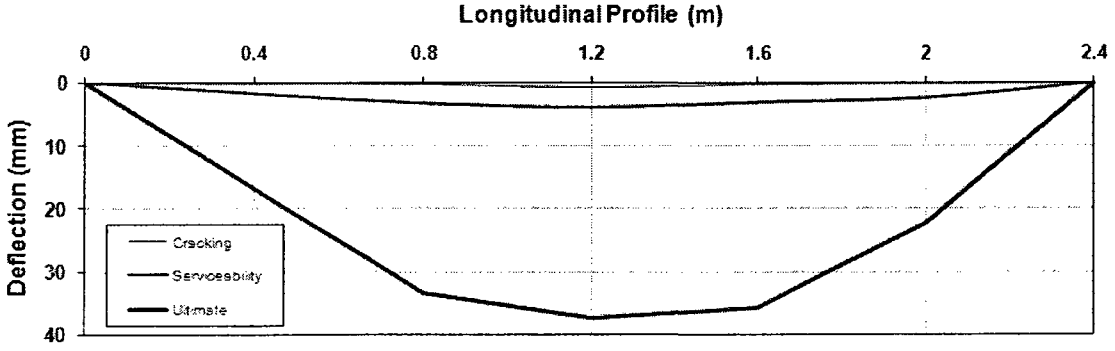

(c)

Figure 4.9 Test results of F-2-2#16-C; a) load-deflection at Mid-Span, b) load-Strain at mid-span c) longitudinal profile at different stages of loading

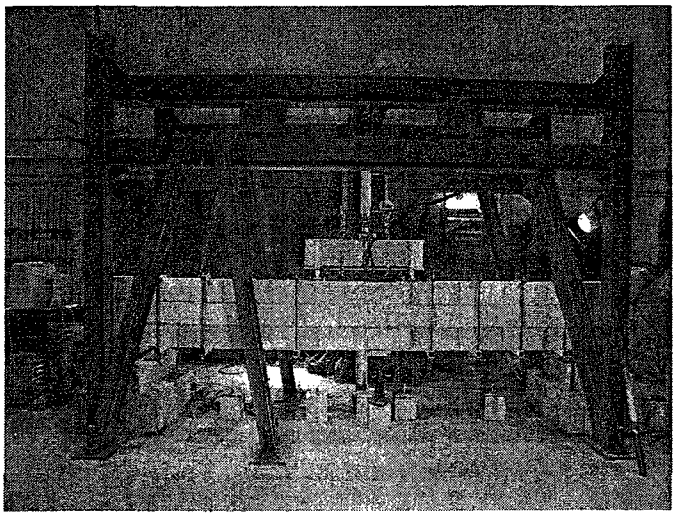

(a)

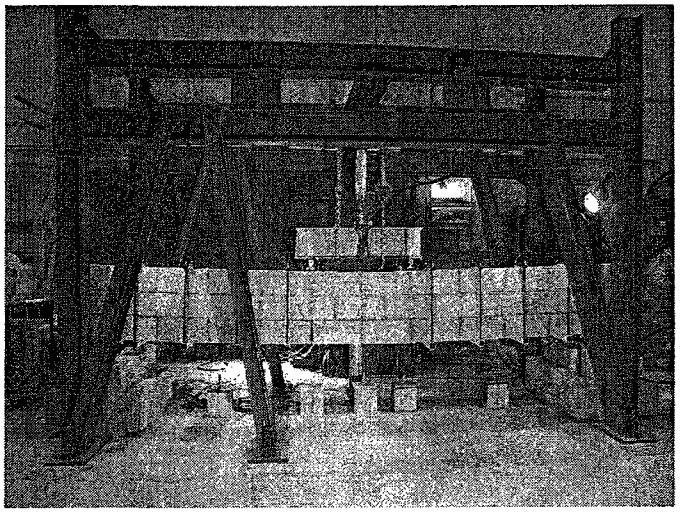

(b)

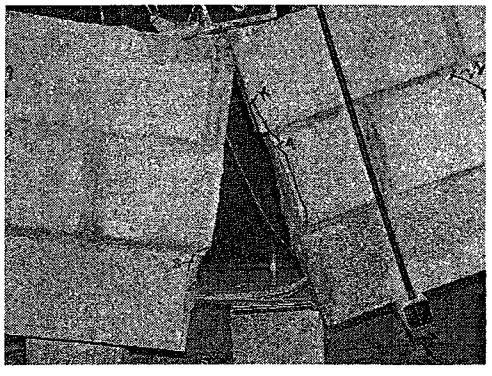

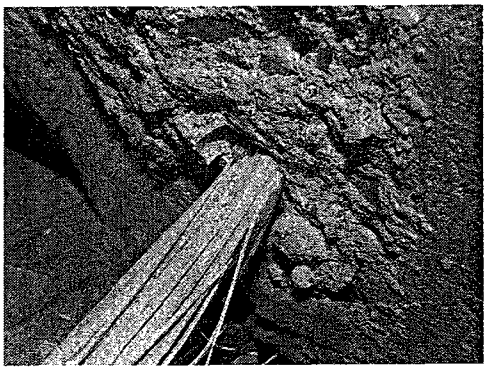

(c)

Figure 4.10 Pictures corresponding to beam F-3-1#13-C; a) beam before commencement of loading, b) close to failure load, c) failed section, rupture of GFRP

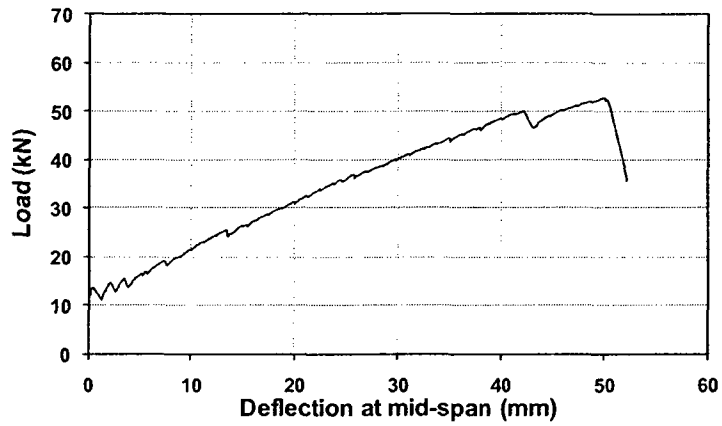

(a)

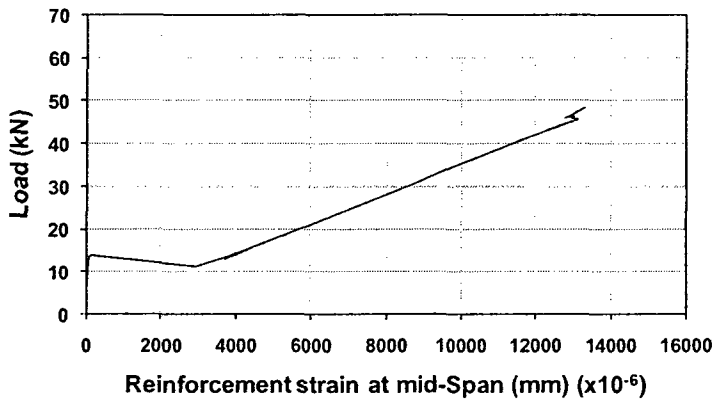

(b)

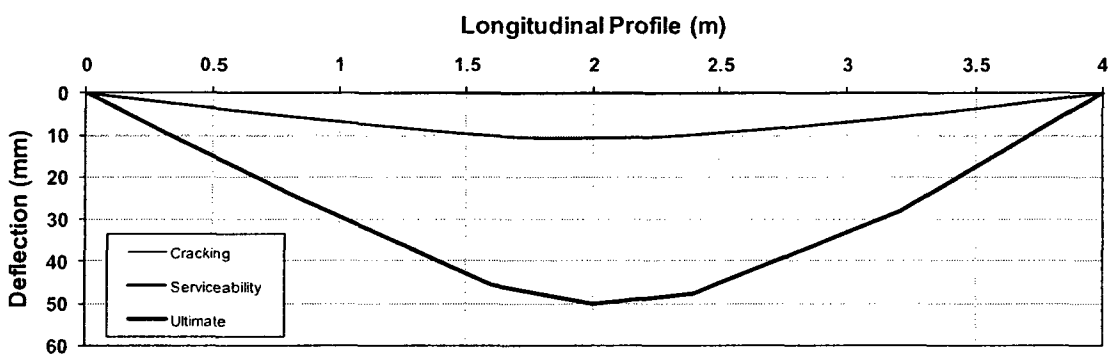

(c)

Figure 4.11 Test results of F-3-1#13-C; a) load-deflection at Mid-Span, b) load-Strain at mid-span c) longitudinal profile at different stages of loading

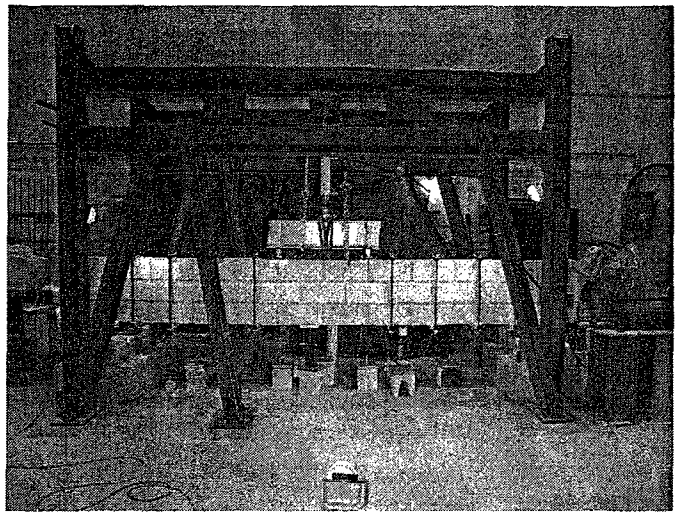

(a)

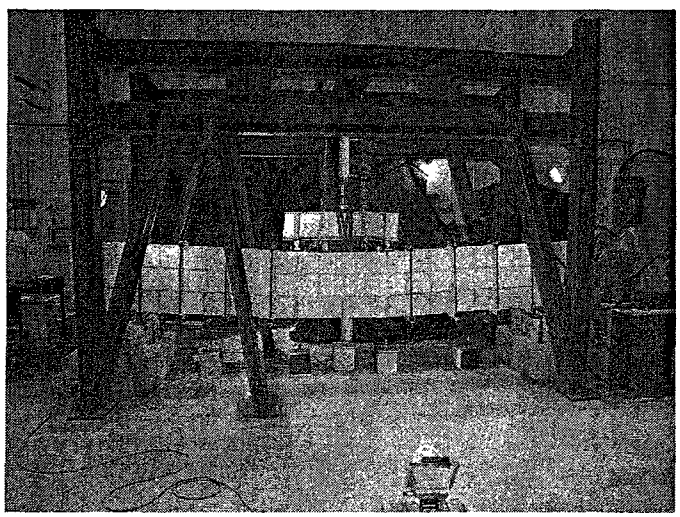

(b)

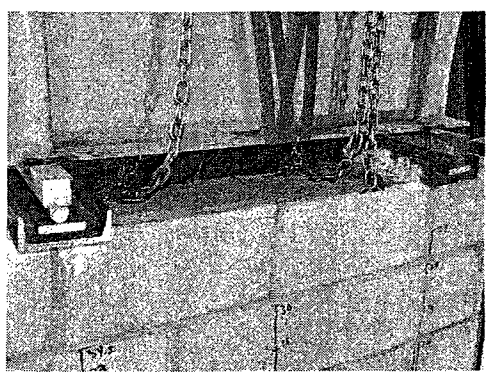

(c)

Figure 4.12 Pictures corresponding to beam F-3-1#19-C; a) beam before commencement of loading, b) close to failure load, c) failed section

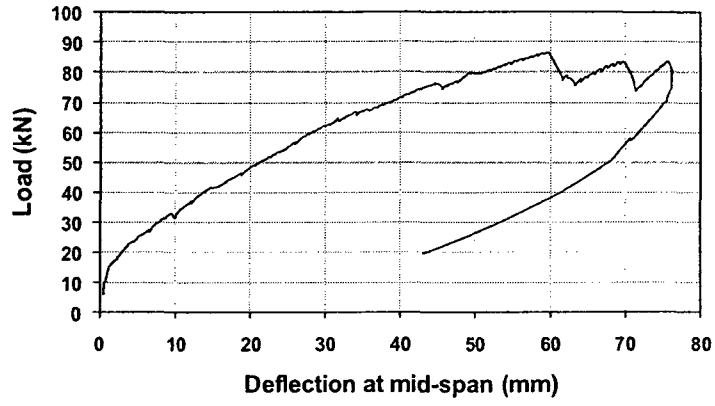

(a)

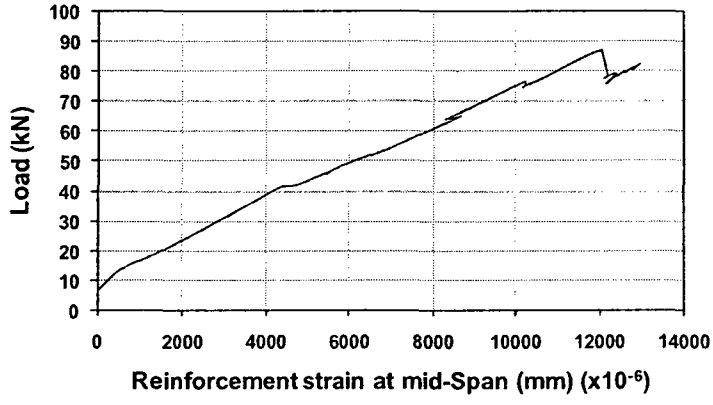

(b)

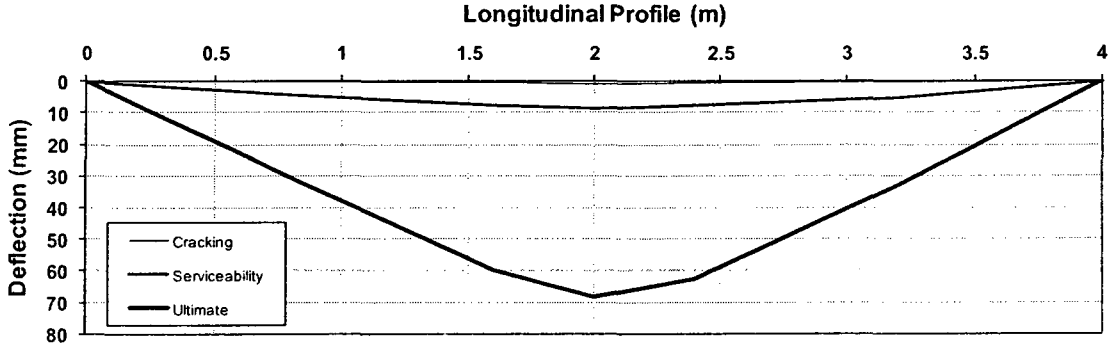

(c)

Figure 4.13 Test results of F-3-1#19-C; a) load-deflection at Mid-Span, b) load-Strain at mid-span c) longitudinal profile at different stages of loading

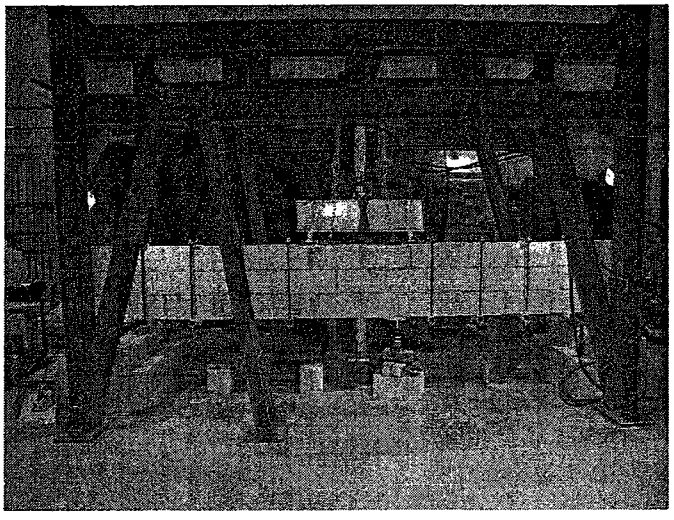

(a)

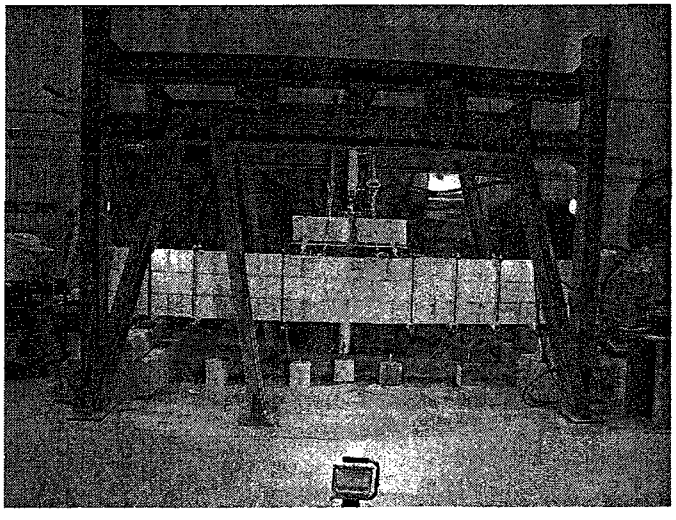

(b)

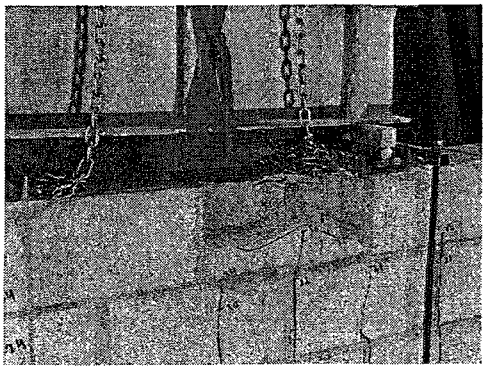

(c)

Figure 4.14 Pictures corresponding to beam F-3-2#16-C; a) beam before commencement of loading, b) close to failure load, c) failed section

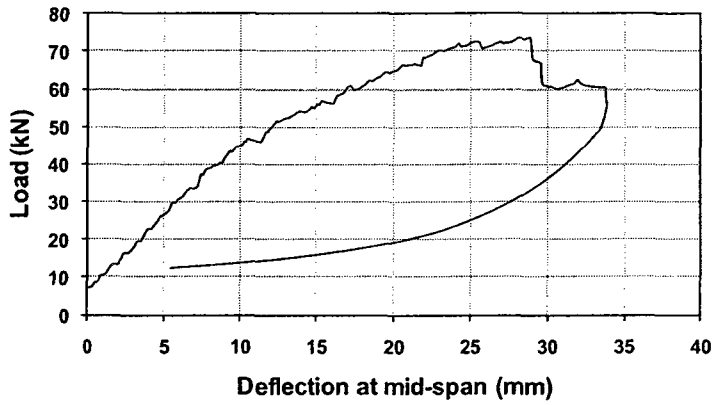

(a)

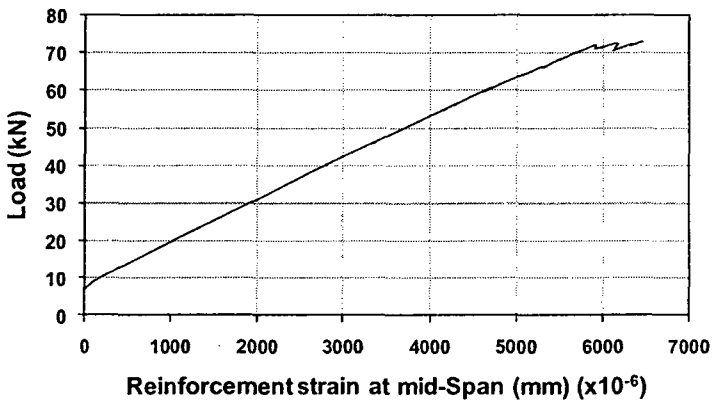

(b)

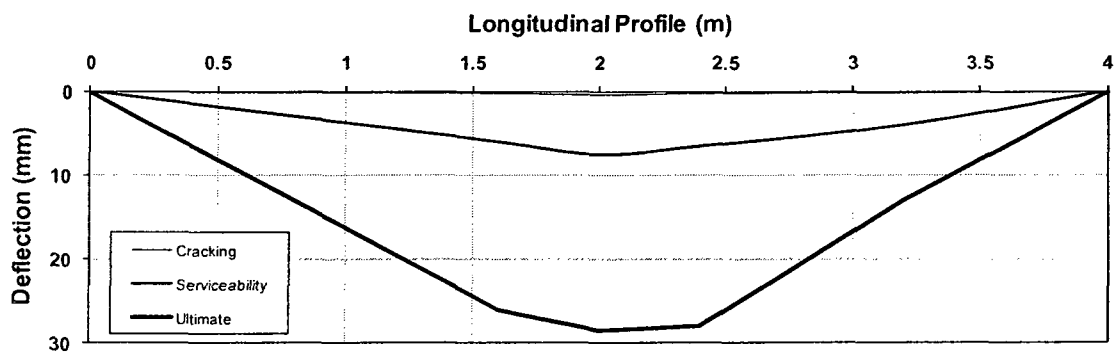

(c)

Figure 4.15 Test results of F-3-2#16-C; a) load-deflection at Mid-Span, b) load-Strain at mid-span c) longitudinal profile at different stages of loading

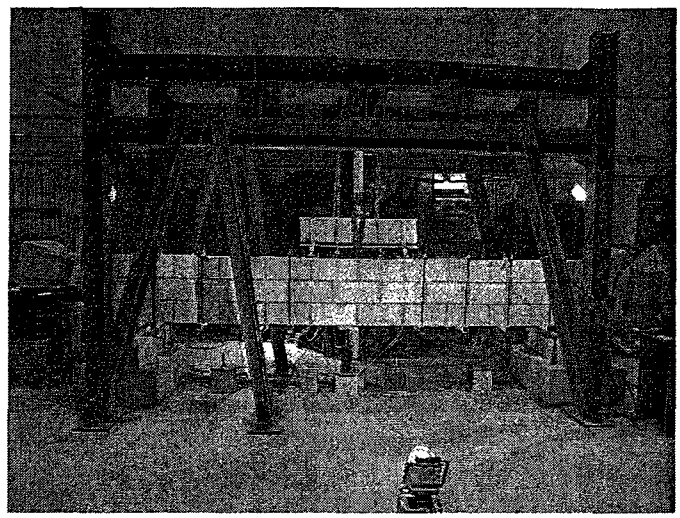

(a)

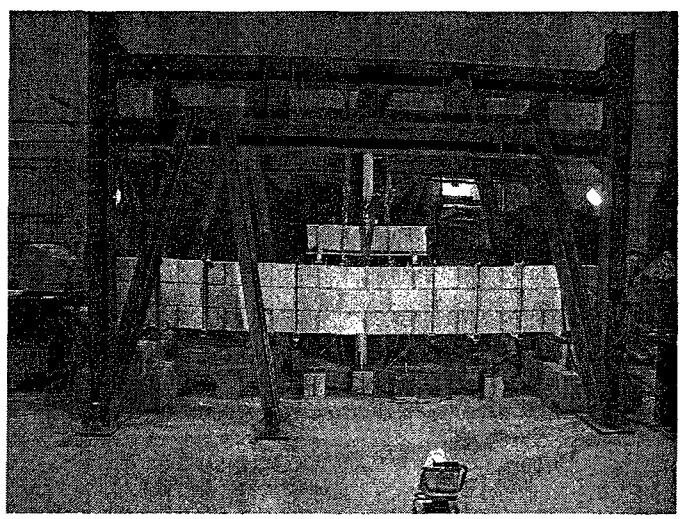

(b)

(c)

Figure 4.16 Pictures corresponding to beam F-3-2#19 & 1#16-C; a) beam before commencement of loading, b) close to failure load, c) failed section

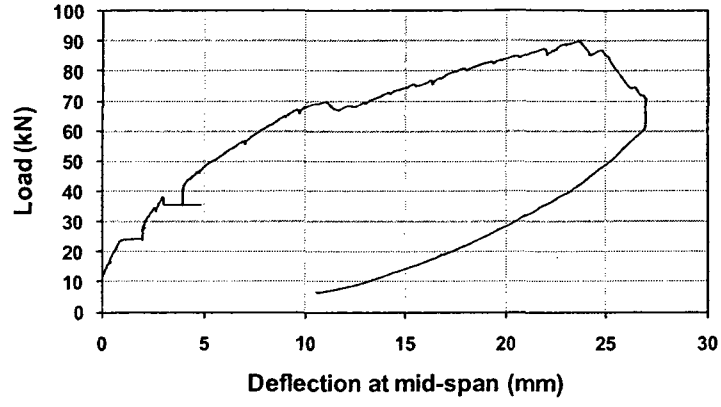

(a)

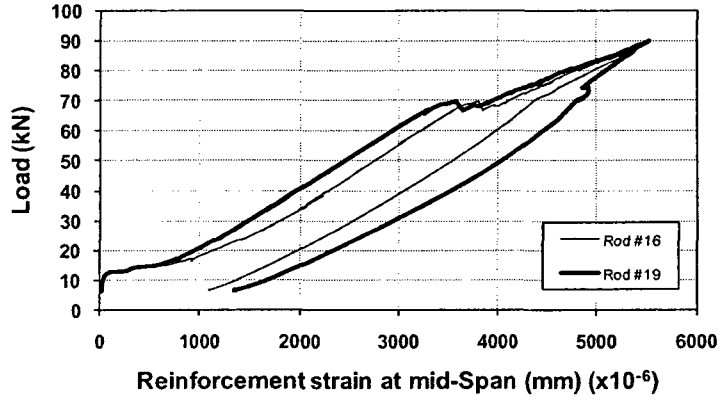

(b)

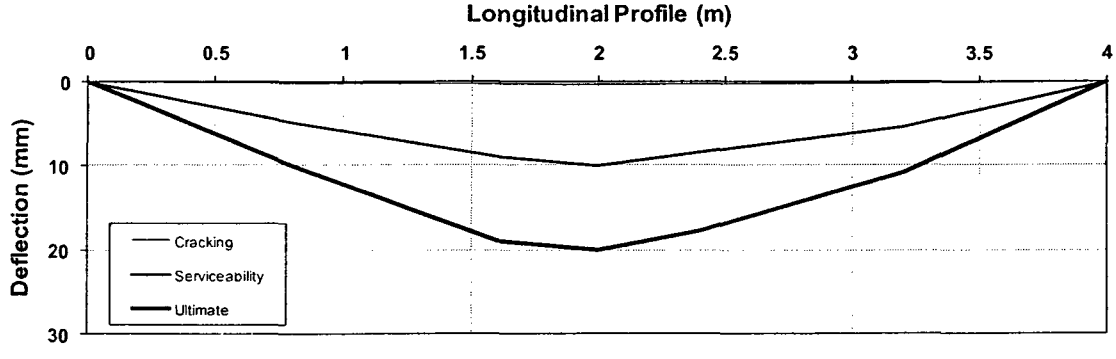

(c)

Figure 4.17 Test results of F-3-2#19 & 1#16-C; a) load-deflection at Mid-Span, b) load-Strain at mid-span c) longitudinal profile at different stages of loading

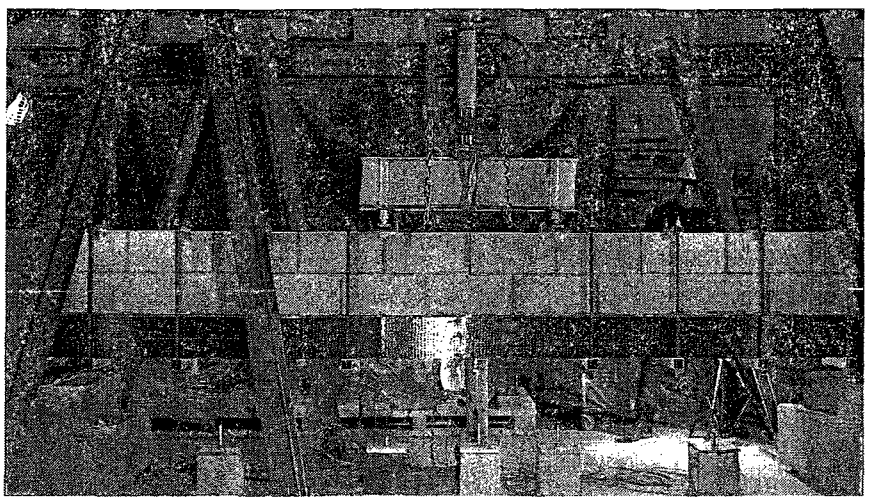

(a)

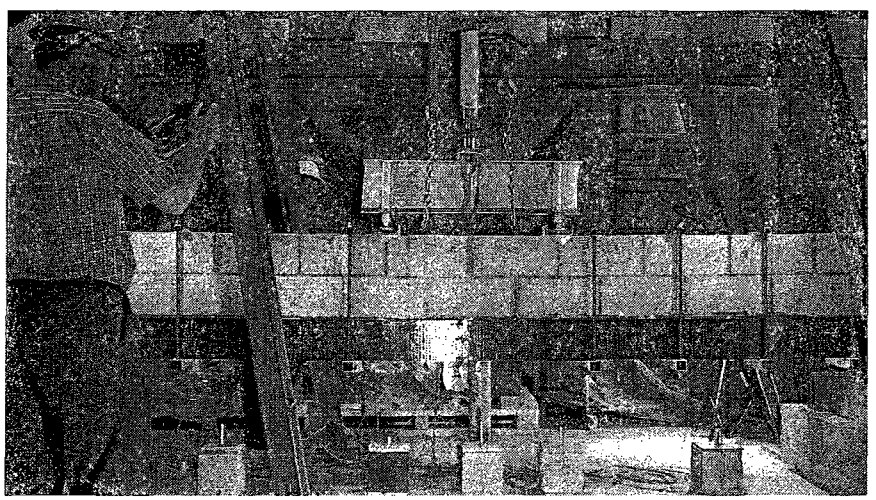

(b)

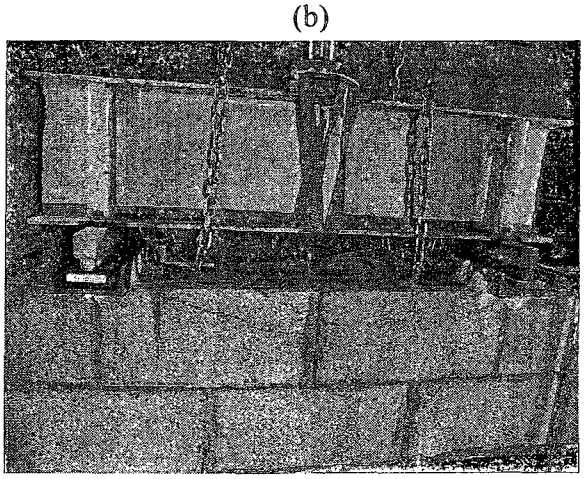

(c)

Figure 4.18 Pictures corresponding to beam S-3-1-15M-C-CFRP; a) beam before commencement of loading, b) close to failure, cracks are nonexistent, c) failed section

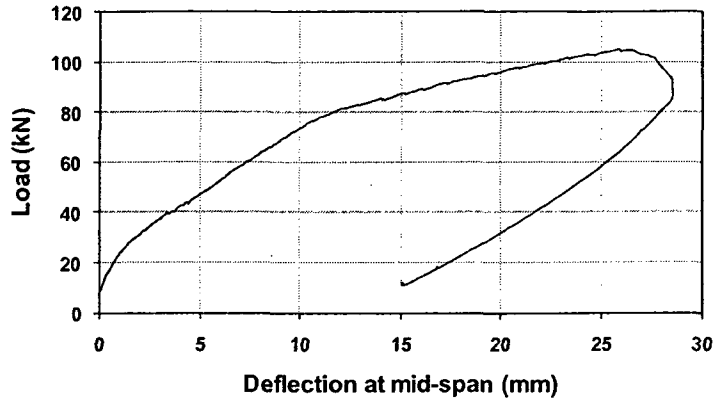

(a)

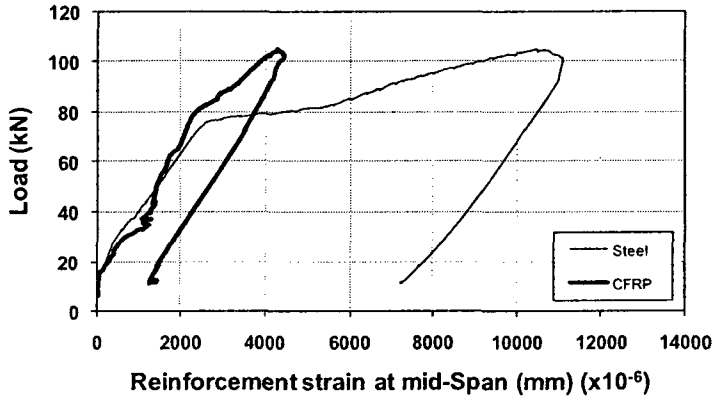

(b)

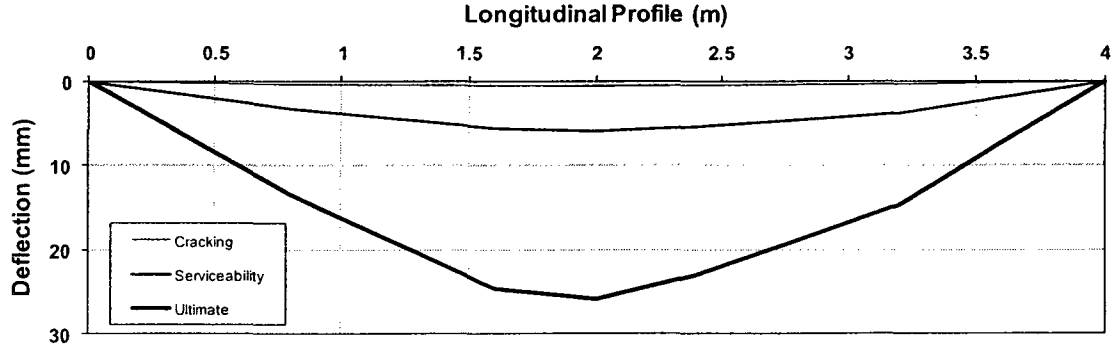

(c)

Figure 4.19 Test results of S-3-1-15M-C-CFRP; a) load-deflection at Mid-Span, b) load-Strain at mid-span c) longitudinal profile at different stages of loading

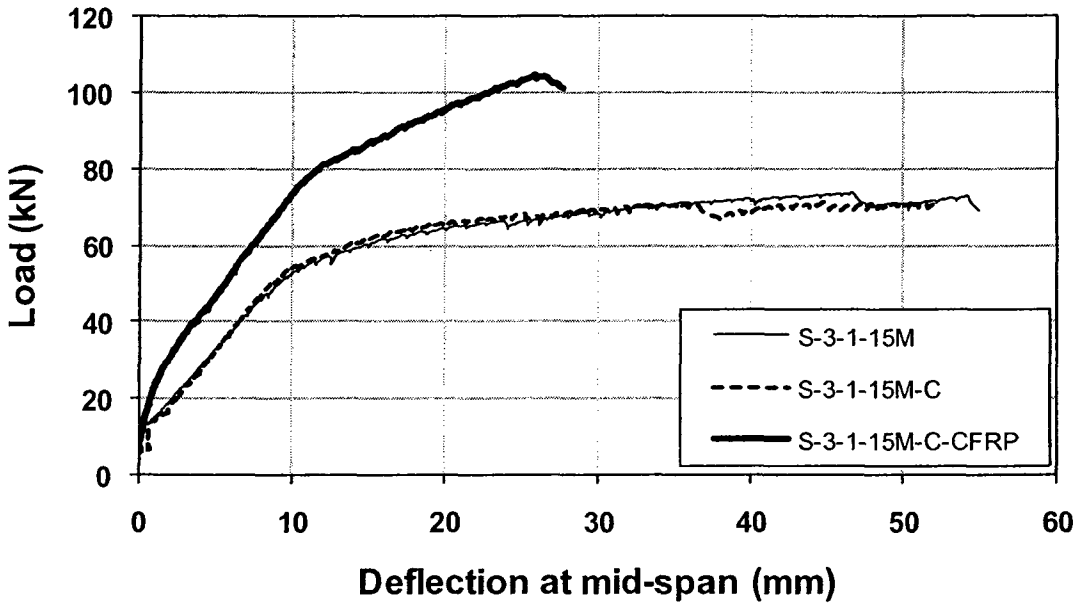

Figure 4.20 Relative load-deflection performance of the steel reinforced concrete masonry beams

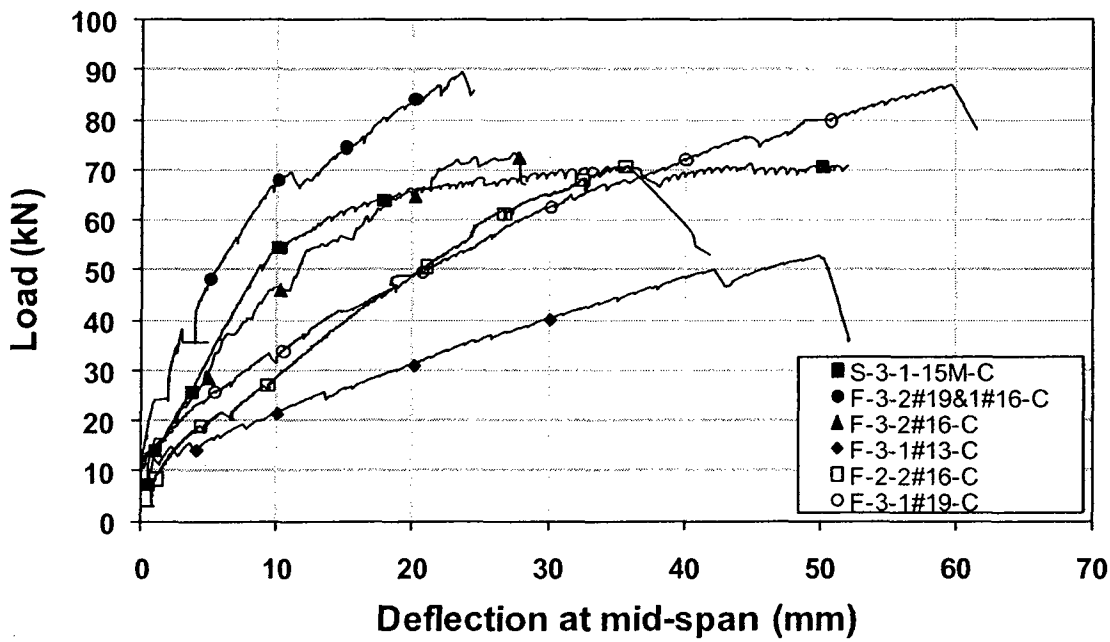

Figure 4.21 Comparison of load-deflection curves of the GFRP-reinforced concrete masonry beams

Table 4.1 Test results of full-scale reinforced concrete masonry beams

Beam	Failure Load (kN)	Failure Moment (kN.m)	Max. Deflection (mm)	Max. Tensile Strain ($x10^{-6}$)	Type of Failure
S-3-1-15M	67	54	46.7	10069	flexure
S-3-1-15M-C	70	56	52.4	13601	flexure
F-2-2#19	48	19	21.6	4909	shear
F-2-2#16-C	70	28	35.9	11976	flexure
F-3-1#13-C	58	46	50.5	13291	flexure
F-3-1#19-C	86	69	68.2	13385	flexure
F-3-2#16-C	80	64	28.6	6468	flexure
F-3-2#19&1#16-C	88	69	16.3	5628	flexure
S-3-1-15M-C-CFRP	111	89	25.9	4473	flexure

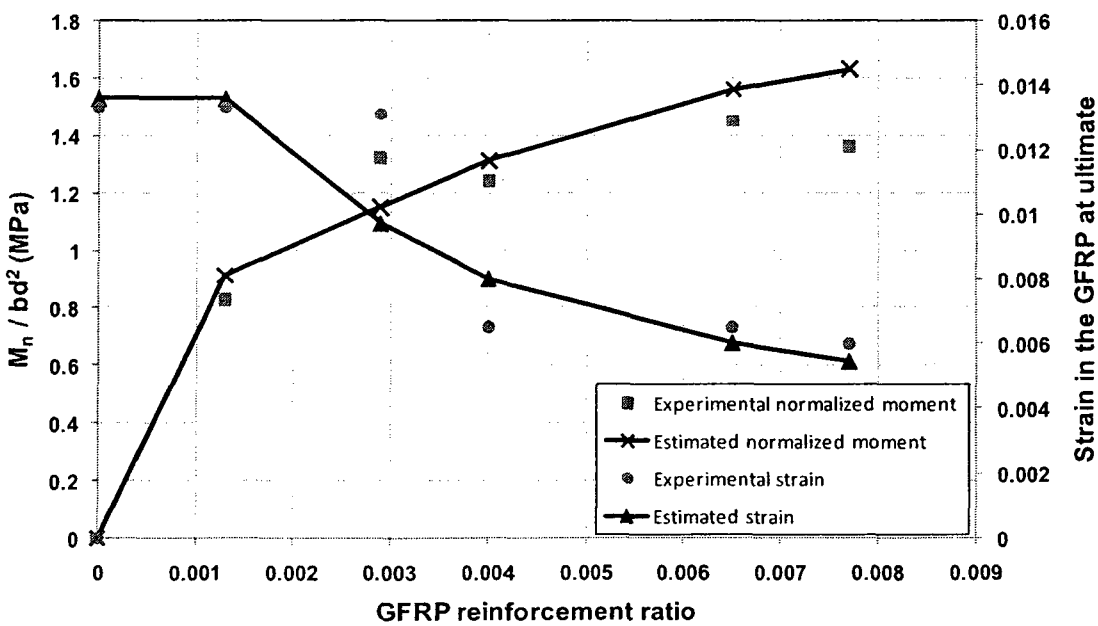

Figure 4.22 Proposed design chart for GFRP-reinforced concrete masonry beams (f'_m=6.9 MPa, $f_{frpu,(ave.)}$=755 MPa, $E_{frp(ave.)}$=47.4 GPa)

CHAPTER 5

ANALYTICAL MODELLING

5.1 Section Analysis

In order to determine the moment resistance of the beams, the following assumptions and constant coefficients were used along with the available design guidelines CSA S304.1 (2004), ISIS Canada (2001) and ACI 440.2R (2002);

- Plane sections remain plane after bending.
- Tensile strength of the section solely depends on the resistance of the longitudinal reinforcement, neglecting the contribution of grouted masonry units.
- GFRP rods exhibit linear elastic behaviour up to the rupture stresses.
- Longitudinal reinforcement is fully bonded to the surrounding grout infill and slippage does not occur.
- Ultimate compressive strain of masonry is taken as $\varepsilon_u = 0.003$
- Modulus of elasticity of masonry is utilized as $E_m = 850 f'_m$
- Intermediate longitudinal reinforcement for crack control was not necessary since CSA S304.1 (2004) requires that only for beams with heights greater than 600mm.
- The direction of the compression (parallel to the bed joint) and discontinuity of the grout in the compression zone of reinforced concrete masonry beams require a corrected f'_m which is obtained by using the factor χ. CSA S304.1 (2004) suggests a factor of 0.5 for compression parallel to the bed joint. In case of lintel blocks in the compression zone, this factor may increase to 0.7. For the analytical capacity estimations of the tested specimens, χ factor is taken as 1.0 since a set of grouted

prisms were tested parallel to their bed joints and obtained the actual f'_m of the grouted masonry units in that direction.

- Depth of the reinforcement (d) varied with the type of longitudinal reinforcement used. In all cases, 50mm cover was assumed.

5.1.1 Steel-Reinforced Masonry Beams

Equivalent rectangular stress block approach suggested by the CSA S304.1 (2004) Clause 11.2.1.6 was used to analyze the flexural capacity of the cross-section. Based on the above mentioned assumptions, in order to obtain an under-reinforced section, primarily the area of steel of balanced condition was checked using:

$$A_{sb} = \frac{\chi(\alpha_1 f'_m) b \beta_1 [\frac{600}{600 + f_y}] d}{f_y} \quad where \ \beta_1 = 0.8, \alpha_1 = 0.85 \qquad 5.1$$

Next to determine the depth of the stress block using the equilibrium of tension and compression forces:

$$\varepsilon_m = \varepsilon_{frpu} (\frac{c}{d-c}) \qquad 5.2$$

where:

ε_{frpu} = Ultimate strain of FRP

d = Depth of the cracked section

c = Depth of the compressive block

$$c = \frac{A_s f_y}{\chi(0.85 f'_m) \beta_1 b} \qquad 5.3$$

Then the expected flexural capacity of the beam is determined using:

$$M_r = \chi(0.85 f'_m) \beta_1 c b (d - \frac{\beta_1 c}{2}) \qquad 5.4$$

5.1.2 GFRP-Reinforced Masonry Beams

Equivalent rectangular stress block approach suggested by the ISIS Canada (2001) for the design of FRP reinforced concrete beams was utilized to analyze the flexural capacity of the cross-section. Compressive stress of concrete (f'_c) was substituted by compressive strength of masonry (f'_m). Moment resistance of the section was calculated by using two different set of values for factors α_1 and β_1; $\beta_1 = 0.8, \alpha_1 = 0.85$ which is suggested by CSA S304.1 (2004) and values recommended by ISIS Canada (2001) depending on the f'_m as well as the reinforcement ratio of the section. Calculated moment resistances of the sections are tabulated on Table 5.1.

5.1.2.1 Tension controlled failure

Although under-reinforced section is not recommended by ISIS Canada (2001), design of an under-reinforced beam was carried out primarily by determination of the balanced condition is checked using:

$$\rho_{frpb} = \frac{\alpha_1 \beta_1 f'_m}{f_{frpu}} \left[\frac{\varepsilon_{mu}}{\varepsilon_{mu} + \varepsilon_{frpu}} \right] \qquad 5.5$$

where:

f_{frpu} = Ultimate tensile strength of the FRP rod

ε_{mu} = Ultimate strain in masonry in compression

As the appropriate number of GFRP rods to satisfy the under-reinforced condition is selected, depth of the compressive block, factors α_1 and β_1 were determined iteratively using the following equation and charts provided in the guideline ISIS Canada:

$$c = \frac{A_{frp} f_{frpu}}{\alpha_1 f'_m \beta_1 b} \qquad 5.6$$

Then the expected flexural capacity of the section is obtained using:

$$M_r = A_{frp} f_{frpu} (d - \frac{\beta_1 c}{2}) \qquad 5.7$$

5.1.2.2 Compression controlled failure

In case of over-reinforced cross-section, following equation was used to determine the stress in the GFRP rod once the quantity of the rods were selected using the balanced section condition:

$$f_{frp} = 0.5 E_{frp} \varepsilon_{mu} \left[\left(1 + \frac{4\alpha_1 \beta_1 f'_m}{\rho_{frp} E_{frp} \varepsilon_{mu}} \right)^{1/2} - 1 \right] \qquad 5.8$$

Moment resistance of the section was calculated by using two different set of values for factors α_1 and β_1; $\beta_1 = 0.8, \alpha_1 = 0.85$ which is suggested by CSA S304.1 (2004) and values recommended by ISIS Canada (2001):

$$\begin{aligned} \alpha_1 &= 0.85 - 0.0015 f'_m \geq 0.67 \\ \beta_1 &= 0.97 - 0.0025 f'_m \geq 0.67 \end{aligned} \qquad 5.9$$

Depth of the compressive block was determined using:

$$c = \frac{A_{frp} f_{frp}}{\alpha_1 f'_m \beta_1 b} \qquad 5.10$$

Then the expected flexural capacity of the section is obtained using:

$$M_r = A_{frp} f_{frp} (d - \frac{\beta_1 c}{2}) \qquad 5.11$$

5.1.3 CFRP-Strengthened Masonry Beams

ISIS Canada (2001) foresees four potential failure modes for CFRP-strengthened reinforced masonry beams; 1) concrete crushing before yielding of steel, 2) steel yielding followed by crushing of concrete, 3) steel yielding followed by rupture in CFRP and 4) debonding of CFRP. Since debonding of CFRP can be eliminated by the use of anchorages, by assuming a failure mode and using equivalent rectangular stress block approach, flexural capacity of the strengthened cross-section could be analyzed. In order to proceed with the numerical analysis, assumption of steel yielding followed by compressive failure was selected. Next, depth of the compressive block, factors α_1 and β_1 were determined iteratively using:

$$\varepsilon_m = \varepsilon_s\left(\frac{c}{d-c}\right) \qquad 5.12$$

$$c = \frac{A_s f_y + A_{cfrp} E_{cfrp} \varepsilon_{cfrp}}{\alpha_1 f'_m \beta_1 b} \qquad 5.13$$

where:

$\varepsilon_{cfrp} = \dfrac{\varepsilon_c (h-c)}{c}$

E_{cfrp} = Modulus of elasticity of CFRP

ε_{cfrp} = Strain in CFRP

Once the correct value for the c determined, the expected flexural capacity of the section is obtained using:

$$M_r = A_s f_y \left(d - \frac{\beta_1 c}{2}\right) + A_{cfrp} E_{cfrp} \varepsilon_{cfrp} \left(h - \frac{\beta_1 c}{2}\right) \qquad 5.14$$

Calculated moment resistance values comparing the tested conventional steel reinforced concrete masonry beams with CFRP-strengthened beam can be found at Table 5.1.

5.2 Load-Deflection Analysis

In order to determine the load-deformation relationship of the specimens, effective moment of inertia (I_{eff}) of the cross section had to be determined. Upon selecting the most suitable approach for estimating the effective moment of inertia for GFRP reinforced concrete masonry beams and CFRP-strengthened steel reinforced concrete masonry beams, various methods were examined and compared.

CSA S304.1 (2004) defines the following equation for estimation:

$$I_{eff} = \left(\frac{M_{cr}}{M_a}\right)^3 I_g + \left[1 - \left(\frac{M_{cr}}{M_a}\right)^3\right] I_{cr} \leq I_g \qquad 5.15$$

where:

$M_{cr} = \dfrac{f_r I_g}{y_t}$

M_{cr} = Cracking moment

M_a = Moment in the member at the load stage at which the deflection is calculated

I_g = Gross moment of inertia

f_r = Modulus of rupture of masonry

y_t = Distance from centroid of the section to the transformed section's extreme fiber in tension

ISIS Canada (2001) suggests two different expressions introduced by Benmokrane et al. (1996), Gao et al. (1998) and Theriault (1998):

$$I_{eff} = \left(\frac{M_{cr}}{M_a}\right)^3 \beta_b I_g + \left[1 - \left(\frac{M_{cr}}{M_a}\right)^3\right] I_{cr} \leq I_g \quad where \quad \beta_b = 0.5\left[1 + \frac{E_{frp}}{E_s}\right] \qquad 5.16$$

$$I_{eff} = \frac{I_g I_{cr}}{I_{cr} + \left(1 - 0.5\left(\frac{M_{cr}}{M_a}\right)^2\right)\left(I_g - I_{cr}\right)} \qquad 5.17$$

For both CSA S304.1 (2004) and ISIS Canada (2001) methods, deflections at any given load are calculated using:

$$\Delta = \frac{Pa}{24EI_{eff}}\left(3l^2 - 4a^2\right) \qquad 5.18$$

Horton and Tadros (1990) recommended the following method for deflection calculation for steel reinforced concrete masonry beams:

$$\Delta = \Delta_{cr}\left[1-\left(\frac{M_{cr}}{M_a}\right)^2\left(2-\frac{M_{cr}}{M_a}\right)\left(1-\frac{I_{cr}}{I_g}\right)\right] \qquad 5.19$$

In addition to the above mentioned methods, specimens were modeled in computer software named Response 2000, developed by Bentz (2000), given the stress-strain properties of the grouted masonry units, GFRP rods, steel rods and CFRP laminates.

Corresponding comparison of load-deflection characteristics of the specimens taking into account all the above mentioned methods as well as the outputs obtained from the software is shown in Table 5.2 and Figures 5.1 to 5.6

5.3 Curvature Analysis

5.3.1 Theoretical Curvature

In addition to the deflection comparisons, tested specimen's curvatures at different bending moment levels were compared as well, in order to better assess and compare the deformability characteristics of GFRP-reinforced concrete masonry beams.

Using different methods of I_{eff} predictions provided by ISIS Canada (2001) and CSA S304.1 (2004), curvature characteristics of the beams were evaluated:

$$\psi = \frac{M}{E_m I_{eff}} \qquad 5.20$$

5.3.2 Experimental Curvature

Moreover, the strains of the GFRP rods obtained from the recorded test data were utilized in a numerical evaluation to mathematically derive the curvature of the cross-section. Curvature was determined through numerical integration based on the actual stress-strain relationship of masonry assemblage proposed by Dhanasekar and Shrive (2002). During the process, some iterative solutions were needed. This numerical method was comprised of the following steps;

Curvature can be calculated using:

$$Radius = \frac{d-c}{\varepsilon_{frp}} \xrightarrow{therefore} \varphi = \frac{1}{Radius} = \frac{\varepsilon_{frp}}{d-c} \qquad 5.21$$

The only unknown in that equation is the height of the compressive block "c" which can be obtained using:

$$c = -\frac{\varepsilon_m}{\varepsilon_m + \varepsilon_{frp}} d \qquad 5.22$$

In the above equation, ε_m is the compressive strain corresponding to the outermost fiber of masonry. In order to determine ε_m equation of equilibrium of the cross-section is used which is:

$$T = C = b\int_0^c \sigma_m dy \qquad 5.23$$

Where, σ_m is the compressive stress in the depth of compression zone (from 0 to c) that can be defined based on Dhanasekar and Shrive (2002) as a function of compressive strain of masonry which varies linearly from 0 at neutral axis to ε_m at the other most fiber:

$$\sigma_m = f'_m(a\varepsilon^3 + b\varepsilon^2 + c\varepsilon + d) \qquad 5.24$$

Therefore, equilibrium equation can be solved for ε_m by substitution, for various load levels.

All of the outcomes obtained from those methods were later compared with the moment-curvature curves of the computer software Response 2000. Corresponding comparison of moment-curvature characteristics of the specimens taking into account all the above mentioned methods as well as the outputs obtained from the software is shown in Table 5.3 and Figures 5.7 to 5.13

5.4 Deformability

5.4.1 Introduction

Deformability can be identified as the structural member's ability to sustain large deformations and related to ductility since ductility as a measure of energy absorption and structural components resistance at inelastic load levels. Ductility of a reinforced masonry beam can be defined using a ductility factor which can be obtained from the ultimate to yield ratios of strains, curvatures, rotations and deflections. Conventional steel reinforced masonry elements absorb energy mainly through plastic deformation of the steel reinforcement. CSA S304.1 (2004) suggests under-reinforced masonry beam design to prevent brittle concrete controlled failure of the structural element and desired ductile failure of the element occurs through plastification of the internal steel rebar.

On the other hand, prediction of the deformability of GFRP-reinforced concrete masonry beams using the conventional assumptions tailored for steel reinforced elements can be misleading due to the linear stress-strain relationship of the FRP reinforcement until rupture. Although GFRP rods have higher ultimate capacities compared to steel

rebars, their low elastic modulus characteristics leads to large deformations which must be taken into account for the design of FRP-reinforced structural members.

In order to estimate the deformability of GFRP-reinforced concrete beams, ISIS Canada (2001) adopts the calculation of a deformability factor which is a ratio of ultimate curvature over curvature at serviceability stage. In this section, the deformations and ductility of the GFRP-reinforced concrete masonry beams were evaluated using several different approaches that exist for deformability and ductility estimation of FRP-reinforced concrete members. The applicability of these methods in deformability estimation of GFRP-reinforced concrete masonry beams is analyzed and discussed.

5.4.2 Curvature Related Deformability

ISIS Canada (2001) adopted the calculation of a deformability factor which is a ratio of ultimate curvature over curvature at serviceability stage:

$$DF = \left|\frac{\Psi_u M_u}{\Psi_s M_s}\right| \qquad 5.25$$

where:

Ψ_u = Curvature at ultimate load

Ψ_s = Curvature at serviceability load

Furthermore, this design guideline assumes that an FRP rod reaches its serviceability stage at 2000 micro strains. According to the guideline, the allowable deformability factor (DF) must be over 4 for rectangular cross-sections. Curvatures of the beams were calculated using the experimental strains of the GFRP rods that were further discussed in the preceding chapter of analytical modeling. Corresponding results are tabulated in Table 5.4

5.4.3 Energy Related Ductility

Total energy absorbed by the specimens was calculated using the area under the load-deflection curves that were plotted using the experimental data. All the specimens excluding the GFRP-reinforced concrete masonry beam F-3-1#13-C were unloaded as soon as the compressive failure occurred at the mid-span as the load and deflection readings were still being monitored. Unloading section of the load-deflection curve represents the border line of the areas namely inelastic energy consumed prior to failure and elastic energy released after failure. While the area on located on the left side of the unloading curve represents the consumed inelastic energy, area located on the right side of the unloading curve represents the released elastic energy. Ductility index of the FRP-reinforced concrete beams were evaluated by Jeong, S. (1994) utilizing the following equation:

$$\mu = 0.5\left[\frac{E_{total}}{E_{elastic}} + 1\right] \qquad 5.26$$

This approach suggests that a ductility index value higher than 2.5 yields that the specimen exhibits ductile behaviour. On the other hand, Grace et al. (1998) reported that the inelastic to total absorbed energy ratio of the specimens should be higher than 75% in order to have ductile behaviour and should be 70% for a semi-ductile behaviour. Corresponding charts and plots showing comparisons and visual explanations of the methods can be examined at Table 5.5.

5.5 Discussions

Since coefficients such as α_1, β_1 and compressive resistance of the masonry assemblage (f'_m) have a great influence on the estimated moment resistances of the tested specimens, their moment resistances were calculated using different values of α_1, β_1 and f'_m suggested by design guidelines CSA S304.1 (2004) and ISIS Canada (2001). Findings were later compared with the test results. Flexural resistance of the section was calculated using two different f'_m, one of which was obtained from the average compressive resistances of the prisms loaded normal to their bed joints. This average strength was later corrected by using the factor χ taken as 0.5 as recommended by CSA 304.1 (2004) Clause 10.2.6. The other f'_m value was obtained by testing prisms loaded parallel to their bed joints.

CSA S304.1 (2004) was able to predict the moment resistance of the steel reinforced control beam S-3-1-15M with 8% error which is reasonable considering the fact that the compressive strength of the masonry assemblage can easily be influenced by the quality of the labor and materials. Using different f'_m values did not result with a noticeable change in the sectional resistance. Response 2000 estimated the resistance of the section correctly as well, having an error of 3%. For steel reinforced beam, f'_m taken as 6.9MPa showed better accordance with the test results.

ISIS Canada (2001) was able to predict the flexural resistances of the GFRP reinforced specimens with minor percentages of errors. Although in case of GFRP reinforced beams, f'_m taken as 6.9 MPa showed better accordance with the test results, While beam F-3-1#19-C exceeded its expected flexural capacity by 15% , beam F-3-2#19&1#16-C, having the highest reinforcement ratio among the other GFRP reinforced

beams, was able to reach 83% of its expected flexural capacity.. Response 2000 estimation of beam F-3-1#19-C was closer to the predictions of ISIS method. Beam F-2-2#19 could not reach the expected ultimate moment since the beam prematurely failed in shear at a much lower load.

As another qualitative comparison, load-deformation relationships of the beams were analyzed and compared. In case of GFRP-reinforced beams, it was observed that the numerical methods used to calculate the deflection patterns over-estimated the deflections of the individual beams. Overall results of the calculations showed that CSA S304.1 (2004) and ISIS Canada (2001) methods yielded similar predictions since they are differentiated by a factor β_b and for GFRP-reinforced concrete masonry beams this factor was in the vicinity of unity. As expected, the stiffness of the GFRP-reinforced beams increased as their reinforcement ratio increased meaning that they experienced lower deformations even at higher loads.

It was also observed that Response 2000 tends to under-estimate the maximum deflections of the GFRP-reinforced masonry beams, while estimating the pattern of the load-deflection curve correctly.

As expected, ductility index and related deformability of the beams decreased as the reinforcement ratios of the cross-section increased however even the specimen with the highest reinforcement ratio went through large deformations before failure in the compression zone. Specimen F-3-2#19&1#16-C had a ductility index of 5.9 which was still within the allowable limits.

On the other hand, by looking at the experimental unloading curves of the specimens, dissipated inelastic and elastic energies of the tested GFRP-reinforced

concrete masonry beams were calculated and the inelastic to total absorbed energy ratio of the specimens was observed to be in the vicinity of 70%

Specimen F-3-1#13-C could not be unloaded since the GFRP bar ruptured as expected, therefore excluded from the calculations. Beam F-2-2#19 that was failed in shear could not be included either.

Table 5.1 Predicted moment resistances of the reinforced masonry beam sections using different methods

Beam	Mn Experimental (kN.m)	CSA* (kN.m)	ISIS* (kN.m)	ISIS** (kN.m)	Response 2000* (kN.m)
S-3-1-15M	53.6	49.2	-	-	52.2
F-2-2#19	19.2	31.3	33.5	27.3	34.1
F-2-2#16-C	28.3	28.1	30.4	24.6	31.7
F-3-1#13-C	46.4	47.3	46.8	46.4	30.4
F-3-1#19-C	69.3	55.3	59.2	49.1	54.8
F-3-2#16-C	63.6	62.7	67.1	55.4	68.2
F-3-2#19&1#16-C	69.4	78.1	83.5	68.4	79.4
S-3-1-15M-C-CFRP	88.7	67.3	70.0	62.1	72.1

*f'm = 6.9 MPa, **f'm = 6.0 MPa

Table 5.2 Predicted deflections of the reinforced masonry beam using different methods

Beam	Experimental result (mm)	CSA (mm)	ISIS (mm)	Horton and Tadros (mm)	Response 2000 (mm)
F-2-2#16-C	35.9	40.3	40.4	16.1	16.3
F-3-1#13-C	50.5	73.8	74.2	95.4	28.3
F-3-1#19-C	68.2	67.2	67.2	68.3	30.6
F-3-2#16-C	28.6	45.9	45.9	45.8	30.7
F-3-2#19&1#16-C	16.3	35.2	35.2	34.5	25.2
S-3-1-15M-C-CFRP	25.9	18.3	-	17.7	21.0

Table 5.3 Predicted curvatures of the reinforced masonry beam using different methods

Beam	Experimental result ($x10^{-6}$/mm)	ISIS (mm)	Response 2000 (mm)
S-3-1-15M-C	26.16	-	26.40
F-2-2#16-C	37.43	19.20	27.32
F-3-1#13-C	25.56	27.44	20.43
F-3-1#19-C	24.68	19.14	18.73
F-3-2#16-C	12.44	13.73	20.72
F-3-2#19&1#16-C	10.82	10.31	16.87
S-3-1-15M-C-CFRP	33.07	-	27.72

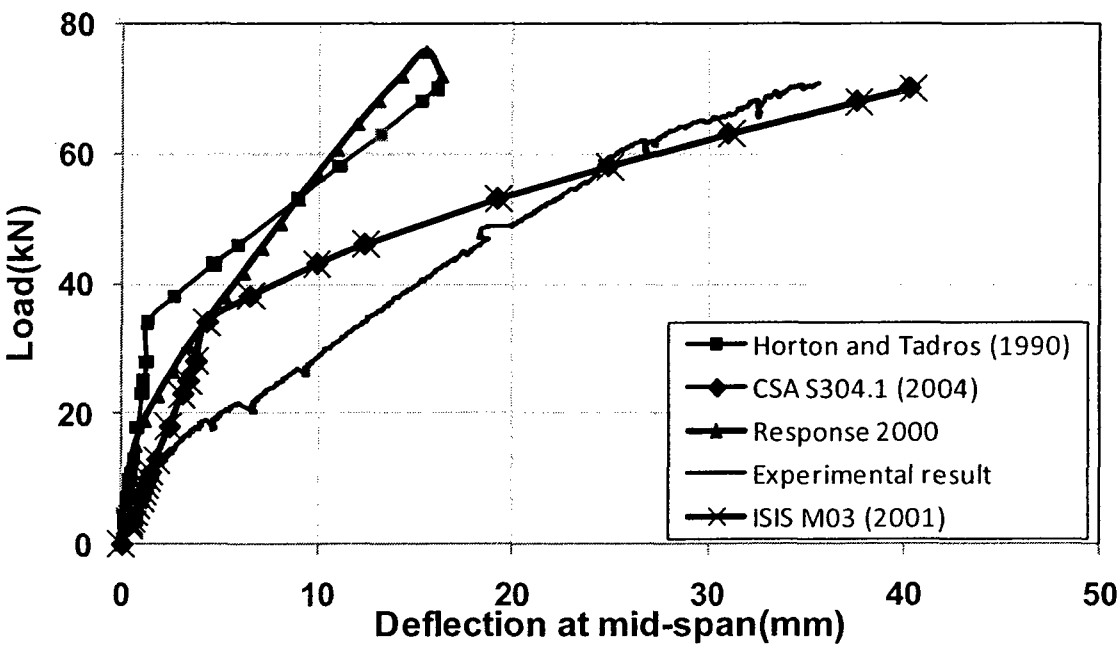

Figure 5.1 Load-deflection predictions for beam F-2-2#16-C

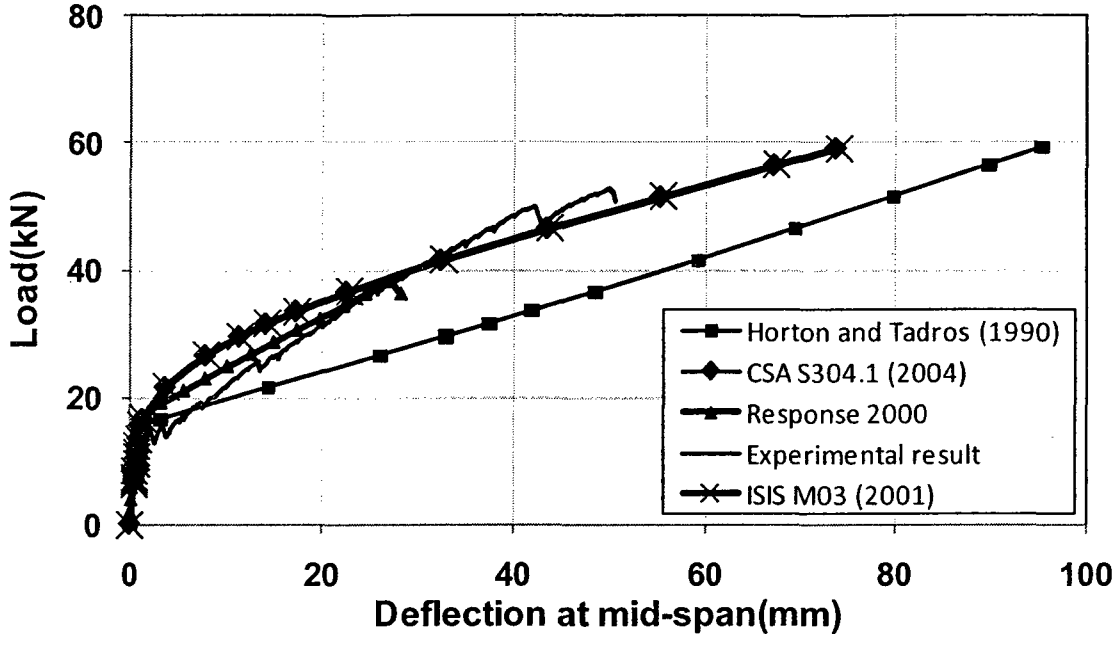

Figure 5.2 Load-deflection predictions for beam F-3-1#13-C

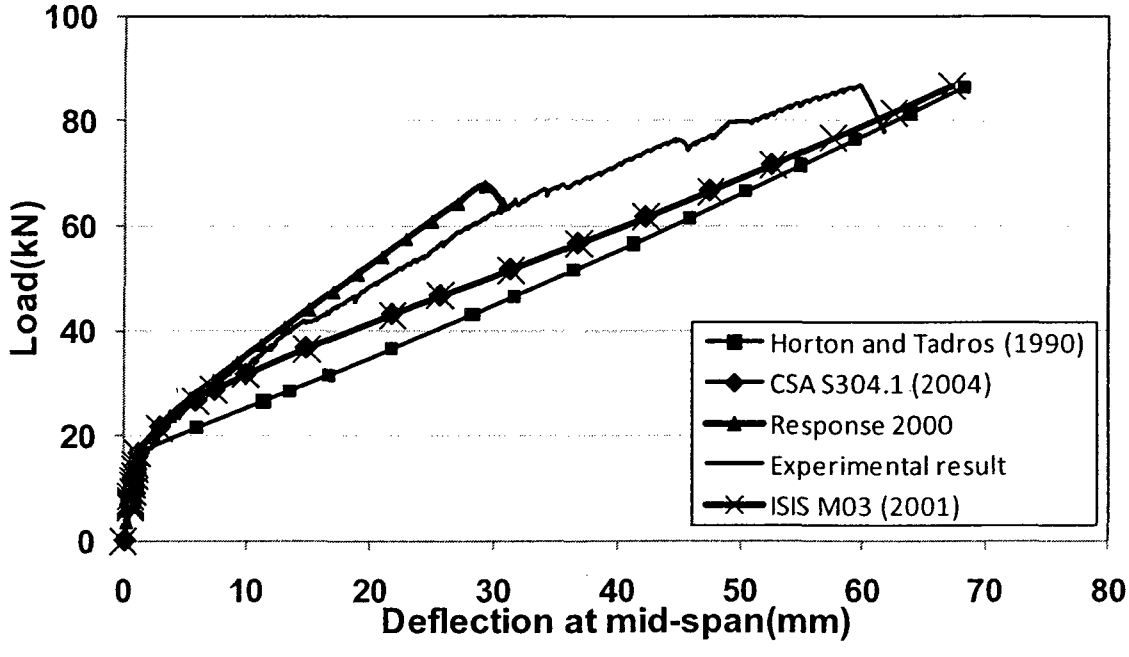

Figure 5.3 Load-deflection predictions for beam F-3-1#19-C

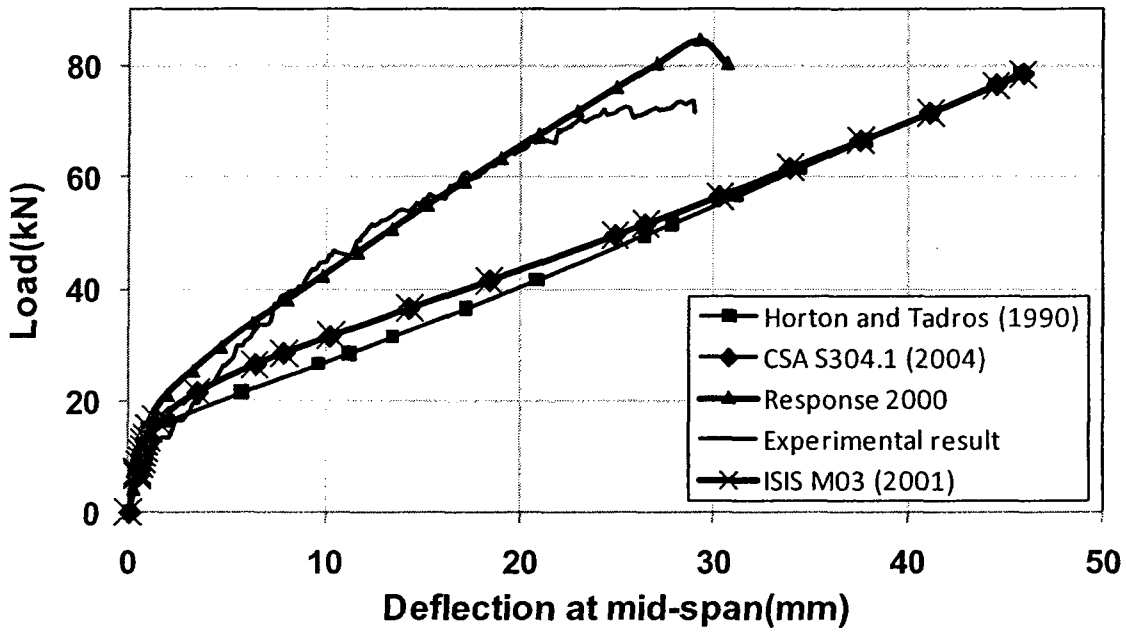

Figure 5.4 Load-deflection predictions for beam F-3-2#16-C

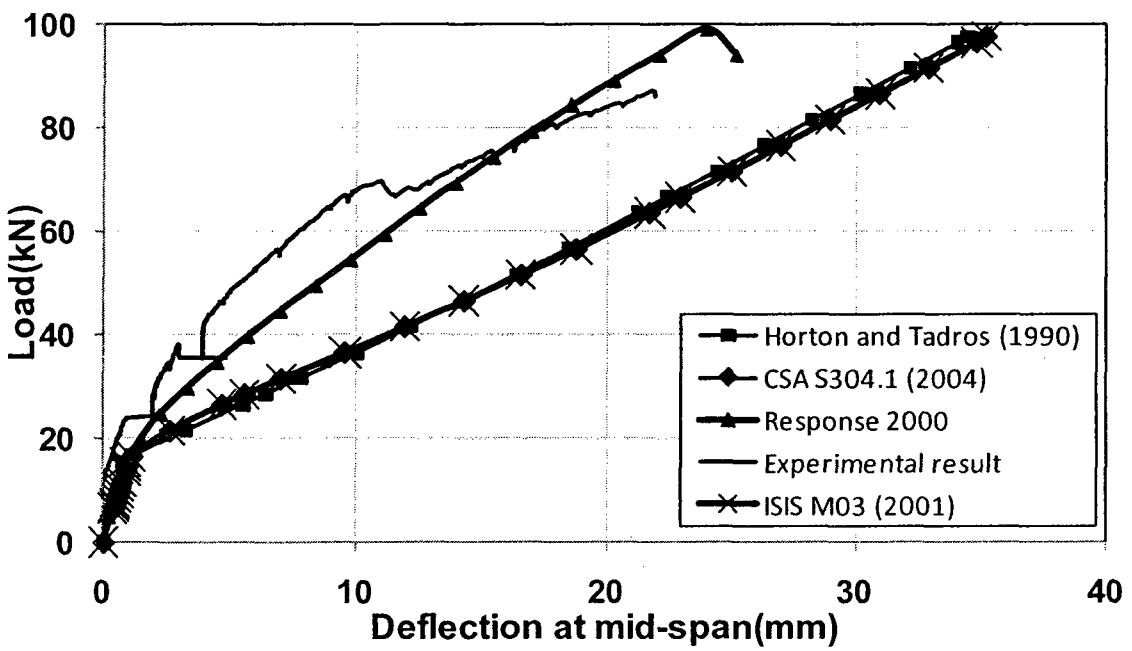

Figure 5.5 Load-deflection predictions for beam F-3-2#19&1#16-C

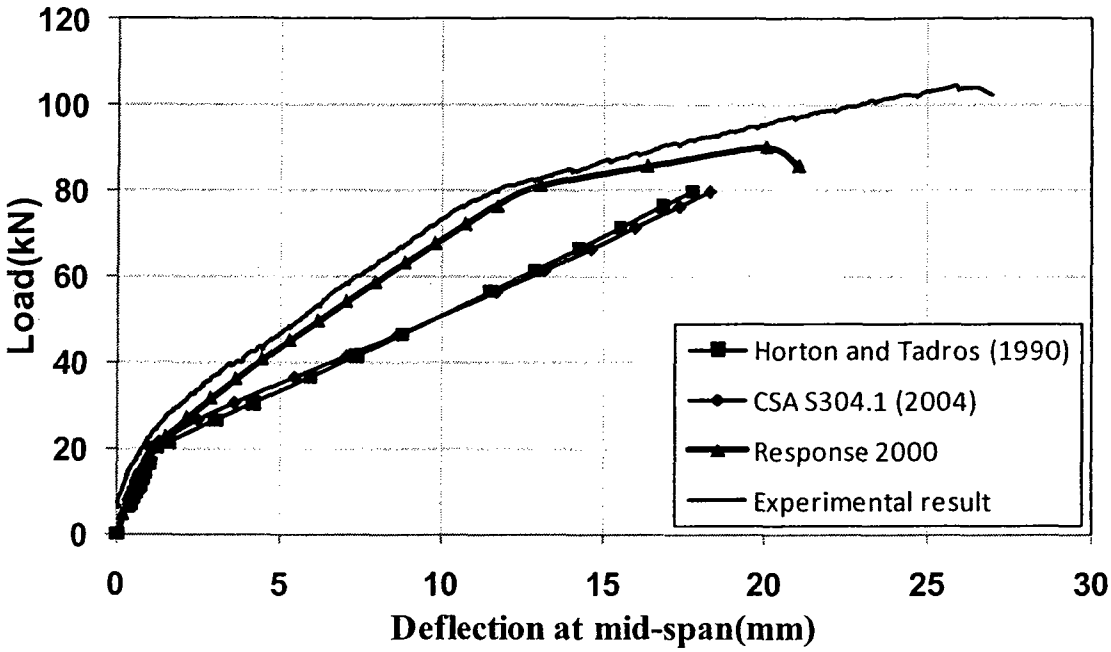

Figure 5.6 Load-deflection predictions for beam S-3-1-15M-C-CFRP

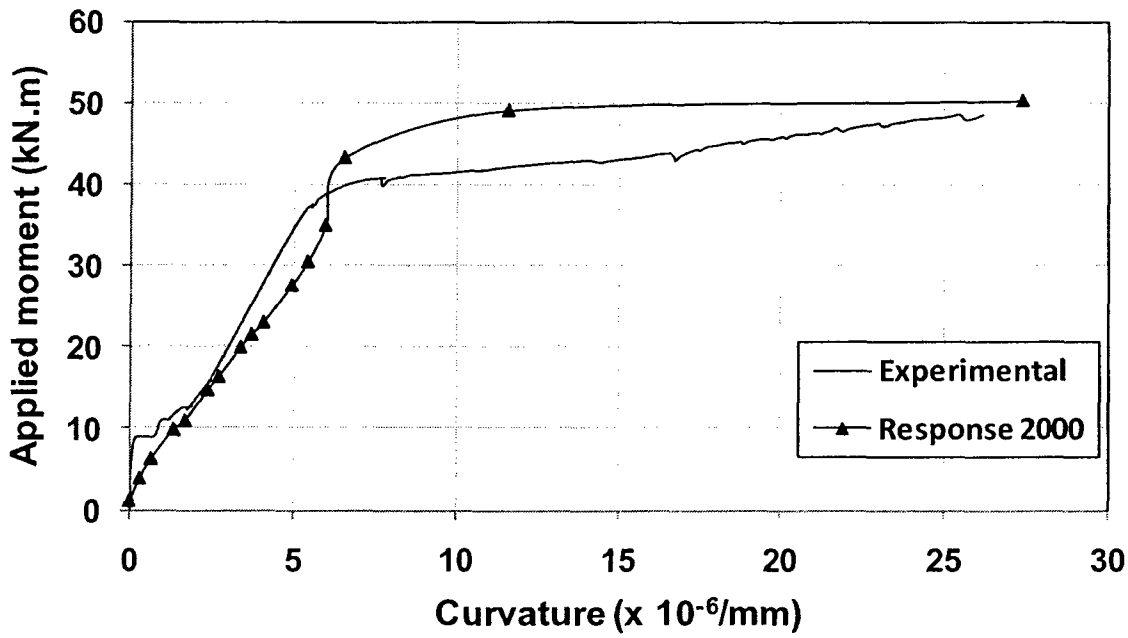

Figure 5.7 Moment-curvature predictions for beam S-3-1-15M-C

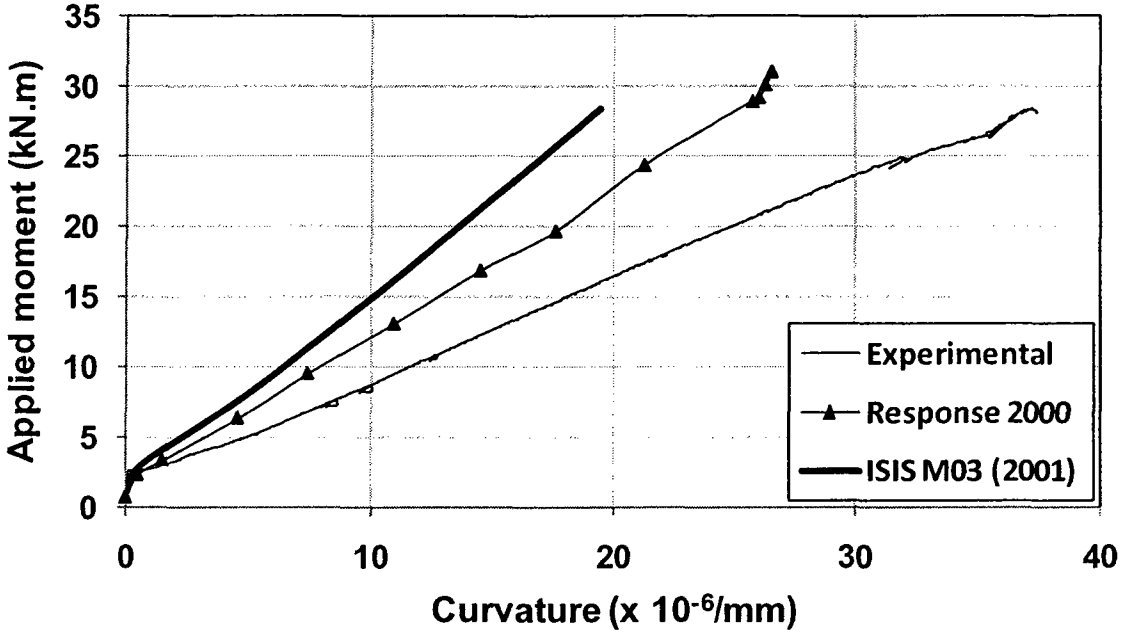

Figure 5.8 Moment-curvature predictions for beam F-2-2#16-C

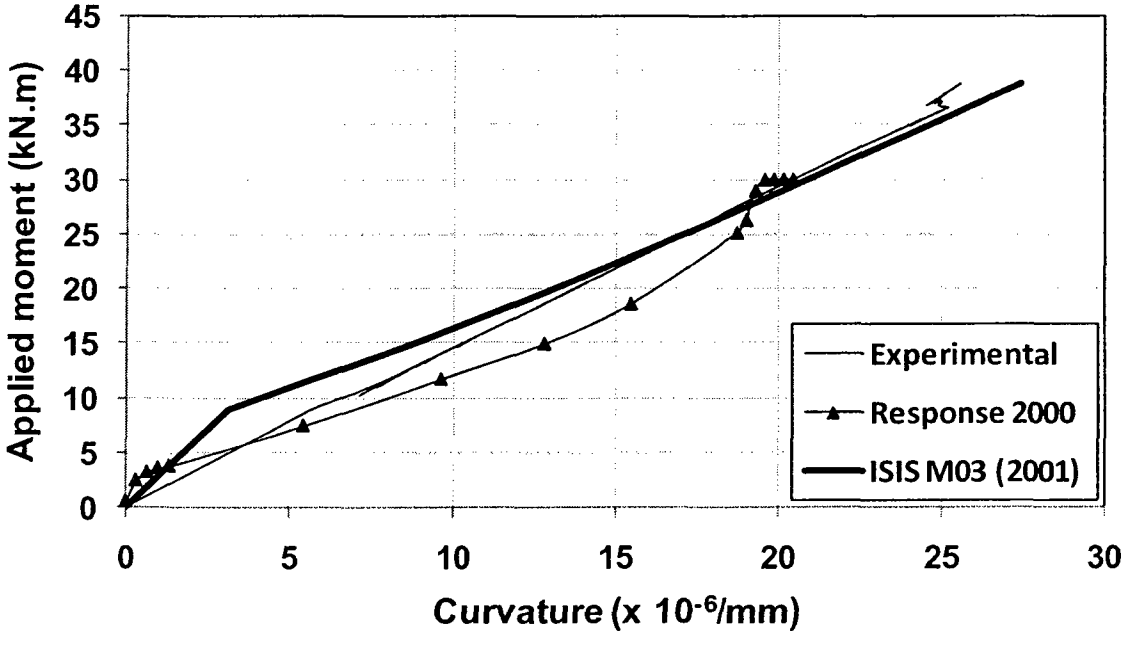

Figure 5.9 Moment-curvature predictions for beam F-3-1#13-C

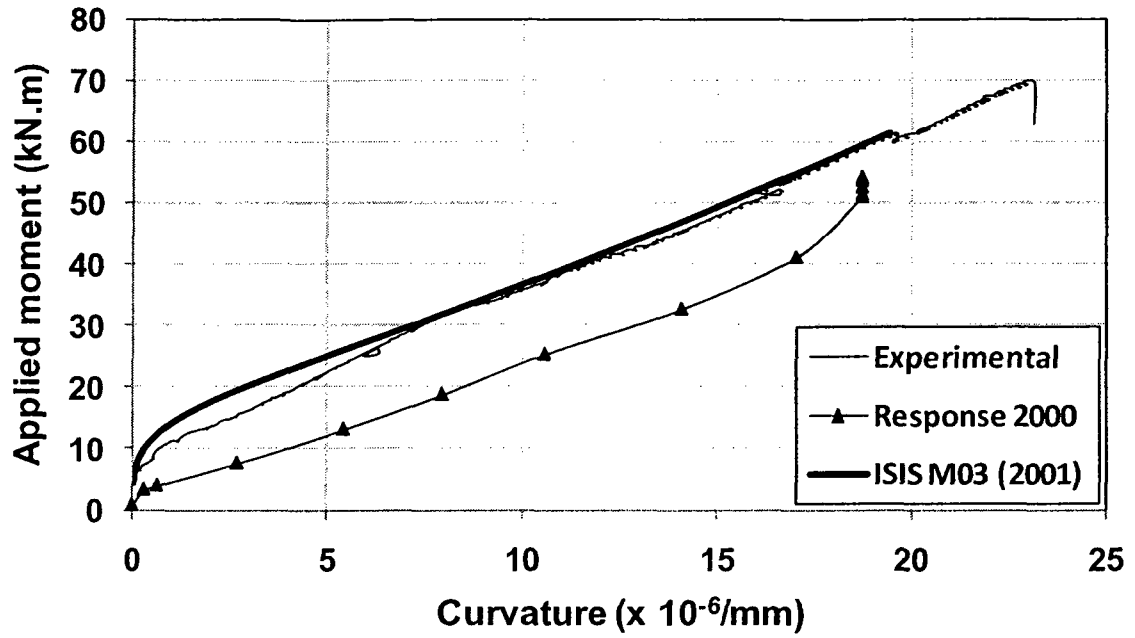

Figure 5.10 Moment-curvature predictions for beam F-3-1#19-C

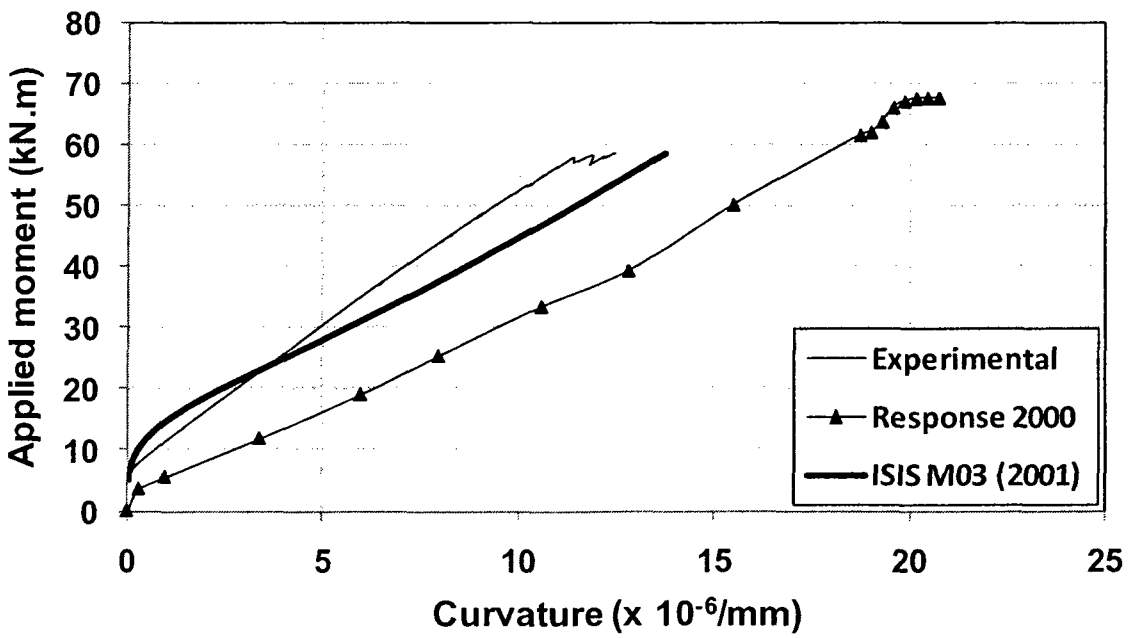

Figure 5.11 Moment-curvature predictions for beam F-3-2#16-C

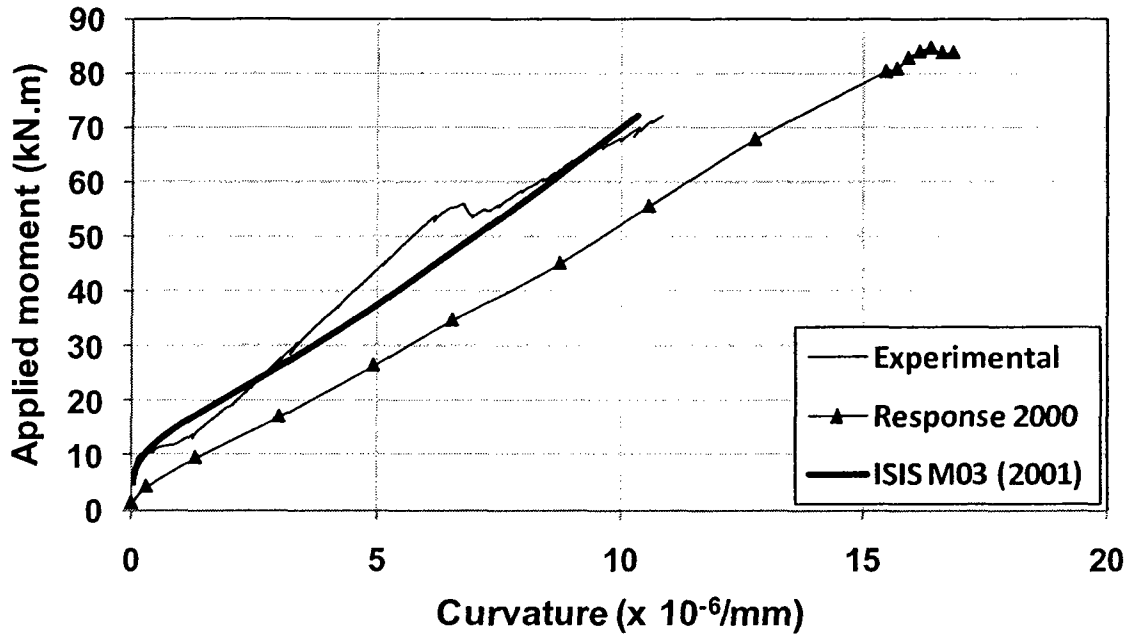

Figure 5.12 Moment-curvature predictions for beam F-3-2#19&1#16-C

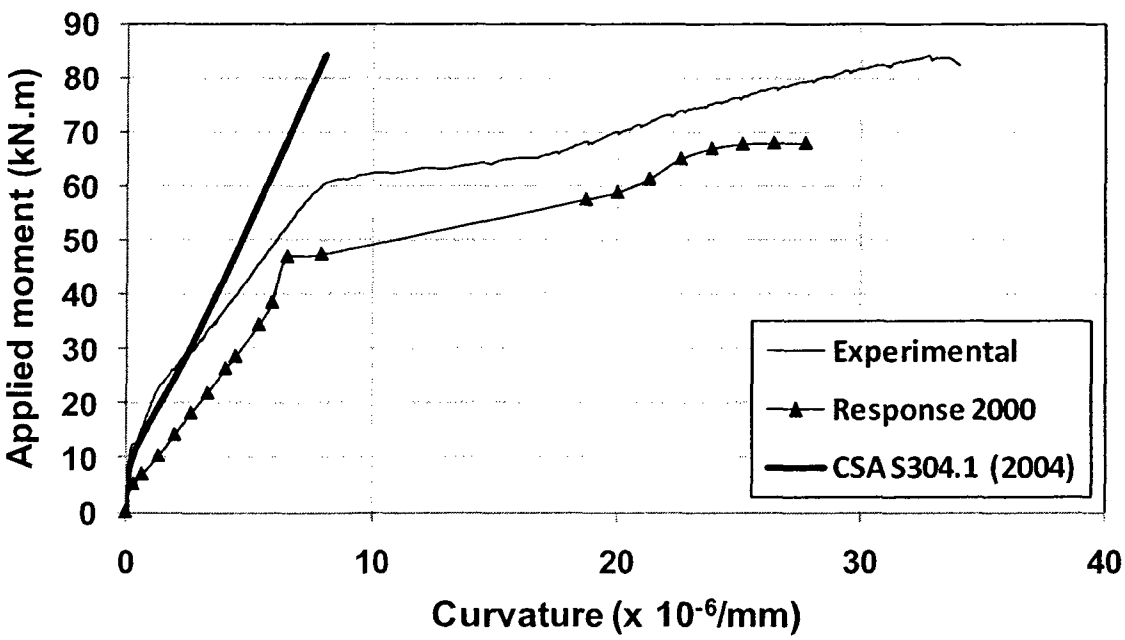

Figure 5.13 Moment-curvature predictions for beam S-3-1-15M-CFRP-C

Table 5.4 Curvature based deformability factor of GFRP-reinforced and CFRP-strengthened concrete masonry beams

Beam	M_s	ψ_s	M_u	ψ_u	Ductility Index
F-2-2#16-C	5.8	6.3	28.1	37.4	28.8
F-3-1#13-C	8.9	5.6	42.2	26.3	21.9
F-3-1#19-C	18.8	3.9	69.3	23.1	22.0
F-3-2#16-C	24.9	3.8	58.4	12.4	7.6
F-3-2#19&1#16-C	34.3	3.9	71.8	10.8	5.9

Table 5.5 Energy based deformability factor of GFRP-reinforced and CFRP-strengthened concrete masonry beams

Beam	Inelastic Energy	Elastic Energy	Total Energy	Inelastic / Total	Ductility
F-2-2#16-C	3.9	1.5	5.4	72%	Semi-ductile
F-3-1#19-C	3.2	1.4	4.6	70%	Semi-ductile
F-3-2#16-C	3.1	1.3	4.4	70%	Semi-ductile
F-3-2#19&1#16-C	3.3	1.2	4.5	73%	Semi-ductile
S-3-1-15M-C-CFRP	3.3	1.3	4.6	71%	Semi-ductile

CHAPTER 6

LONGITUDINALLY-DRILLED CONCRETE MASONRY BLOCKS

6.1 Introduction

Grout filled hollow concrete units are stronger when axially loaded normal to the bed joints and tend to fail at lower stresses if the axial load is parallel to the bed joints. Keeping this characteristic of the hollow masonry units in mind, grout filled masonry units with holes going through their webs are expected to be stronger compared to regular hollow units when axially loaded parallel to the bed joints. This is due to their continuous cylindrical grout cores acting against the compression force. In addition to this advantage, individual concrete masonry units are lighter than regular hollow concrete units allowing them to be a lot easier to handle compared to their predecessors.

In order to have masonry units with holes going through their webs, more than 100 hollow concrete blocks were drilled using a core driller and carbide drill bits of different diameters. Sufficient number of masonry units with 2", 3" and 4" holes were prepared in order to have five compressive prisms for each hole size. An extra set of masonry units with all three different sizes of hole was drilled to be tested for fragility (Table 6.3).

Pictures of the setup prepared for the core driller and sample drilled masonry units can be seen in Figures 6.1, 6.2 and 6.3.

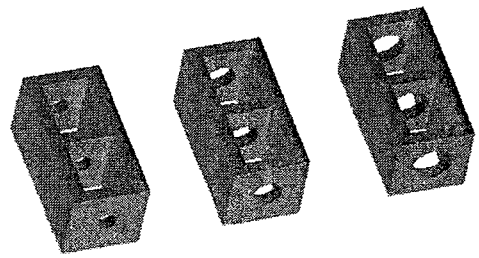

Figure 6.1 Schematic 3D view of the drilled concrete masonry units

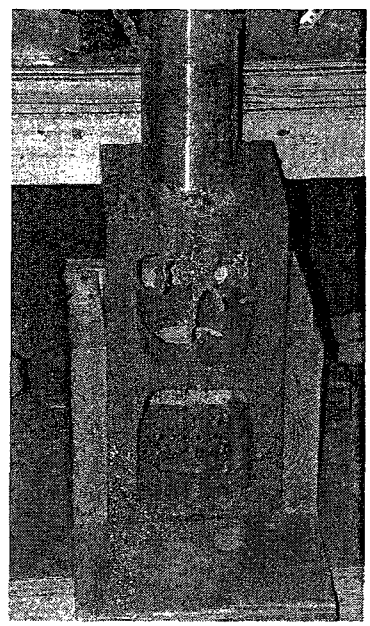

Figure 6.2 Drilling the holes into a concrete masonry unit using 4" carbide mesh

Table 6.1 Compressive strength test data of the grout cylinders

Cylinder Number	Age (days)	Failure Load(kN)	Compressive Strength(MPa)
1		144.5	18.4
2		128.5	16.4
3	28	136.7	17.4
4		137.8	17.5
5		129.1	16.4

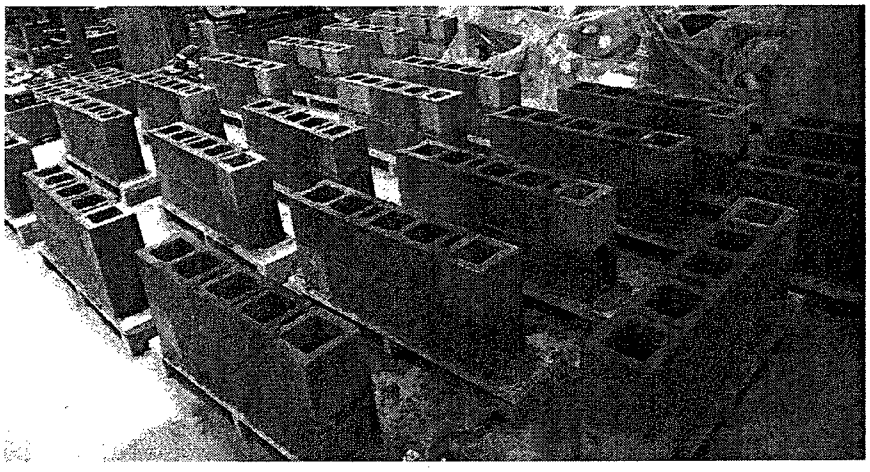

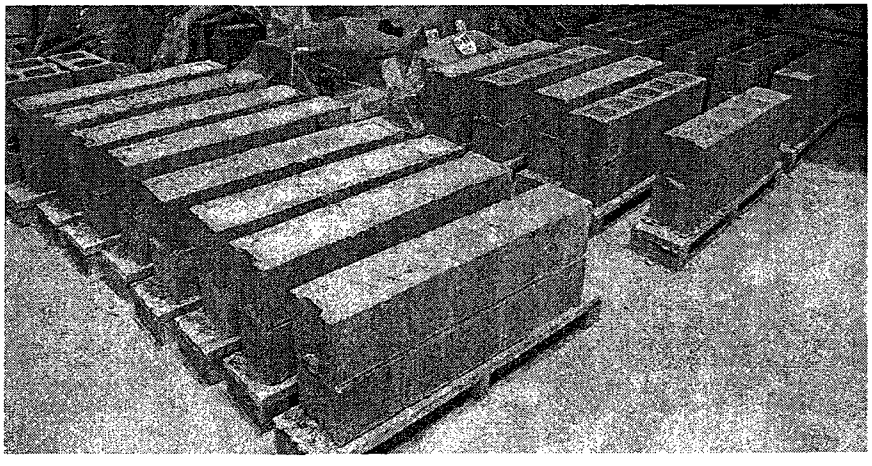

Figure 6.3 Construction of the prisms

6.1.1 Compressive Strength of Longitudinally-Drilled Blocks Loaded Parallel to the Bed Joint

One block wide and five-block high unreinforced grouted masonry prisms were prepared using longitudinally-drilled masonry units to be tested under axial load parallel to their bed joints. In total twenty prisms were constructed. Five of the prisms were built using masonry blocks with 2" holes, five were built using 3" hole blocks and ten other were built using 4" hole masonry units. Among the ten 4" hole masonry unit prisms, five prisms had 150 mm long conventional steel 10M reinforcing bars passing through the web holes located at mortar joints in order to examine the effect of compression reinforcement on the strength of prisms. Identical test setup was used as the previously tested compressive prisms. Detailed results of the prism tests are shown in Table 6.2

Table 6.2 Comparison of compressive strengths of masonry prisms

	Strength Normal to the Bed Joint	Strength Parallel to the Bed Joint				
Specimen	Control (MPa)	Control (MPa)	2" Holes (MPa)	3"Holes (MPa)	4"Holes (MPa)	4"+Steel (MPa)
1	13.4	6.5	10.0	11.6	11.2	10.7
2	13.3	5.8	7.8	11.7	9.6	9.0
3	14.6	6.1	10.7	12.2	9.5	9.7
4	13.2	5.7	9.0	12.5	8.3	8.7
5	13.8	-	7.6	13.7	10.2	10.6
Average	**13.7**	**6.0**	**9.0**	**12.4**	**9.8**	**9.7**

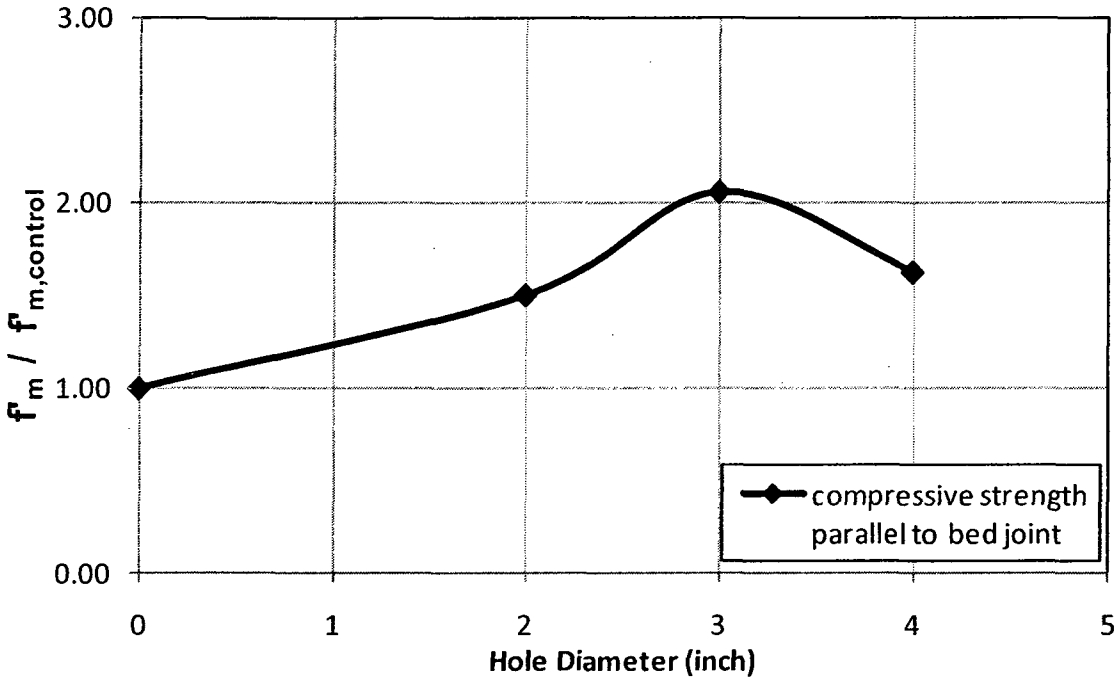

Figure 6.4 Relationship between the compressive strength of the masonry assemblage and the hole diameter

Table 6.3 Fragility comparison of the proposed masonry units

	Drop Height (meters)		
Hole Diameter (inches)	0.75	1.0	1.5
0	Intact	Intact	Broke
2"	Intact	Fracture	Broke
3"	Intact	Fracture	Broke
4"	Intact	Broke	Broke
Lintel	Broke	Broke	Broke

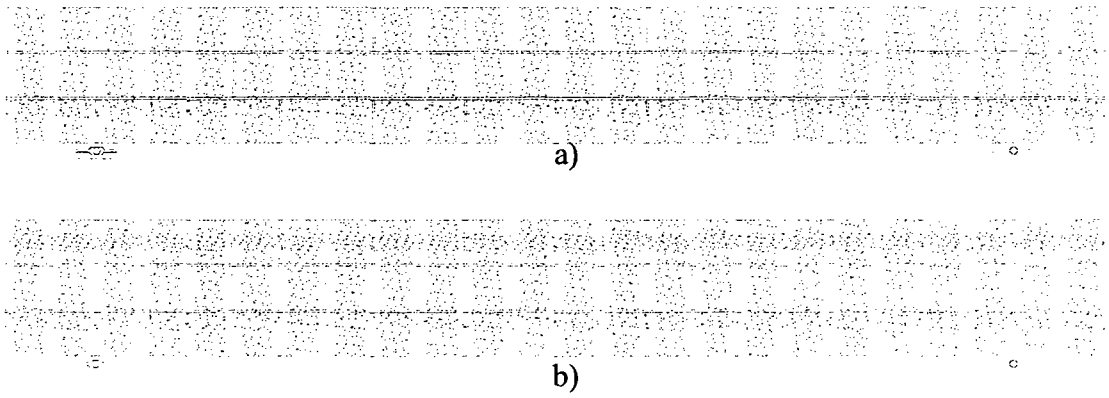

Figure 6.5 a) Schematic elevation view of a reinforced masonry beam, demonstrating the orientation of the grouted areas using regular concrete masonry units b) Schematic elevation view of a reinforced masonry beam, demonstrating the orientation of the grouted areas using longitudinally-drilled concrete masonry units at the top course.

6.2 Discussions

Tests conducted on the compressive strength prisms loaded parallel to their bed joints proved the following:

- As expected, although prisms with 2" grout cores showed better compressive strength than ones without holes, they failed at lower loads compared to the other specimens with wider grout cores. The common failure mode was face shell separation and conical break. On the other hand, even though these prisms were the weakest in compression with an average compressive stress of 9.0 MPa, their compressive strength was still 50% higher than the control prisms that were prepared using regular concrete masonry blocks. Tested specimens after failure are shown in Figure 6.6
- Although prisms with 4" grout cores were able to exceed the compressive resistance of 2" grout core specimens, they unexpectedly failed at lower stresses than specimens with 3" grout cores. Average compressive strength of the prisms

was 9.8 MPa which is 63% higher than the capacity of the control specimens. The common failure mode of the all five specimens was face shell separation. Visible cracks started to develop on the surface at early stages of loading. Cracks gradually widened as the loading continued and eventually the specimen failed as one of the masonry unit's shell separated. By looking at the test results, it was concluded that the 4" holes passing through the webs of the concrete masonry units, decreased the compressive resistance of the block in the direction of the loading. Addition of 10M steel reinforcing bars to the head joints between the blocks changed neither the compressive stress capacity nor their failure types. Tested specimens after failure are shown in Figures 6.8 and 6.9

- Prisms having 3" grout cores exhibited a relatively better performance than rest of the specimens. The average compressive strength was 12.4 MPa, demonstrating more than 100% increase in the compressive resistance when compared to the control prisms. Therefore it was proven that the compressive strength of the assembly not only increased significantly, but also approached to the compressive strength of prisms loaded normal to their bed joints. Splitting and separation of the face shells was not experienced. In general, deep diagonal and conical shear cracks developed on the surface of the specimens prior to failure. It was concluded that the optimal core size for the tested concrete masonry blocks with dimensions 390x190x190 mm is 3". Tested specimens after failure are shown in Figure 6.7

- 3" grout cores passing through the concrete masonry blocks provide:
  1) Improved compressive strength (f'_m) of the reinforced concrete masonry beams up to 100%, which accordingly increases the flexural capacity of the section significantly,
  2) Increased workability due to the reduced weight of the concrete masonry units(16.9 kg vs. 15.5 kg),
  3) Improved bonding through the head joints between the masonry units due to the grout cores linking the masonry units (Figure 6.5),
  4) Elimination of several masonry unit types such as lintel blocks and blocks with grooves for reinforcement, leading to a facilitated construction procedure and internal longitudinal reinforcement can easily be placed in the circular cores passing through the webs of the concrete masonry units.

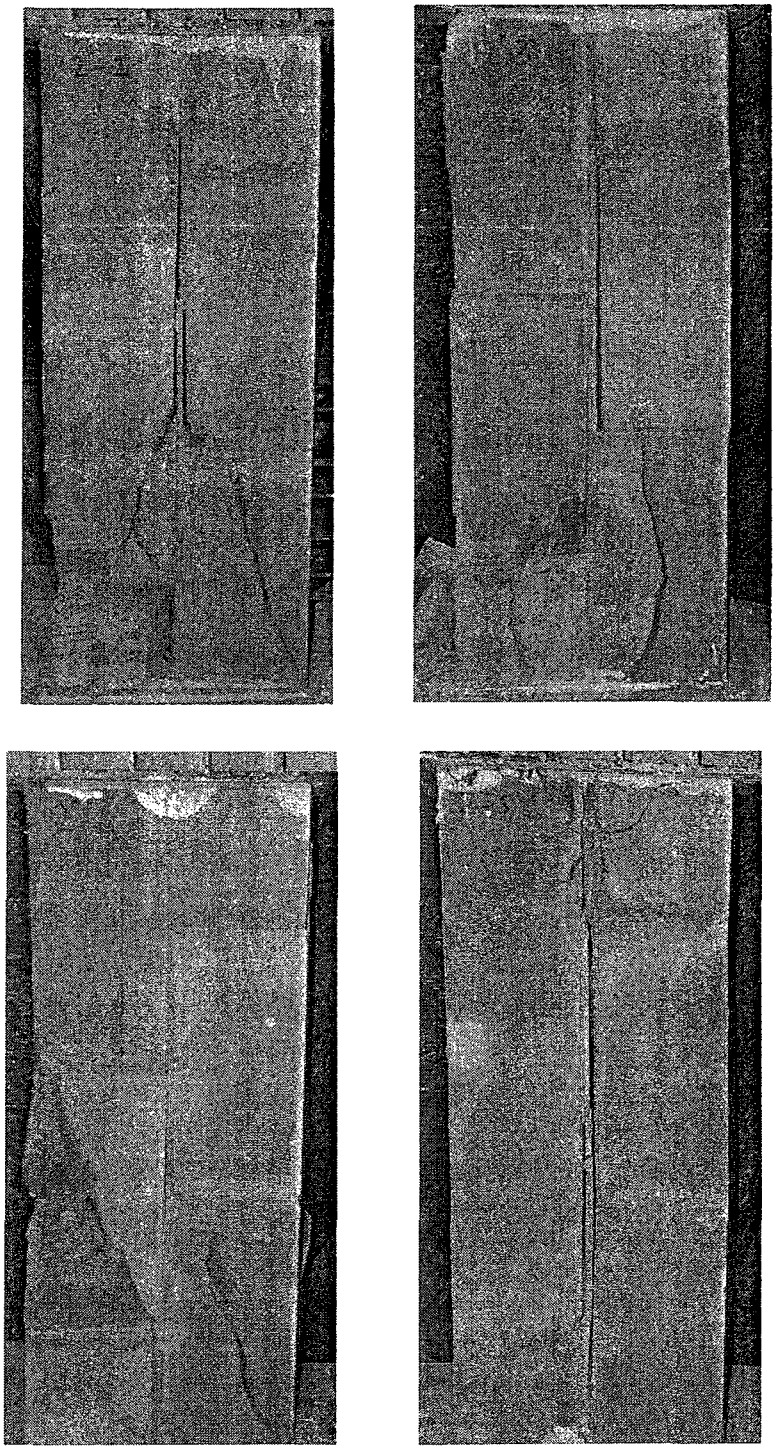

Figure 6.6 Failed compressive masonry prisms with 2" cores, loaded parallel to their bed joints.

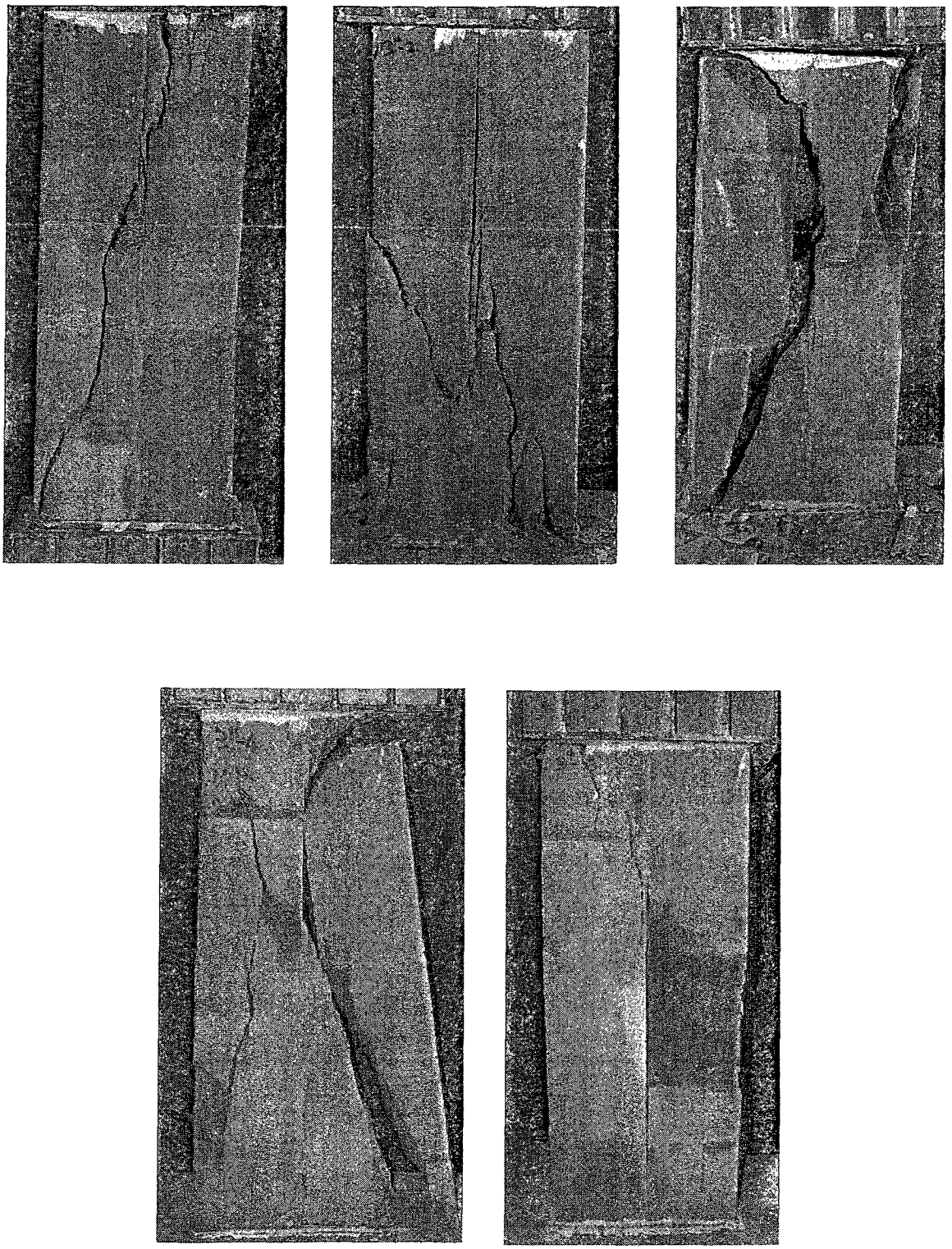

Figure 6.7 Failed compressive masonry prisms with 3" cores, loaded parallel to their bed joints.

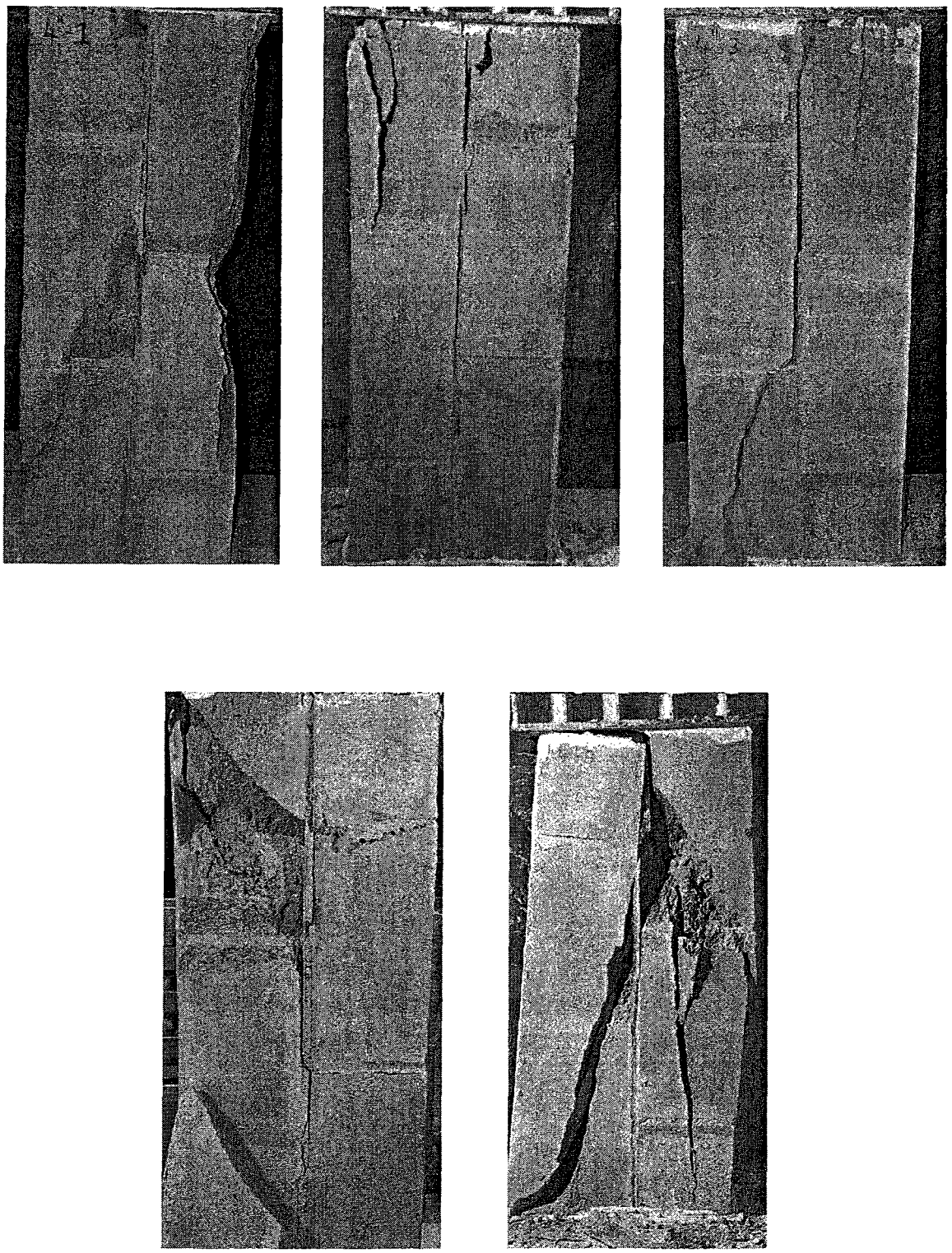

Figure 6.8 Failed compressive masonry prisms with 4" cores, loaded parallel to their bed joints.

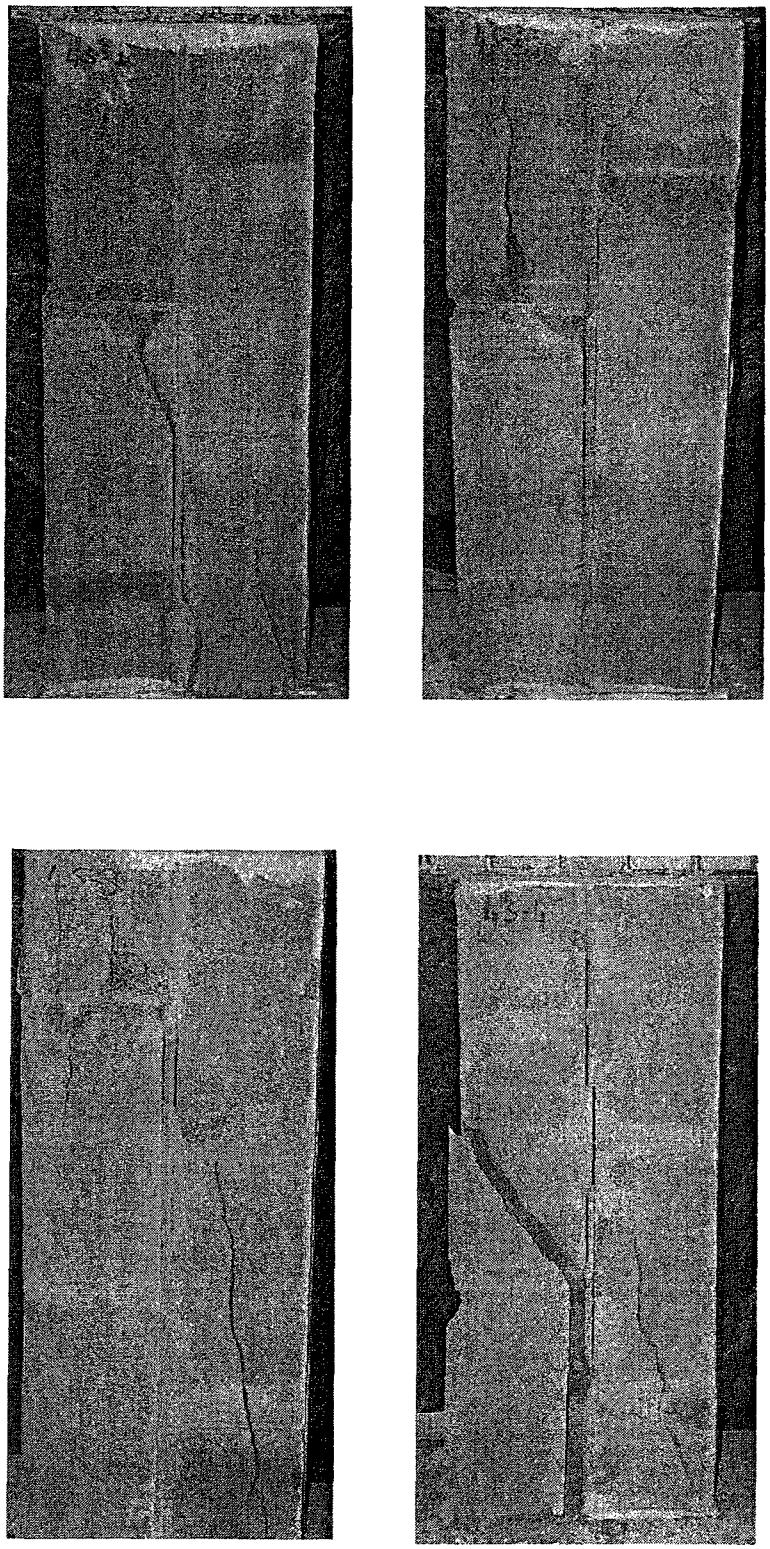

Figure 6.9 Failed compressive masonry prisms with 4" cores having 10M steel rebars at the head joints, loaded parallel to their bed joints.

CHAPTER 7

CONCLUSIONS AND RECOMMENDATIONS

7.1 Summary

Masonry is one of the ancient construction methods and has been used by several civilizations for centuries. Beams in masonry construction are mostly utilized as bond beams or lintel beams. They are located at the roof level or at floor levels and may have multiple functions such as tying the structure around its perimeter, transferring the diaphragm action of the roof to the shear walls and spanning over the openings in the walls supporting the gravity loads coming from above. The contemporary limit states design (LSD) design guideline for reinforced masonry structures such as CSA S304.1 (2004) does not permit the use of unreinforced masonry beams since tensile strength of masonry alone cannot be relied upon. Although conventional steel reinforcement solves the tensile strength problem of the grouted masonry assemblage, design difficulties may be encountered with conventional steel bars due to the limited width of the masonry units. Considering the under-reinforced design principle of the reinforced concrete, design of larger beam cross-sections is inevitable for most of the cases, giving rise to higher material and labor costs. In addition, corrosion problem of the conventional steel reinforcement gives rise to high maintenance costs in the long run.

The primary objective of this study was to introduce and implement FRP as a reinforcing and strengthening method to the design of reinforced concrete masonry beams and to verify the flexural performance of the GFRP-reinforced and CFRP-strengthened masonry beams. FRP-reinforced concrete has been extensively examined by

researchers in the past decades and has been identified as a promising alternate construction material for reinforcing and strengthening reinforced concrete. FRP reinforcement comes along with several significant advantages over steel such as high durability, non-corrosiveness, high strength-to-weight ratio and resistance against fatigue. Moreover, unlike conventional steel reinforcement, FRP uses over-reinforced design approach meaning that there will not be any upper limit for reinforcement ratio as long as the deflections and deformability of the beams meet the design guidelines of ISIS Canada (2001) and ACI 440-2R (2002).

In addition, existing ancient structures constructed using unreinforced masonry do not meet the requirements of current buildings codes, mostly have been severely deteriorated and are prone to failure when subjected to excessive lateral loads such as seismic loads and wind loads. Nowadays, CFRP sheets are being used in the construction industry in order to rehabilitate, retrofit and strengthen existing reinforced concrete structural members. CFRP exhibits similar properties as other fiber reinforced polymers such as high strength-to-weight ratio, non-corrosiveness and high durability.

In order to fulfill the objectives, nine reinforced masonry beams were constructed to be tested. Two beams with clear spans of 2.4 m had two courses of hollow concrete masonry units, and the remaining seven beams with clear spans of 4.0 m had three courses. Three masonry beams were reinforced using conventional steel rebars two of which were considered as the control specimens, while the third one was strengthened using two layers of CFRP sheets that were externally bonded to both sides of the beam. The remaining six beams were internally reinforced using GFRP rods with different reinforcement ratios. Comparisons were conducted between the GFRP-reinforced and

steel-reinforced control beams as well as CFRP-strengthened and steel-reinforced control beam with regard to the flexural capacity, deformation and strains of the tested specimens. Using the outcomes of the experimental and analytical studies, the performance of GFRP-reinforced masonry beams in flexure as well as the efficiency of CFRP sheets in strengthening existing steel-reinforced masonry beams was evaluated.

As the tests on the full-scale reinforced concrete masonry beams were completed, insufficient compressive resistance of the grouted masonry units in the direction parallel to their bed joints was highlighted by the performance of the tested beams. In order to improve the masonry assemblages compressive stress (f'_m) which is directly related to the moment resistance of the section, additional compressive prisms were prepared using concrete masonry units having 2", 3" and 4" drilled cores passing through their webs. Comparisons were conducted between the compressive resistances of the tested masonry prisms axially loaded both in the direction parallel and normal to the bed joints, accompanied by proposal of a new block type that has the potential to increase the flexural capacity of the reinforced concrete masonry beams.

7.2 Conclusions

The following conclusions were drawn from the experimental and analytical analysis and comparisons conducted on the tested full-scale GFRP-reinforced and CFRP-strengthened concrete masonry beams:

1. As anticipated, cross-sectional moment resistance and stiffness of the reinforced concrete masonry beams significantly improved as the internal GFRP reinforcement ratio increased.

2. GFRP over-reinforced specimens failed due to compressive failure of the top masonry course at the constant moment region. During each test, compression zone failures started with crushing of the mortar joints (head joints) at mid-span. As the load increased, cracks on both faces of the blocks widened and the block shells eventually separated resulting with a significant drop in the load resistance capacity of the specimen.

3. The flexural resistance of the conventional steel reinforced beam was predicted with 8% of error based on the f'_m value of 6.9 MPa.

4. For the majority of the GFRP-reinforced full-scale masonry beams, experimental results had good agreement with analytical method described in ISIS Canada (2001) while having minor percentages of errors assuming f'_m value of 6.9 MPa. Differences in the capacities could be due to the varying compressive strength of grouted masonry units loaded in the direction parallel to the bed joints.

5. Strains in the GFRP rods linearly increased with the increase in the applied load up to the failure load.

6. It was observed that the numerical methods used to calculate the deflection patterns overestimated the deflections of the GFRP-reinforced concrete masonry beams.

Overall results showed that the methods suggested by CSA S304.1 (2004) and ISIS Canada (2001) yielded similar predictions. It was also concluded that Response 2000 tends to slightly underestimate the maximum deflections of the GFRP-reinforced masonry beams, while estimating the pattern of the load-deflection curve correctly.

7. Methods used to calculate curvatures of the GFRP-reinforced and CFRP-strengthened masonry beams at different bending moment levels showed good agreement with each other, while Response 2000 slightly underestimated the curvature values.

8. It was observed that the cracks did not necessarily follow the mortar joints and propagated through the masonry blocks as well. In this sense, GFRP-reinforced concrete masonry beams exhibited similar crack patterns with the GFRP-reinforced concrete beams. Clamps placed in the shear zones did not limit the formation of shear cracks but worked as internal shear reinforcement (stirrups) and prevented shear cracks from widening.

9. Curvature-based deformability factor of the GFRP-reinforced beams as well as the CFRP-strengthened reinforced masonry beams were within the allowable limits set by ISIS Canada (2001). On the other hand, energy based ductility estimations demonstrated that the GFRP-reinforced concrete masonry beams exhibited semi-ductile behaviour having energy ratio values in the vicinity of 70%.

10. CFRP-strengthening applied on the steel-reinforced concrete masonry beam not only increased the flexural capacity of the section by 60%, but also significantly prevented the propagation of flexural and shear cracks that improved the stiffness of the beam. CFRP sheets applied on the both sides of the masonry beam did not show any

signs of debonding and remained intact until the failure even though they were not mechanically anchored to the surface of the beam.

The following conclusions were drawn from the experimental and analytical analysis and comparisons conducted on the tested compressive masonry prisms:

1. CSA S304.1 (2004) estimates the compressive strength of grouted masonry loaded in the direction parallel to the bed joints as 50% of the compressive strength of the prism when loaded normal to the bed joints. Compression tests conducted on masonry prisms demonstrated that this method slightly overestimates the actual compressive resistance f'_m however provided good results when used along with ISIS Canada (2001) to estimate the flexural capacity of the GFRP-reinforced sections. Average experimental f'_m parallel to the bed joint was 6.0 MPa while CSA S304.1 (2004) estimated it to be 6.9 MPa.

2. Tests conducted on the prisms that were constructed using the longitudinally-drilled masonry blocks and loaded parallel to their bed joints proved that the optimum core size for the concrete masonry units is 3". 2" grout core specimens increased the compressive strength 50%, 4" grout core specimens increased the compressive strength 63% and finally 3" grout core specimens increased the compressive strength more than 100% compared to the control compressive prisms. It was also concluded that higher compressive strength provided by these new blocks can lead to higher flexural capacities using identical mortar and grout mix design. In the meantime, they can replace and eliminate the need for lintel blocks since internal reinforcement can be positioned inside the grout cores. Moreover, lighter blocks will allow faster construction and increase workability of the blocks.

7.3 Recommendations for Future Work

Although it had been demonstrated and discussed throughout this thesis that the clamps in the shear zone did not have a significant effect on the deflections and crack patterns of the beams, deflections of the GFRP-reinforced and CFRP-strengthened concrete masonry beams must be revisited using high ratio of internal steel stirrups instead of external shear reinforcement.

Since the experimental program of this research focused on GFRP-reinforced concrete masonry beams, only one CFRP-strengthened beam tested and compared with the conventional steel reinforced control beam. In order to be able to further analyze and comprehend the flexural resistance, deflection, deformation and curvature characteristics of the strengthened masonry beam, more tests have to be conducted on masonry beams strengthened using different patterns and amounts of CFRP sheets.

Moreover, beams using the proposed longitudinally-drilled concrete masonry units have to be constructed to better visualize and analyze their performance under actual loading conditions. Design of these new concrete masonry units can be fine-tuned by testing hollow and fully-grouted blocks with holes with various other shapes and sizes.

Lastly, since a combination of steel and GFRP as an internal reinforcement is not recommended by ISIS Canada (2001), reinforced concrete masonry beams designed to have longitudinal and transverse GFRP rods have to be tested to investigate the performance and efficiency of GFRP as stirrups for reinforced concrete masonry beams.

REFERENCES

Abdalla, H.A, (2002) "Evaluation of Deflection in Concrete Members Reinforced with FRP Bars", Composite Structures Vol. 56, pp.63-71

Alagusundaramoothy P, Harik, I. E. and Choo, C. C. (2003), "Flexural Behavior of R/C Beams Strengthened with Carbon Fiber Reinforced Polymer Sheets or Fabric", Journal of Composites for Construction Vol. 7, No.4, pp. 293-301

American Concrete Institute (ACI). (2006). "440.1R-06: Guide for the Design and Construction of Concrete Reinforced with FRP Bars." Farmington Hills, MI.

American Concrete Institute (ACI). (2002). "440.2R-02: Guide for the Design and Construction of Externally Bonded FRP Systems for Strengthening Concrete Structures" Farmington Hills, MI.

American Society of Testing and Materials (ASTM). (2002). "C1314-02: Standard Test Method for Compressive Strength of Masonry Prisms." West Conshohocken, PA.

American Society of Testing and Materials (ASTM). (2002). "C270-02: Standard Specification for Mortar for Unit Masonry." West Conshohocken, PA.

American Society of Testing and Materials (ASTM). (2002). "C476-02: Standard Specification for Grout for Masonry." West Conshohocken, PA.

American Society of Testing and Materials (ASTM). (2002). "C780-02: Standard Test Method for Preconstruction and Construction Evaluation of Mortars for Plain and Reinforced Unit Masonry." West Conshohocken, PA.

American Society of Testing and Materials (ASTM). (2002). "E518-02: Standard Test Method for Flexural Bond Strength of Masonry." West Conshohocken, PA.

Altin, S., Tankut, T., Anil, O. and Demirel, Y. (2003) "Response of Reinforced Concrete Beams with Clamps Applied Externally: An Experimental Study", Engineering Structures Vol.25, pp.1217-1229

Anil, O. (2007) "Strengthening of RC T-Section Beams with Low Strength Concrete Using CFRP Composites Subjected to Cyclic Load", Construction and Building Materials Vol.22, pp. 2355-2368

Ashour, A.F, (2006) "Flexural and shear capacities of concrete beams reinforced with GFRP bars", Construction and Building Materials Vol.20, pp.1005-1015

Bahn B.Y., and Harichandran, R.S., (2008), "Flexural Behaviour of Reinforced Concrete Beams Strengthened with CFRP Sheets and Epoxy Mortar", Journal of Composites for Construction Vol.12, No.4, pp. 387-395

Benmokrane, B. and Theriault, M. (1998) "Effects of FRP Reinforcement Ratio and Concrete Strength on Flexural Behavior of Concrete Beams", Journal of Composites for Construction Vol.2, No.1, pp.7-16

Bennett, R. M., McGinley, W.M. and Bryja, J., (2007) "Deflection Criteria for Masonry Beams", Journal of ASTM International Vol.4, No.1, pp.39-48

Canadian Standards Association (CSA). (2004). "A179-04: Mortar and Grout for Unit Masonry." Mississauga, Ontario.

Canadian Standards Association (CSA). (2004). "S304.1-04: Design of Masonry Structures." Mississauga, Ontario.

Canadian Standards Association (CSA). (2006). "S6-06: Canadian Highway Bridge Design Code (CHBDC)." Mississauga, Ontario.

Canadian Standards Association (CSA). (2006). "S806-02: Design and Construction of Building Components with Fibre-Reinforced Polymers." Mississauga, Ontario.

Dhanasekar and Shrive, (2002), " Strength and Deformation of Confined and Unconfined Grouted Concrete Masonry", ACI Structural Journal Vol.99, No.6, pp.819-826

Drysdale, R.G. and Hamid, A.A. (2005). "Masonry structures – Behaviour and design." Canada Masonry Design Centre, Mississauga, Ontario.

Esfahani, M.R. (2007), "Flexural Behaviour of Reinforced Concrete Beams Strengthened by CFRP Sheets", Engineering Structures Vol.29, No.10, pp.2428-2444

Fyfe Co. (2008), " Tyfo SCH-11UP Composite using Tyfo S Epoxy", San Diego, USA

Galati, N., Tumialan, G. and Nanni, A. (2005) "Strengthening with FRP Bars of URM Walls Subject to Out-of-Plane loads", Construction and Building Materials Vol. 20, pp.101-110

Garden H.N. and Holloway L.C. (1998) "An Experimental Study of the Influence of Plate End Anchorage of Carbon Fibre Composite Plates Used to Strengthen Reinforced Concrete Beams", Composite Structures 42, pp. 175-188

Ghobarah, A., Galal, K. E. (2004). "Out-of-Plane Strengthening of Unreinforced Masonry Walls with Openings", Journal of Composites for Construction Vol.8, No.4, pp.298-305

Grace N.F. (1998), " Behavior and Ductility of Simple and Continuous FRP Reinforced Beams", Journal of Composites for Construction, Vol.2, No.4, pp. 186-194

Hao, Z. (2007), "Application of CFRP Laminates in the Retrofit of Masonry Deep Beams", Master Thesis, University of Alberta, Edmonton, Canada, pp.1-125

Horton, R.T. and Tadros, M.K., (1990), "Deflection of Reinforced Masonry Beams", ACI Structural Journal, Vol. 87, No.4, pp. 453-463

Jeong, S. (1994), "Evaluation of Ductility in Prestressed Concrete Beams Using Fibre Reinforced Plastic Tendons", PhD Thesis, University of Michigan, MI, pp.1-268

Khalaf, M. (1981), "A Study of Flexure in Reinforced Masonry Beams", Masters Thesis, University of Manitoba, pp.1-201

Kim, W. and White, N. (1999), "Shear-Critical Cracking in Slender Reinforced Concrete Beams", Structural Journal, Vol.96, No.5, pp.657-765

Kiss R.M, Kollar, L. P., Jai, J., Krawinkler, H., (2002) "FRP Strengthened Masonry Beams", Journal of Composite Materials, Vol. 36, No.5, pp. 521-536

Lee, S. and Moy, S., (2007), "A Method for Predicting the Flexural Strength of RC Beams Strengthened with Carbon Fiber Reinforced Polymer", Journal of Reinforced Plastics and Composites, Vol.26, No.14, pp. 1383-1400

Moon, F.L., Yi, T., Leon, R.T. and Kahn, L.F (2007) "Testing of Full-Scale Unreinforced Masonry Building Following Seismic Strengthening", Journal of Structural Engineering, Vol.133, No.9, pp. 1215-1226

Ombres, L. and Aiello, M.A, (2000), "Load-Deflection Analysis of FRP Reinforced Concrete Flexural Members", Journal of Composites for Construction, Vol.4, No.4, pp. 164-171

Paulay T. and Priestley, M.J (1992), "Seismic Design of Reinforced Concrete and

Masonry Buildings", Applied Mechanics Reviews, Vol.45, No.11, pp.158

Saikia, B., Kumar, P., Thomas, J., Rao, K. S. N., and Ramaswamy, A. (2007) "Strength and Serviceability Performance of Beams Reinforced with GFRP Bars in Flexure", Construction and Building Materials, Vol.2, pp.1709-1719

Sasanian, Navid (2009) "Out-of-Plane Flexural Performance of GFRP Reinforced Concrete Masonry Walls", Master's Thesis, Concordia University, Canada

Simard-Beaudry. (2001). "Blocs de béton: résumé des données techniques." St-Eustache, Québec.

Suter, G.T and Fenton, G.A, (1986). "Flexural Capacity of Reinforced Masonry Members", ACI Journal, Vol.83, No.15, pp. 126-136

Taly, Narendra, (2000). "Design of Reinforced Masonry Structures", McGraw- Hill

Turco, V., Secondin, S., Morbin, A., Valluzzi, M. R., and Modena, C. (2006). "Flexural and shear strengthening of un-reinforced masonry with FRP bars. "Composites Science and Technology, Vol.66, 289–296.

Voon, K.C. and Ingham, J.J, (2005) "Experimental Study of Partially Grouted Concrete Masonry Walls with Openings", 10th Canadian Masonry Symposium, Alberta

APPENDIX A: SECTION ANALYSIS OF GFRP-REINFORCED CONCRETE MASONRY BEAM

Section analysis using rectangular stress block approach of specimen F-3-1#19-C is explained in detail in this section in order to demonstrate the method that was used to determine the flexural capacity of the GFRP-reinforced concrete masonry beam sections in this project.

Using #19 GFRP rod for design:

$A_{frp} = 285$ mm^2, $\varepsilon_{frpu} = 0.017$
$E_{frp} = 47.6$ GPa, $f_{frpu} = 728$ MPa
$\varepsilon_{mu} = 0.003$, $f'_m = 6.9$ MPa
$h = 590$ mm, $d = 520$ mm, $b = 190$ mm

Next determining masonry stress block factors:

$$\alpha_1 = 0.85 - 0.0015 f'_m = 0.85 - 0.0015(6.9) = 0.84$$
$$\beta_1 = 0.97 - 0.0025 f'_m = 0.97 - 0.0025(6.9) = 0.95$$

Next the balanced condition has to be checked to make sure that the section is over-reinforced:

$$\rho_{frpb} = \frac{\alpha_1 \beta_1 f'_m}{f_{frpu}} \left[\frac{\varepsilon_{mu}}{\varepsilon_{mu} + \varepsilon_{frpu}} \right] = 1.13 \text{ x } 10^{-3}$$

$\rho_{frpb} = 1.13$ x 10^{-3} (190 x 320)= 112 mm^2 < 285 mm^2

Assuming compression failure at ultimate load in order to determine the stress in the GFRP rod:

$$\varepsilon_m = \varepsilon_{mu} = 0.003, f_{frp} < f_{frpu} = 723 \text{ MPa}$$

$$f_{frp} = 0.5E_{frp}\varepsilon_{mu}\left[\left(1+\frac{4\alpha_1\beta_1 f'_m}{\rho_{frp}E_{frp}\varepsilon_{mu}}\right)^{1/2} - 1\right] = 455.5 \text{ MPa}$$

Next using equilibrium equation the depth of the compressive block is found:

$$c = \frac{A_{frp}f_{frp}}{\alpha_1 f'_m \beta_1 b} = 122.6 \text{ mm}$$

Finally, the flexural resistance of the cross-section can be determined using:

$$M_r = A_{frp}f_{frp}(d - \frac{\beta_1 c}{2}) = 59 \text{ kN.m}$$

APPENDIX B: DEFLECTION ANALYSIS OF GFRP-REINFORCED CONCRETE MASONRY BEAM

In order to determine the load-deformation relationship of the specimens, effective moment of inertia (I_{eff}) of the cross section was calculated using several approaches of CSA S304.1 (2004), ISIS Canada (2001) and Horton and Tadros (1990) at any given applied moment. Next, the deflections depending on the previously calculated effective moment of inertias are estimated. The excel sheet corresponding to the specimen F-3-1#19-C is shown below comprised of step by step calculation of the effective moment of inertias and corresponding deflections of the specimen.

w(kN/m)	P(kN)	Equivalent Load	M(kNm)	$I_{eff(CSA S304.1)}$	$\Delta_{(CSA S304.1)}(mm)$	$\Delta_{(cr for Horton)}(mm)$	$\Delta_{(Horton)}(mm)$	$I_{eff(ISIS)}$	$\Delta_{(ISIS)}(mm)$
0	0	0	0	3.30E+09	0	0	0	3.30E+09	0
2.6	0	6.5	5.2	3.30E+09	0.43	5.46	0.43	3.30E+09	0.43
2.6	0.25	6.75	5.4	3.30E+09	0.44	5.67	0.44	3.30E+09	0.44
2.6	0.5	7	5.6	3.30E+09	0.46	5.88	0.46	3.30E+09	0.46
2.6	1	7.5	6	3.30E+09	0.49	6.30	0.49	3.30E+09	0.49
2.6	2	8.5	6.8	3.30E+09	0.56	7.14	0.56	3.30E+09	0.56
2.6	3	9.5	7.6	3.30E+09	0.62	7.98	0.62	3.30E+09	0.62
2.6	4	10.5	8.4	3.30E+09	0.69	8.82	0.69	3.30E+09	0.69
2.6	5	11.5	9.2	3.30E+09	0.76	9.66	0.76	3.30E+09	0.76
2.6	6	12.5	10	3.30E+09	0.82	10.50	0.82	3.30E+09	0.82
2.6	7	13.5	10.8	3.30E+09	0.89	11.34	0.89	3.30E+09	0.89
2.6	8	14.5	11.6	3.30E+09	0.95	12.18	0.95	3.30E+09	0.95
2.6	10	16.5	13.2	3.30E+09	1.09	13.86	1.09	3.26E+09	1.10
2.6	15	21.5	17.2	1.63E+09	2.86	18.06	5.98	1.62E+09	2.88
2.6	20	26.5	21.2	9.91E+08	5.79	22.26	11.31	9.84E+08	5.84
2.6	22	28.5	22.8	8.48E+08	7.29	23.94	13.43	8.41E+08	7.34
2.6	25	31.5	25.2	6.95E+08	9.83	26.46	16.58	6.90E+08	9.90
2.6	30	36.5	29.2	5.39E+08	14.69	30.66	21.72	5.36E+08	14.77
2.6	36.5	43	34.4	4.30E+08	21.69	36.12	28.20	4.28E+08	21.79
2.6	40	46.5	37.2	3.94E+08	25.60	39.06	31.61	3.92E+08	25.69
2.6	45	51.5	41.2	3.58E+08	31.19	43.26	36.39	3.57E+08	31.28
2.6	50	56.5	45.2	3.34E+08	36.70	47.47	41.09	3.33E+08	36.79
2.6	55	61.5	49.2	3.17E+08	42.10	51.67	45.73	3.16E+08	42.18
2.6	60	66.5	53.2	3.04E+08	47.35	55.87	50.31	3.04E+08	47.43
2.6	65	71.5	57.2	2.95E+08	52.47	60.07	54.85	2.95E+08	52.54
2.6	70	76.5	61.2	2.89E+08	57.48	64.27	59.35	2.88E+08	57.54
2.6	75	81.5	65.2	2.83E+08	62.37	68.47	63.82	2.83E+08	62.43
2.6	80	86.5	69.2	2.78E+08	67.20	72.67	68.26	2.78E+08	67.25